RESPONSE AND FAILURE OF FLUID-FILLED TANKS UNDER BASE EXCITATION

Thesis by
Sotirios Natsiavas

In Partial Fulfillment
of the Requirements for the Degree of
Doctor of Philosophy

California Institute of Technology
Pasadena, California
1988

(Submitted April 1987)

ACKNOWLEDGMENTS

The author takes this opportunity to sincerely thank Professor C.D. Babcock for his advice and encouragement during the course of this work. The support and friendship of Professor P.C. Jennings is also gratefully acknowledged. The financial support, education and help provided by the Caltech community throughout my graduate studies is much appreciated.

Most of the text of this thesis was typed by Mrs. Marta Goodman. I want to thank her for her help and friendship.

Finally, I would like to thank my wife, Anatoli, for her understanding and patience during the period of this study.

ABSTRACT

An analytical model is developed that leads to better understanding of the response of fluid-filled tanks whose bottom may separate from and lift off the foundation, during base excitation. First, the hydrodynamic problem is solved in closed form, for the most general motion of the structure. This eliminates the fluid response unknowns and therefore only the structural degrees-of-freedom need to be considered. Then, application of Hamilton's Principle in the structural domain sets up the system equations of motion. During this procedure, the uplifting behavior is modeled by an appropriate rotational spring, placed between the foundation and the bottom of the tank. Equivalent springs are also used for modeling the ground/structure interaction. Moreover, shell flexibility and liquid sloshing effects are also incorporated and investigated.

Using this model, results are obtained and compared with experimental data. This comparison reveals some interesting effects of the base uplift on the system response. Ground flexibility is found to reduce the effective beam-type stiffness of the structure, but this reduction is much smaller than the substantial stiffness reduction induced by the possibility of uplifting. For the cases examined, the stiffness reduction due to the base uplift changes dramatically the dynamics of the system, which in turn alters the developed hydrodynamic loads, through the fluid/structure coupling process. Also, the shell flexibility effects - which can be important for the anchored tank case - are found to be negligible for an unanchored tank. Knowledge of the structural response leads to direct calculation of the hydrodynamic loads and consequently to prediction of failure. Buckling phenomena observed experimentally at the top and the bottom of scale model tanks are studied and explained.

TABLE OF CONTENTS

Chapter 1

GENERAL INTRODUCTION

1.1. Motivation.

Circular cylindrical tanks are extensively used structures for the storage of liquids. This is due to the fact that they are easy and economical to fabricate and they are structurally efficient in sustaining the hydrostatic pressure caused by the contents. This hydrostatic pressure is carried by tensile membrane stresses while bending stresses are significant only in local areas where changes in tank geometry occur.

A tank designed only for statical content loads can be quite thin in the sense that the radius-to-thickness ratio can be very high. Values of this ratio in the range 400-800 are the common case. As long as the membrane stresses remain tensile and below the allowable stress, the strength of the shell is not an issue. However, if compressive stresses are generated due to operational or environmental loads, a buckling failure may occur.

High compressive membrane stresses can be developed in fluid-filled ground-supported tanks during strong earthquakes. Severe loading can lead to stress or buckling failures and subsequent loss of contents. This, apart from the economical losses, may result in disastrous consequences if flammable liquids or hazardous substances are released.

The earthquake loads in a storage tank are caused by the mass of the tank itself and the contents being accelerated by the ground motion. For most tanks the loads caused by the contents are much greater than the loads caused by the tank structure. This is not true for tanks with low fluid levels which is not an important case since the combined loads are then so small that failure is not of concern.

Content loads basically depend on earthquake intensity, direction (horizontal, vertical) and frequency content, on tank and soil flexibility and on tank base fixity. Depending on the base fixity, the tanks are divided into anchored and unanchored. A fixed base tank requires a fairly substantial foundation and attachment mechanism in order to carry successfully the considerable overturning loads that occur during an earthquake. This implies high constructional cost which is the main reason why most of the tanks in the field are not properly anchored.

The calculation of the earthquake induced loads is more complicated in unanchored tanks due to the fact that these tanks lift off the ground around the perimeter, if the ground shaking is sufficiently high. This uplifting causes severe loading on the sidewall/bottom joint as well as high bottom plate stresses. It also considerably reduces the effective beam-type stiffness of the tank, as verified by relative data from static tilt tests [35,37][1] and results of the present analysis. This reduces the frequency of the predominant response mode of the tank and changes the behavior and motion of the tank, which in turn affects the distribution of the fluid pressures through the fluid/structure coupling effects.

Depending on the height to diameter ratio, the tanks are divided into tall and broad. If the diameter of the tank is less than its height the tank is called tall. In the opposite case the tank is called broad. From field observations, tall tanks are more susceptible to earthquake damage.

Tank failure modes due to ground motion [1-5,25,30] are quite diverse in nature. Most common are buckling and failure at joints. Buckling at the bottom of the tank usually appears in two patterns. The first one is the typical diamond-shaped post buckling mode which occurs because the tank is subjected to axial membrane stress resulting from the overturning moment (Figure 1.1). The other one is the so called "elephant's foot" bulge (Figure 1.2). This is an outward bulge observed most or all the way around the shell bottom. Its almost axisymmetrical shape makes many

1. Numbers in brackets correspond to references.

investigators believe that vertical acceleration is the cause. Similar patterns have also been observed in places of the tank where shell courses of different thicknesses are connected (Figure 1.3). Buckling is also observed at the top of the tank (Figure 1.4). Its pattern is similar to those observed for shells under external pressure (one half wave in the axial direction and several waves in the circumferential direction of the shell). As it is proved in this work, the required external pressure is created by negative hydrodynamic pressures developed near the liquid free surface which locally overcome the hydrostatic pressure, during sufficiently strong earthquake excitation.

Joint or seam failure usually occurs at the sidewall/bottom connection or at the sidewall/roof connection. This latter failure is believed to be caused by the sloshing waves impacting the roof. Complete collapse of tanks has also been observed. This is probably due to a stress or buckling induced rupture at the base followed by rapid loss of the tank contents (Figure 1.5). The resulting partial vacuum causes a buckling collapse of the entire tank.

Connection failures are quite common on unanchored tanks. This, again, leads to rapid loss of contents and perhaps tank buckling due to inadequate venting. Tank connections that can accommodate uplift of unanchored tanks can be designed but considerable uplift must be considered. The uplift of a large tank (R= 50 ft) of the order of 14 inches has been observed [3] (Figure 1.6).

1.2. Historical Background.

Over the past 50 years a large number of studies have been conducted on the dynamic response of liquid storage tanks. The earliest studies were due to Jacobsen et al. [6,7], who reported analytical and experimental results on the hydrodynamic pressure developed in rigid tanks subjected to horizontal base motion and anchored to a rigid foundation.

In the late 1940s and in the 1950s, during intensive work and fast evolution in aerospace technology, a number of studies were devoted to the investigation of the

dynamic behavior of fuel containers [56,59]. These analytical developments and studies examined the influence of the containers' vibrational characteristics on the flight control system of space vehicles by considering the container to be rigid and focusing on the dynamic response of the contained liquid. By considering the exact solution for simple geometries, it was pointed out that the fluid/container system can be represented by a simplified discrete model whose parameters are determined as functions of the liquid depth to tank radius ratio. These parameters were found by requiring duplication of forces and moments at some important point - usually center of mass or base - of the system.

In 1957, based on results of the above works, Housner used an approximate simplified approach, avoiding the complexities of the exact solution, and developed formulae for models of containers having two-fold symmetry. This analysis, which easily identifies the base shear and overturning moment [8,9], found widespread application in practice and comprises the basis of today's seismic design codes for liquid containers.

The research in the aerospace industry was vigorously pursued with attempts to incorporate the tank flexibility and nonlinear sloshing effects analytically [53-55,57,58,60]. Comprehensive lists of investigations on the dynamic behavior of fuel tanks of space vehicles, up until 1966, can be found in [51,52]. On the other hand, seismic analysis methods for ground-supported tanks evolved slowly until the 1964 Alaska earthquake. The response and the large-scale damage of modern design storage tanks during that earthquake brought into question the adequacy of the seismic design procedures and demonstrated the need for more realistic and reliable design. Also, the fast evolution of the digital computer technology and the parallel development of appropriate numerical methods had significantly enhanced solution capability by that time. These factors, in addition to helpful knowledge which came out of investigations in related aerospace areas, profoundly influenced the subsequent research in the field. Experiments and more refined analytical and numerical analyses were carried out.

First, the accuracy of the tank rigidity assumption was assessed by a number of investigators. In 1969, Edwards [11] considered the interaction between the contained liquid and the elastic tank wall by employing the finite element method in modeling the flexibility of the tank wall. Application of this analysis to a broad tank, allowing no cross-section distortions, and comparison of the results with those obtained from the corresponding mechanical analog revealed that the tank flexibility effects were important for the case examined. Arya, Thakkar and Goyal [12] used a different approach to study the dynamic characteristics of elastic fluid containers. Their analysis was based on an energy method treatment by Baron and Skalak [10] who utilized the idea of the virtual mass of the liquid and used the mode shapes of the empty shell as generalized coordinates for the coupled system. A similar type of analysis was used by Wu, Mouzakis, Nash and Colonell [14] who did not utilize the virtual mass idea but instead used a series expression for the liquid potential function as well as for the shell displacements. At about the same time, Hsiung and Weingarten [13] applied the finite element method to investigate the free vibrational characteristics of fluid/shell systems by discretizing both the shell and the fluid. Shortly after, Shaaban and Nash [15] investigated the seismic response of partially filled ground-supported anchored cylindrical containers. Again, finite elements were used to descretize both the shell and the fluid. Later, Balendra [16] extented this work by including an elastic axisymmetric dome attached to the top of the tank. A common conclusion of all these works was that the response of the coupled system can be determined through superposition of the motions of the shell and the liquid neglecting the liquid free surface waves together with the sloshing of the liquid in a rigid tank. This means that the liquid sloshing is not much affected by the tank flexibility, for an anchored tank.

During the same time, another approach was presented by Veletsos [19] for formulating the tank flexibility. First he neglected the fluid sloshing and assumed that the tank cross-section does not deform during vibration. By then prescribing the axial variation of the tank deflection he actually represented the system by a single

degree-of-freedom oscillator. A more complete formulation as well as an extension of that work was presented by Veletsos and Yang [20,21]. The hydrodynamic pressure distribution and the loads at the base of the tank corresponding to several assumed axial modes of vibration were presented and it was concluded that the flexibility effects may be important depending on the system characteristics and the seismic excitation.

In all the previous works, the beam-type modes were mainly treated since the tanks were considered to be perfect and anchored to a rigid foundation. Then, according to classical linear analysis, only those modes can be excited during horizontal base excitation. However, shaking table and static tilt experiments conducted at U.C. Berkeley by R.W. Clough et al. [33-37], showed that the out-of-roundness modes had significant amplitudes. Those experiments dealt with both anchored and unanchored tanks and they also examined the effects of other parameters on the tank response. Such parameters were the roof type, water depth, excitation type and intensity, effect of initial shell imperfections and the stiffness of the foundation material. In addition to dynamic pressure, water surface displacements, membrane strains, radial and tangential tank displacements, base uplift displacements were also measured. In an effort to explain the out-of-round response, Veletsos and Turner [22] presented an analysis and they concluded that this response is probably due to the interaction between the initial shell imperfections and the pressure exerted by the contained liquid.

In 1980, Haroun [24] presented a discretization scheme in which the shell wall was modeled by finite elements but the fluid region was treated as a continuum, thereby reducing the number of unknowns of the problem. Apart from the flexibility effects for anchored tanks, he also examined the effect of the initial hoop stresses due to hydrostatic pressure, the roof effect and the effect of coupling between liquid sloshing and shell vibrations. A study on the foundation flexibility effect concluded that the fundamental frequency of deformable containers [26] was reduced. Soil/structure interaction effects were also examined analytically by

Daysal and Nash [17] and experimentally by Cambra [36] and by Manos and Clough [37].

Except for some analysis included in [20] and some experimental results reported in [34] all the above works ignored the vertical loading effects. Some current studies, though, tried to identify the effects of such an excitation. The most significant effect appears to be the increased fluid pressure which in turn causes a higher hoop stress in the tank wall. Marchaj [39] developed a simple analysis trying to stress the importance of the increased hoop stresses due to the vertical excitation, in the design of liquid containers. Kumar [23] presented analytical results on the subject while Haroun and Tayel [27] extended the work in [24] to include the vertical excitation component for anchored tanks. Both approaches yielded eigenfrequencies and mode shapes for partially filled tanks and concluded that liquid sloshing and liquid compressibility effects are negligible for the most commonly used liquids.

Most of the above mentioned effects were studied simultaneously by other investigators, mainly in Europe and Japan [40,43-47], but the refinements and developments which came out of these considerations have not found extensive application in seismic design procedures. A common characteristic of all these works is that they are concerned with tanks anchored to their foundation. However, many of the tanks in the field are essentially unanchored, since proper anchoring is expensive. Some information on damage of unanchored and/or not sufficiently anchored tanks can be found in [1-3,5,25,30]. The analytical formulation of the dynamic behavior of tanks which lift off their foundation during strong ground motion is quite complicated and inherently nonlinear. As a result, only some experimental results were published on the subject at the beginning. This is so, despite the fact that the uplift of the tank causes important changes in the tank behavior under strong seismic motion.

Results from tests with unanchored tanks were first conducted at U.C. Berkeley by R.W. Clough et al. [33-38]. According to these results, the response of the unanchored tank is dominated by the uplift mechanism. Also, in some cases [34,37,38], the compressive axial membrane stresses at the shell bottom were measured to be considerably higher than the corresponding allowable code value, without any sign of failure. More recently, Shih and Babcock performed scale model tests for both anchored and unanchored tanks in an effort to gain a better understanding of the response and the appropriate failure criterion [28,29]. For the anchored case it was observed that the buckling is predominantly influenced by the response of the beam-type fundamental mode, while the higher order shell modes even with lower frequencies seemed to be unimportant. Also, the buckling stress was considerably higher than that proposed by codes using a "knockdown" factor. Much higher stresses were developed in unanchored tanks than in anchored tanks, for the same loading conditions. The buckling was again found to be highly influenced by the response of the rocking mode of the tank. The results of these experiments provide good information and data for comparison with analytical works.

During the course of the present investigation, some works have been reported in an effort to analytically formulate various aspects of the behavior of unanchored tanks. In 1985, Ishida and Kobayashi presented a four degree-of-freedom mechanical model in an attempt to approximately analyze the rocking response of tanks [42]. The rocking motion of the tank is modeled by a rotational spring, placed at the tank bottom. This spring is supposed to take into account both the foundation flexibility effects and the partial uplift at the tank bottom, simultaneously. The properties of such a spring are obtained under certain assumptions for the foundation and the bottom plate properties as well as for the distribution of the vertical forces at the tank base.

At the same time, Auli, Fischer and Rammerstorfer presented an approach which allows for an approximate modeling of the vertical restraining action of the base plate and foundation on the shell [41]. This is done by representing the bottom

plate and the foundation action on the shell with axial springs, placed all around the lower edge of the shell. These springs have nonlinear characteristics, derived either analytically - by considering strips of the bottom plate - or by employing finite element methods. The second approach is more comprehensive since it includes the membrane action in the base plate, it incorporates the foundation flexibility by modeling it as a Winkler foundation and it accounts for an elastic-plastic material behavior of the plate and the shell. In both cases, axisymmetric conditions are considered by making the assumption that the deformation of the uplifted region varies slowly in the circumferential direction. The uplifted area and the compressive axial membrane stresses at the shell bottom are computed for two tanks. In those calculations, the hydrodynamic pressure developed for the anchored tank cases was used. However, as it is shown by results of the present analysis, this is completely unjustified. The uplift changes dramatically the behavior of a tank and consequently the developed hydrodynamic loads. Finally, it was concluded that the buckling of those tanks is unaffected by the shell geometrical imperfections and that the critical axial compressive stress is about the same as the classical buckling value.

Similar analytical concepts were developed by Peek [31], independently. However, since for some cases - broad, roofless tank - the modeling with nonlinear springs was not satisfactory, the solution of the two-dimensional contact problem was attempted, using a finite difference energy method. Both methods were developed for static lateral loads on the tank. The membrane stresses were found to carry most of the load on the uplifted portion of the base plate. Apart from the characteristics of the nonlinear springs modeling the base uplift, other important quantities like the loads and stresses in the bottom plate as well as the stresses in the shell wall can be computed by this analysis. Such results are presented in [31] for static tilt tests with tanks tested by Peek as well as by others [29,35,37]. Comparison of the analytical and experimental results revealed that the computed stresses are in good agreement with the experimental values and that in some cases

these stresses exceed those calculated by current design codes by more than a factor of two.

1.3. Design Procedures.

Design procedures [48-50] consider one axis lateral ground acceleration. Most procedures first find the tank overturning moment caused by the tank mass and the pressures exerted on the tank wall by the fluid contents. This latter calculation includes the impulsive and convective terms assuming a rigid tank anchored on a rigid foundation and may consider a correction due to tank wall flexibility. This correction is derived from anchored tank analysis but is used for both anchored and unanchored tanks. The calculations are based on a specified response spectrum for the sloshing and tank flexibility correction and a maximum acceleration for the impulsive type load. Also, there is no consideration for the ground flexibility effects and the vertical ground excitation component.

Once the overturning moment is found, the anchored and unanchored design procedures differ. For the anchored tank, the tank wall stresses are found from the moment using structural mechanics considerations. These stresses are compared to the allowable stresses using either a stress or a buckling limitation.

The unanchored tank presents more difficulty to the designer. First, the resistance to tank overturning is calculated, despite the fact that overturning prior to other failure has never been observed. This calculation is based upon an empirical model where tank resistance to overturning is provided by the tank shell and a portion of the tank contents [48]. This portion depends on the width of the bottom annular ring which may lift off the foundation. The calculation of this width ignores the membrane stresses developed in the bottom plate upon large amount of uplift. In some experiments, the uplift length was measured to be more than three times of that predicted by this model [38]. Next, the axial stresses in the tank wall are calculated using much the same empirical model used for the overturning calculations. This model assumes that the stresses approach infinity at overturning so a stress or

buckling failure always precedes overturning. The stresses resulting from this calculation are compared to the allowable stress in the same manner as for the anchored tank. This method of stress calculation is not supported by tests or analyses.

1.4. Objective and Organization of the Present Investigation.

Most of the previous studies on the subject have focused on the dynamic response of rigid or flexible tanks, anchored on a rigid foundation and subjected to horizontal base excitation. Recently, some works have dealt with the formulation of the ground flexibility [17,26], the vertical excitation effects [23,27,39] and some aspects of the uplifting phenomenon [29-38,41,42,46].

The objective of the present work is to create - based upon observations and results provided by previous investigations - a simplified analytical model for the dynamic behavior of fluid-filled tanks, that will lead to a better understanding of the response and consequently the failure mechanisms of unanchored tanks. For these tanks, the difficulty associated with the exact analytical modeling of the nonlinear uplifting phenomenon implies directly the need for simplified approaches. The present model formulates this uplift behavior, determines the tank response under base excitation and identifies the hydrodynamic loads on a tank so that failure analyses can then be performed. The work is mostly concerned with the formulation of the behavior of unanchored tanks. However, the response of anchored tanks is also easily obtained from this analysis, as a special case. For this case, special attention is paid to the formulation of the ground/structure interaction effects.

In the following chapter, the response of a fluid inside a cylindrical tank is examined for the most general motion of the tank. The corresponding hydrodynamic pressure and base loads are obtained analytically, in closed form. Finally, a simplified model for the behavior of a rigid tank undergoing both translation and rocking is developed.

The third chapter is devoted to the derivation of a set of equations describing the behavior of the coupled fluid/stucture/ground system. Special attention is paid to the formulation of the base uplift but effects due to ground and shell flexibility and liquid sloshing are also included. Beam-type deformation - but allowing for circumferential straining and in-plane shearing of the cylindrical shell - and horizontal base excitation are assumed.

Numerical results from the application of this analysis, are presented in chapters 4 and 5. In chapter 4, results for anchored tanks are derived, so that comparison with results of previous investigations can be done. In addition, effects due to ground flexibility are primarily considered. Also, buckling phenomena observed at the top of a fluid-filled tank are explained. A strange dynamic response of this tank, encountered during the nonlinear ground/structure interaction formulation, is also examined and investigated.

In the last chapter, results are obtained for unanchored tanks. The effect of the base uplift on the system dynamics is first examined. Then, the coupling between the sloshing and structural modes and the shell flexibility effects in an unanchored tank are considered. Finally, an explanation is provided for previously performed buckling experiments [29]. In those experiments, the tanks were subjected to either harmonic or transient base excitation and their behavior was very different depending on their base fixity condition only.

Chapter 2

FLUID RESPONSE IN A CYLINDRICAL TANK

2.1. Introduction.

A basic step in the analytical formulation of the fluid/structure interaction, occurring in a liquid storage tank during dynamic excitation, is that of determining the fluid response associated with a given structural response. It is more convenient to analyze the fluid response problem separately, before the general formulation of the coupled problem. In this way, the physics and the fundamental parameters governing the fluid behavior can be examined and presented more efficiently, which then results in a better understanding of the complete problem.

For the purposes of the present work, the fluid is assumed to be ideal (inviscid, incompressible) and the flow irrotational. The fluid velocity field is then expressed in terms of a scalar potential function Φ, satisfying the Laplacian throughout the fluid domain. Considering small amplitude surface waves, conservative body forces and matching the appropriate fluid and structural velocities the boundary value problem for Φ is set. Then, the solution for Φ is found for the most general case of tank motion, the corresponding hydrodynamic pressure is obtained and the resultant hydrodynamic base shear and overturning moment are also determined. In each case, the so-called "impulsive" and "convective" terms can be easily identified.

In the formulation of the boundary value problem for Φ, the structural velocities are assumed to be known and the derived hydrodynamic pressures and loads are functions of these velocities. To completely determine the fluid as well as the structural response, the coupled fluid/structure interaction problem must be considered, in the general case. This task is the subject of the next chapter, while in the end of this chapter a simplified mechanical model is presented, which easily identifies the resultant hydrodynamic loads at the bottom of a rigid cylindrical tank,

undergoing both translation and rocking.

2.2. Mathematical Formulation of the Fluid Behavior.

The geometry of the system under consideration is shown in Figure 2.1. The tank has radius R and contains a liquid of density ρ_l, up to a level H. Its base is assumed to follow the ground motion, whose displacement along the x-axis has history $x_g(t)$. Polar coordinates r, θ, z are used for the space description of the system variables and U_r, U_θ, U_z are the corresponding velocities in the radial, circumferential and axial direction. Symbol t stands for the time variable.

For the considered system and the most commonly used liquids, the viscosity and compressibility liquid effects are believed to be negligible. Then, if the flow is originally irrotational, it will remain so and the fluid velocity field can be expressed by:

$$\underset{\sim}{U} = \nabla\Phi \ ,$$

the continuity equation reduces to

$$\nabla^2\Phi = 0$$

and for conservative body forces, the equilibrium equations can be represented in an integrated form by a single scalar (Bernoulli) equation

$$\frac{\partial\Phi}{\partial t} + \frac{P}{\rho_l} + \frac{1}{2}\nabla\Phi\cdot\nabla\Phi - G = F(t) \ ,$$

where

$$\nabla^2 \equiv \frac{\partial^2}{\partial r^2} + \frac{1}{r}\frac{\partial}{\partial r} + \frac{1}{r^2}\frac{\partial^2}{\partial\theta^2} + \frac{\partial^2}{\partial z^2} \qquad \text{and} \qquad G = \frac{P_o}{\rho_l} - g(z-H) \ .$$

Φ is a scalar function known as the "velocity potential," g is the gravity acceleration, P is the total pressure and is a function of space and time, P_o is the external pressure on the fluid surface and F(t) is a time function coming out of the integration of the equilibrium equations.

Assuming small amplitude surface waves - compared to their wavelengths - Bernoulli's equation reduces to:

$$\frac{\partial \Phi}{\partial t} + \frac{P-P_o}{\rho_l} + g\eta = 0 \ ,$$

where F(t) is absorbed into Φ and $\eta=z-H$. Then, imposing the linearized kinematic free surface condition

$$\frac{\partial \Phi}{\partial z} = \frac{\partial \eta}{\partial t} \qquad at \quad z = H \ ,$$

the linearized Bernoulli's equation, at z=H, takes the form

$$\frac{\partial^2 \Phi}{\partial t^2} + \frac{1}{\rho_l} \frac{\partial (P-P_o)}{\partial t} + g \frac{\partial \Phi}{\partial z} = 0 \ .$$

Neglecting free surface tension effects, the last equation becomes

$$\frac{\partial^2 \Phi}{\partial t^2} + g \frac{\partial \Phi}{\partial z} = 0 \qquad on \quad z = H \ .$$

Finally, matching of the normal velocities of the fluid and the structure in their common area requires that:

$$U_z = \frac{\partial \Phi}{\partial z} = f(r,\theta,t) \qquad at \quad z = 0$$

$$U_r = \frac{\partial \Phi}{\partial r} = h(\theta,z,t) \qquad at \quad r = R$$

where f, h are the corresponding normal velocities at the bottom and the wetted cylindrical part of the structure, respectively.

With Φ determined, the fluid velocity field is given by

$$U_r = \frac{\partial \Phi}{\partial r} \ , \qquad U_\theta = \frac{1}{r} \frac{\partial \Phi}{\partial \theta} \ , \qquad U_z = \frac{\partial \Phi}{\partial z} \tag{2.1}$$

the free surface displacement by

$$\eta(r,\theta,H,t) = -\frac{1}{g} \frac{\partial \Phi}{\partial t}(r,\theta,H,t) \tag{2.2}$$

and the pressure distribution in the fluid domain by

$$P(r,\theta,z,t) = P_o + \rho_l g(H-z) - \rho_l \frac{\partial \Phi}{\partial t}(r,\theta,z,t) \tag{2.3}$$

Clearly, the pressure consists of two parts. The hydrostatic part

$$P_{st} = P_o + \rho_l g(H-z) \tag{2.4}$$

and an additional (hydrodynamic) part, resulting from the fluid motion

$$P_d = -\rho_l \frac{\partial \Phi}{\partial t} \ . \tag{2.5}$$

2.3. Solution of the General Fluid Response Problem.

First, the velocity potential Φ and the structural velocities can be expanded in Fourier Series in the θ-direction. Utilizing the linearity of the system and the orthogonality properties of the sine and cosine functions in the considered domain, it becomes clear that instead of the initial system, only the following problem for each Fourier component of Φ, f and h, say Φ_n, f_n and h_n, respectively, has to be solved:

$$\nabla^2 \Phi_n(r,z,t) = 0 \qquad \textit{in the fluid domain} \tag{2.6}$$

$$\frac{\partial^2 \Phi_n}{\partial t^2} + g \frac{\partial \Phi_n}{\partial z} = 0 \qquad on \quad z = H \tag{2.7}$$

$$\frac{\partial \Phi_n}{\partial z} = f_n(r,t) \qquad at \quad z = 0 \tag{2.8}$$

$$\frac{\partial \Phi_n}{\partial r} = h_n(z,t) \qquad at \quad r = R \tag{2.9}$$

Then, assuming the initial conditions

$$\Phi_n = \dot{\Phi}_n = 0 \qquad at \quad t = 0 \tag{2.10}$$

and using standard separation of variables techniques, it is found (Appendix A) that the general solution of this problem has the following form:

$$\Phi_n(r,z,t) = (\frac{r}{R})^n \left[a_n(t) \frac{z}{H} + b_n(t)\right] + \sum_{s=1}^{\infty} \{J_n(k_{ns} \frac{r}{R}) \left[A_{ns}(t) \cosh(k_{ns} \frac{z}{R}) + \right.$$

$$\left. + B_{ns}(t) \sinh(k_{ns} \frac{z-H}{R})\right] + I_n(\lambda_s \frac{r}{H}) C_{ns}(t) \cos(\lambda_s \frac{z}{H})\}$$

where J_n is the Bessel function and I_n is the modified Bessel function of the first kind of order n and

$$J_n'(k_{ns}) = 0$$
$$\lambda_s = s\pi \qquad s = 1, 2, \cdots \ , \ n = 0, 1, \cdots$$

Decomposing h_n in the form

$$h_n(z,t) \equiv \alpha_n(t)\ z + \bar{h}_n(z,t)$$

and applying the boundary conditions of the system, the time functions a_n, b_n, A_{ns}, B_{ns} and C_{ns} are determined to be as follows, for zero initial conditions:

$$a_n(t) = \frac{1}{n} RH\alpha_n(t) \ , \quad b_n(t) = \frac{R}{nH} \int_o^H \bar{h}_n(z,t)\ dz \ , \quad (\ a_o(t) = 0 = b_o(t)\ )$$

$$C_{ns}(t) = \frac{2}{\lambda_s\ I_n'(\lambda_s\ \frac{R}{H})} \int_o^H \bar{h}_n(z,t)\ \cos(\lambda_s\ \frac{z}{H})\ dz$$

$$B_{ns}(t) = 2R^2\ \frac{b_{ns}(t) - \alpha_n(t)\ J_n(k_{ns})}{k_{ns}\ (k_{ns}^2 - n^2)\ J_n^2(k_{ns})\ \cosh(\mu_{ns})}$$

$$A_{ns}(t) = D_{ns}(t) - \omega_{ns} \int_o^t [E_{ns}(\tau) + D_{ns}(\tau)]\ \sin\omega_{ns}(t-\tau)\ d\tau$$

with

$$b_{ns}(t) = \left(\frac{k_{ns}^2}{R^3}\right) \int_o^R r\ J_n(k_{ns}\ \frac{r}{R})\ f_n(r,t)\ dr$$

$$E_{ns}(t) = \frac{2\ n\ a_n(t)}{\mu_{ns}\ (k_{ns}^2 - n^2)\ J_n(k_{ns})\ \sinh(\mu_{ns})} + \frac{B_{ns}(t)}{\sinh(\mu_{ns})}$$

$$D_{ns}(t) = -2\ \frac{n\ [a_n(t) + b_n(t)] + d_{ns}(t)}{(k_{ns}^2 - n^2)\ J_n(k_{ns})\ \cosh(\mu_{ns})}$$

$$d_{ns}(t) = \sum_{p=1}^{\infty} \left[(-1)^p\ \frac{(\lambda_p\ \frac{R}{H})\ I_n'(\lambda_p\ \frac{R}{H})}{1 + (\lambda_p/\mu_{ns})^2}\ C_{np}(t) \right]$$

$$\mu_{ns} = k_{ns}\ (\frac{H}{R}) \qquad \text{and} \qquad \omega_{ns}^2 = g\ \frac{k_{ns}}{R}\ \tanh(\mu_{ns}) \ .$$

2.4. Fluid Response for Some Special Cases.

For the scope of this study, the solution of the fluid response problem is only needed for some simple cases. In all these cases n=1 and the form of the solution is much simpler than the form of the general solution. For this reason and for their practical importance, these solutions are given next, by dropping the n=1 subscript - except for J_1 and I_1 - for simplicity.

2.4.1. *Tank with Flexible Cylindrical Shell.* In this case, assuming a rigid bottom plate and radial velocity for the cylindrical part of the form $w_m(z)\ \dot{\psi}_m(t)\cos\theta$, it is:

$$f(r,\theta,t) = 0 \quad \text{and} \quad h(\theta,z,t) = w_m(z)\ \dot{\psi}_m(t)\cos\theta\ .$$

Then, it easily follows from the general solution that

$$C_s(t) = \frac{2\ R\ \alpha_{ms}\ \dot{\psi}_m(t)}{(\lambda_s \frac{R}{H})\ I_1(\lambda_s \frac{R}{H})}\ ,\quad A_s(t) = D_s(t) - \omega_s \int_o^t D_s(\tau)\ \sin\omega_s(t-\tau)\ d\tau$$

where

$$\alpha_{mo} = \frac{1}{H}\int_o^H w_m(z)\ dz \tag{2.11}$$

$$\alpha_{ms} = \frac{1}{H}\int_o^H w_m(z)\cos(\lambda_s \frac{z}{H})\ dz \qquad (s = 1, 2, \cdots) \tag{2.12}$$

$$D_s(t) = -\ 2R\frac{S_{ms}\ \dot{\psi}_m(t)}{(k_s^2-1)\ J_1(k_s)\cosh(\mu_s)}\ ,\quad S_{ms} \equiv \alpha_{mo} + 2\sum_{p=1}^{\infty}\left[\frac{(-1)^p\ \alpha_{mp}}{1+(\lambda_p/\mu_s)^2}\right] \tag{2.13}$$

The velocity potential in this case has the form:

$$\Phi_m(r,\theta,z,t) = \cos\theta\ \{r\ \alpha_{mo}\ \dot{\psi}_m(t) + \sum_{s=1}^{\infty}[J_1(k_s \frac{r}{R})\ A_s(t)\cosh(\mu_s \frac{z}{H}) +$$

$$+ I_1(\lambda_s \frac{r}{H})\ C_s(t)\cos(\lambda_s \frac{z}{H})]\}\ ,$$

while the hydrodynamic pressure is given by:

$$P_m(r,\theta,z,t) = -\rho_l R\cos\theta \{ f_m(r,z)\ \ddot{v}_m(t) + \sum_{s=1}^{\infty}[f_{ms}(r,z)\ \bar{A}_{ms}(t)]\} \tag{2.14}$$

with

$$f_m(r,z) = \frac{r}{R}\ a_{mo} + \sum_{s=1}^{\infty}\left[2\ a_{ms}\ r_s(r)\ \cos(\lambda_s\frac{z}{H}) - f_{ms}(r,z)\right]$$

$$f_{ms}(r,z) = c_{ms}\,\bar{f}_s(r,z)\ ,\quad \bar{f}_s(r,z) = 2\frac{J_1(k_s\frac{r}{R})\cosh(\mu_s\frac{z}{H})}{(k_s^2-1)J_1(k_s)\cosh(\mu_s)}$$

$$c_{ms} = S_{ms}\ ,\quad r_s(r) = \frac{I_1(\lambda_s\frac{r}{H})}{(\lambda_s\frac{R}{H})\ I_1'(\lambda_s\frac{R}{H})} \tag{2.15}$$

$$\bar{A}_{ms}(t) = \int_o^t \omega_s\ \ddot{v}_m(\tau)\ \sin\omega_s(t-\tau)\ d\tau \tag{2.16}$$

2.4.2. *Tank Rigid Body Translation along the x-axis.* In this case, assuming that the ground displacement is $x_g(t)$ along the x-axis, the solution can be obtained from the previous solution, by just letting $w_m(z) = 1$ and $v(t) = x_g(t)$. Then, the previously obtained formulae are further simplified (since $a_{mo} = 1$ and all others $a_{ms} = 0$) and the velocity potential is given by:

$$\Phi_x(r,\theta,z,t) = \cos\theta \{ r\ \dot{x}_g(t) + \sum_{s=1}^{\infty}[J_1(k_s\ \frac{r}{R})\ A_s(t)\ \cosh(\mu_s\ \frac{z}{H})]\}\ ,$$

while the associated hydrodynamic pressure by:

$$P_x(r,\theta,z,t) = -\rho_l R\cos\theta \{ f_x(r,z)\ \ddot{x}_g(t) + \sum_{s=1}^{\infty}[f_{xs}(r,z)\ \bar{A}_{xs}(t)]\} \tag{2.17}$$

with

$$A_s(t) = -2R\frac{\dot{x}_g(t) - \omega_s\int_o^t \dot{x}_g(\tau)\ \sin\omega_s(t-\tau)\ d\tau}{(k_s^2-1)\ J_1(k_s)\ \cosh(\mu_s)}$$

$$f_x(r,z) = \frac{r}{R} - \sum_{s=1}^{\infty} f_{xs}(r,z)\ ,\quad f_{xs}(r,z) = \bar{f}_s(r,z)$$

$$\bar{A}_{xs}(t) = \int_o^t \omega_s \ddot{x}_g(\tau) \sin\omega_s(t-\tau)\, d\tau. \tag{2.18}$$

2.4.3. *Tank Rigid Body Rotation about the y-axis.* If the tank rotates about the y-axis so that:

$$f(r,\theta,t) = -\, c\, r\, \dot{\phi}(t) \cos\theta \quad \text{and} \quad h(\theta,z,t) = z\, \dot{\phi}(t) \cos\theta\ ,$$

it easily follows from the general solution that

$$B_s(t) = \frac{-\,2\,(c+1)\,R^2\,\dot{\phi}(t)}{k_s\,(k_s^2-1)\,J_1(k_s)\cosh(\mu_s)}\ ,\quad A_s(t) = 2R^2\,\frac{\bar{\mu}_s(t) - \mu_s\,\dot{\phi}(t)}{k_s\,(k_s^2-1)\,J_1(k_s)\cosh(\mu_s)}$$

with

$$\bar{\mu}_s(t) = \left[\mu_s(t) + \frac{(c+1) - \cosh(\mu_s)}{\sinh(\mu_s)}\right]\omega_s \int_o^t \dot{\phi}(\tau)\sin\omega_s(t-\tau)\, d\tau\ .$$

Then, the velocity potential is given by:

$$\Phi_\phi(r,\theta,z,t) = \cos\theta\{rz\dot{\phi}(t) + \sum_{s=1}^{\infty} J_1(k_s\,\frac{r}{R})[A_s(t)\cosh(\mu_s\,\frac{z}{H}) + B_s(t)\sinh(\mu_s\frac{z-H}{H})]\}$$

and the corresponding hydrodynamic pressure is:

$$P_\phi(r,\theta,z,t) = -\,\rho_l R\cos\theta\,\{f_\phi(r,z)\,R\ddot{\phi}(t) + \sum_{s=1}^{\infty}[f_{\phi s}(r,z)\,R\bar{A}_{\phi s}(t)]\} \tag{2.19}$$

with

$$f_\phi(r,z) = \frac{rz}{R^2} - 2\sum_{s=1}^{\infty} J_1(k_s\frac{r}{R})\,\frac{\mu_s\cosh(\mu_s\frac{z}{H}) - (c+1)\sinh(\mu_s - \mu_s\frac{z}{H})}{J_1(k_s)\,k_s\,(k_s^2-1)\cosh(\mu_s)}$$

$$f_{\phi s}(r,z) = c_{\phi s}\,\bar{f}_s(r,z)\ ,\quad c_{\phi s} = \frac{(c+1) - \cosh(\mu_s) + \mu_s\sinh(\mu_s)}{k_s\sinh(\mu_s)}$$

$$\bar{A}_{\phi s}(t) = \int_o^t \omega_s\,\ddot{\phi}(\tau)\sin\omega_s(t-\tau)\, d\tau\ . \tag{2.20}$$

Clearly, the case c=1 corresponds to the rigid body rotation of the tank through an angle $\phi(t)$ about the y-axis. On the other extreme case, when c=0, only the cylindrical shell undergoes the rocking motion, while the bottom plate remains horizontal.

2.4.4. *Discussion.* At this point it is noted that in all the cases examined the hydrodynamic pressure is proportional to $\cos\theta$. Also, the dependence of this pressure on the time functions associated with the corresponding tank mode is fairly standard. Namely, in all these cases, the hydrodynamic pressure is comprised of two distinct parts. One part which is directly proportional to the acceleration of the mode plus another part which is given in terms of an infinite series involving the same time function but in an integral form. In the relative literature, the first part is - not so properly - called "impulsive." Physically it is caused by the part of the fluid moving in unison with the tank. The second part, which is known as "convective" pressure, represents the sloshing at the free surface of the liquid. This part contains integral terms involving the sloshing frequencies and the time function associated with the tank deflection pattern.

In order to get some of the flavor of what is included in the various spatial functions appearing in the pressure expressions, Figures 2.2-2.3 are presented. The depicted distributions are computed at r=R and are given as functions of z/H and for H/R= 0.5, 1, 2, 4, which covers the range of practical interest. The corresponding distributions for the flexible modes were obtained by assuming

$$w_m(z) = \sin[(2m-1)\frac{\pi z}{2H}] \ ,$$

while for the deformation of the bottom plate the value c=1 was chosen. One difference between the impulsive and the sloshing terms is that the former are important all over the wetted surface, while the latter are usually important only near the free surface of the liquid. Also, the sloshing effects become less important as the tank becomes taller and as the order of the sloshing mode increases.

Finally, it is noted that interpreting what is shown in these figures, one must bear in mind that the pressures on the shell wall are obtained after multiplication of the normalizing constants and the corresponding time functions.

2.5. Hydrodynamic Loads at the Tank Base.

Knowledge of the pressure distribution on the shell wall and the bottom plate leads to straightforward computation of the resultant loads induced by the fluid motion, at any point of the shell. In the majority of the cases, the most severe stressing and failure occurs at the bottom of the tank. Therefore it is of practical importance to identify the loads there in order to be able to find the corresponding stress distribution and to predict possible failure at the bottom of the tank.

Clearly, if $P(r,\theta,z,t)$ is the pressure distribution inside the tank, the resultant shear force at the base of the tank is found from:

$$Q(t) = \int_0^H \int_0^{2\pi} P(R,\theta,z,t) \cos\theta \; R \; d\theta \; dz \quad ,$$

while the resultant moment with respect to point 0 and along the y-axis is given by:

$$M(t) = M_c(t) + M_b(t) \quad ,$$

where

$$M_c(t) = \int_0^H \int_0^{2\pi} P(R,\theta,z,t) \; z \; \cos\theta \; R \; d\theta \; dz$$

is the moment exerted through the cylindrical part of the tank and

$$M_b(t) = \int_0^R \int_0^{2\pi} P(r,\theta,0,t) \; r^2 \cos\theta \; d\theta \; dr$$

is the moment exerted from the fluid on the bottom plate.

Because of the form of the pressure P and the orthogonality properties of the cosine and sine functions in $0 \leq \theta < 2\pi$, it is obvious from the above formulae that only the $\cos\theta$ modes contribute to the resultant loads on the tank. Using results of the previous section, the resultant shear force at the bottom of the tank, during rigid body translation $x_g(t)$ along the x-axis, is found in the form:

$$Q_x(t) = - \; m_l \; \{ q_x \; \ddot{x}_g(t) + \sum_{s=1}^{\infty} [q_{xs} \; \bar{A}_{xs}(t)] \} \qquad (2.21)$$

where $m_l = \rho_l(\pi R^2 H)$ is the mass of the contained liquid. The corresponding moments are given by:

$$M_{xc}(t) = - m_l H \{\beta_x \ddot{x}_g(t) + \sum_{s=1}^{\infty}[\beta_{xs} \bar{A}_{xs}(t)]\} \tag{2.22}$$

$$M_{xb}(t) = - m_l H \{\gamma_x \ddot{x}_g(t) + \sum_{s=1}^{\infty}[\gamma_{xs} \bar{A}_{xs}(t)]\} \tag{2.23}$$

Similar expressions are derived for the resultant base loads for the case of rigid body rotation $\phi(t)$ about the y-axis and for the case where the radial velocity of the shell is of the form $w_m(z)\dot{v}_m(t)\cos\theta$. In these cases the subscript x in the above expressions for the base loads is replaced by ϕ and m, respectively. The q, β and γ's appearing in these base loads expressions are functions of the ratio H/R and the corresponding tank mode. Their explicit forms are given in Appendix B. The impulsive and convective parts in all the obtained relations for the hydrodynamic loads can again be readily identified. As far as the role of the important relative system parameters is concerned, Figures 2.4-2.6 help in illustrating the following points.

First, the sloshing effects are generally important only for relatively small values of the ratio H/R. As this ratio increases the impulsive terms become dominant, as expected intuitively. Also, from all the sloshing modes, usually only the first one may be of practical importance for realistic values of H/R. Finally, by comparing Figures 2.5-2.6, it is seen that the moments exerted by the liquid at the bottom of the tank are small compared to the moments exerted at the shell, for large H/R. The form of the flexible modes in obtaining the corresponding base loads was the same as that assumed for calculating the pressure distributions and c=1 was chosen again.

2.6. Simplified Mechanical Model for a Rigid Tank.

Apart from the ground displacement history $x_g(t)$, all the other time functions involved in the pressure and resultant loads expressions - as presented in the previous section - are yet to be found. Once these time functions are determined, the histories of the hydrodynamic loads on the structure become completely known, since their spatial dependence is already known.

In the general case, these time functions - and others associated with the structural response - may be determined by considering the coupled fluid/structure system. This task is not always that straightforward. One way of approaching the coupled problem is presented in the next chapter of this work. However, for the case of a rigid cylindrical tank, one can follow a simplified approach. Namely, as is shown next, one can substitute the contained liquid in a rigid tank by a number of oscillators whose position and dynamic characteristics can be analytically obtained by requiring the same base loads from both the container and the corresponding mechanical model, when they exhibit the same motion. Historically, this was the way the problem was approached at first [59,56,55,52,9,8]. Due to its simplicity and the clear physical interpretation it provides, this simplified model found widespread application in practice and a version of it - accounting for rigid body translation only - still comprises the basis of today's seismic design codes.

2.6.1. *Base Loads for a Rigid Tank.* By allowing a rigid tank to translate by $x_g(t)$ along the x-axis and rotate through a small angle $\phi(t)$ about the y-axis, the developed resultant base shear and base moment are given by

$$Q(t) = Q_x(t) + Q_\phi(t) \qquad \text{and} \qquad M(t) = M_x(t) + M_\phi(t) \ ,$$

respectively. Using the corresponding formulae for the base loads and applying the identity

$$\sum_{s=1}^{\infty} \left[\frac{1}{k_s^2(k_s^2-1)} \right] = \frac{1}{8} \ ,$$

after some trivial algebraic manipulations one can rewrite the base loads as:

$$Q(t) = - m_o \left[\ddot{x}_g(t) + h_o \ddot{\phi}(t)\right] - \sum_{s=1}^{\infty} m_s \left[\bar{A}_{xs}(t) + h_s \bar{A}_{\phi s}(t)\right] \tag{2.24}$$

$$M(t) = - m_o h_o \ddot{x}_g(t) - I_o \ddot{\phi}(t) - \sum_{s=1}^{\infty} m_s h_s \left[\bar{A}_{xs}(t) + h_s \bar{A}_{\phi s}(t)\right] \tag{2.25}$$

with

$$\frac{m_o}{m_l} = 1 - 2\frac{R}{H}\sum_{s=1}^{\infty}\left[\frac{\tanh(\mu_s)}{k_s(k_s^2-1)}\right] \tag{2.26}$$

$$\frac{m_s}{m_l} = 2\frac{R}{H}\,\frac{\tanh(\mu_s)}{k_s(k_s^2-1)} \tag{2.27}$$

$$\frac{h_o}{h} = \frac{m_l}{m_o}\left\{\frac{1}{2} + \frac{1}{2}(\frac{R}{H})^2 - 2(\frac{R}{H})^2\sum_{s=1}^{\infty}\left[\frac{\mu_s\sinh(\mu_s) + 2}{k_s^2\,(k_s^2-1)\cosh(\mu_s)}\right]\right\} \tag{2.28}$$

$$\frac{h_s}{H} = \frac{m_l}{m_s}\,2\,(\frac{R}{H})^2\left[\frac{\mu_s\,\sinh(\mu_s) - \cosh(\mu_s) + 2}{k_s^2\,(k_s^2-1)\cosh(\mu_s)}\right] \tag{2.29}$$

$$\frac{I_o}{m_l H^2} = \frac{1}{3} + (\frac{R}{2H})^2 - 2(\frac{R}{H})^3\sum_{s=1}^{\infty}\left[\frac{4\mu_s+(\mu_s^2-4)\sinh(\mu_s)}{k_s^3\,(k_s^2-1)\cosh(\mu_s)}\right] \tag{2.30}$$

An immediate obvious consequence is that

$$m_l = m_o + \sum_{s=1}^{\infty} m_s \quad .$$

2.6.2. *Mechanical Model for a Rigid Tank.* Consider now the mechanical system shown in Figure 2.7. It consists of a rigid body, having mass m_o and moment of inertia I_o with respect to point 0, together with an infinite number of oscillators with masses m_s (s= 1, 2, ...). The rigid body is attached rigidly to the tank wall at a distance h_o from the base, while each mass m_s is attached at a height h_s from the base through a spring of stiffness K_s, where

$$K_s = m_s\omega_s^2 = m_s g\,\frac{k_s}{R}\tanh(\mu_s) \tag{2.31}$$

Then, if $y_s(t)$ is the displacement of the s^{th} oscillator relative to the tank wall, its equation of motion is

$$m_s\,(\ddot{x}_s + \ddot{y}_s) + K_s\,y_s = 0 \tag{2.32}$$

where

$$x_s(t) = x_g(t) + h_s\,\phi(t) \quad .$$

For zero initial conditions, the solution of (2.32) is given by:

$$y_s(t) = -\frac{1}{\omega_s^2}\,\bar{A}_{rs}(t) \quad ,$$

with

$$\bar{A}_{rs}(t) \equiv \int_o^t \ddot{x}_s(\tau)\,\omega_s \sin\omega_s(t-\tau)\,d\tau = \bar{A}_{xs}(t) + h_s\,\bar{A}_{\phi s}(t) \quad .$$

Then, the base shear developed due to this oscillator is equal to

$$K_s\,y_s = -\,m_s\,\bar{A}_{rs}(t) \quad ,$$

while the corresponding base moment is equal to

$$(K_s\,y_s)\,h_s = -\,m_s\,h_s\,\bar{A}_{rs}(t) \quad .$$

Now, choose the parameters (masses, moment of inertia, heights, springs) of the considered mechanical system from equations (2.26-2.30). Then, it is clear that this mechanical system is equivalent to the initial rigid tank/liquid system, in the sense that it reproduces the same base loads, when subjected to the same $x_g(t)$ and $\phi(t)$ motions. From the above derivation it is obvious that the rigid body (m_o, I_o) in the model represents the impulsive part of the base loads, while each oscillator represents that part of the base loads, which is associated with a corresponding sloshing mode.

In order to get an idea of how the various elements of the derived mechanical model depend on the parameter H/R, Figure 2.8 presents graphically what is contained in equations (2.26-2.31), for a practical range of values of H/R. Obviously, these elements depend only on H/R and not on the motion of the system.

Clearly, the sloshing effects can be important for small values of H/R, while the impulsive effects dominate for large H/R, as expected. Also, for all practical purposes, only the first sloshing mode seems to be important. The higher sloshing modes may be important only through resonance, which does not seem to be of severe nature in real systems [57]. The results on Figures 2.8.a and 2.8.c are identical to similar ones obtained in reference [20], even though the corresponding equations appeared in different forms.

Finally, it is noted that the symbol I_c, in Figure 2.8.b, represents the centroidal moment of inertia of the rigid mass, i.e.,

$$I_c = I_o - m_o h_o^2$$

and that there is no centroidal moment of inertia associated with the sloshing masses.

2.6.3. *Equilibrium Equations for the Rigid Mechanical System.* In the previous section it was shown that the liquid contained in a rigid cylindrical tank can be substituted by a simple mechanical model. This model can be further simplified by ignoring the contribution of all the sloshing modes but the first one.

Ground flexibility and base uplift phenomena are two practical reasons for a tank to rotate on its base when subjected to a horizontal excitation. In such a case and when the flexibility effects of the cylindrical part of the tank can be neglected, the real system may be approximately represented by the simplified model shown in Figure 2.9.

In that system, the elements m_o, I_o, m_1 and K_1 represent the liquid impulsive and first sloshing mode, while m_r, m_s, m_f and I_r, I_s, I_f are the mass and the centroidal moments of inertia of the roof, the shell and the foundation respectively. Symbols h_r, h_s represent the roof and shell center of mass distances from the tank base, respectively.

The equations of motion for the simplified discrete model can be derived by employing Lagrance's equations:

$$\frac{d}{dt}\left(\frac{\partial T}{\partial \dot{q}_i}\right) + \frac{\partial V}{\partial q_i} = F_i \ ,$$

where T is the kinetic and V the potential energy of the system, q_i are the generalized coordinates and F_i the corresponding generalized forces. In the considered case

$$q_1 = y_1 \ , \quad q_2 = \phi \ , \quad \textit{while} \quad F_1 = 0 \quad \text{and} \quad F_2 = M_g \ ,$$

where y_1 is the displacement of the oscillating mass m_1 relative to the tank wall and M_g is the moment exerted by the ground on the bottom of the tank. If the following notation is used

$$\bar{h} = h + h_g \ ,$$

where h_g is the vertical distance between the bottom of the tank and the ground point G, which purely translates by x_g, then, by assuming small ϕ, the kinetic energy of the considered system is given by:

$$T(t) = \frac{1}{2} m_1(\dot{x}_g + \bar{h}_1\dot{\phi} + \dot{y}_1)^2 + \frac{1}{2} m_o(\dot{x}_g + \bar{h}_o\dot{\phi})^2 + \frac{1}{2} I_c\dot{\phi}^2 + \frac{1}{2} m_f(\dot{x}_g + h_f\dot{\phi})^2 +$$

$$+ \frac{1}{2} I_f\dot{\phi}^2 + \frac{1}{2} m_r(\dot{x}_g + \bar{h}_r\dot{\phi})^2 + \frac{1}{2} I_r\dot{\phi}^2 + \frac{1}{2} m_s(\dot{x}_g + \bar{h}_s\dot{\phi})^2 + \frac{1}{2} I_s\dot{\phi}^2 \ ,$$

while the potential energy can be expressed as

$$V(t) = \frac{1}{2} K_1 y_1^2 - m_1 g y_1\phi - g(m_o\bar{h}_o + m_1\bar{h}_1 + m_r\bar{h}_r + m_s\bar{h}_s + m_f h_f)\frac{1}{2}\phi^2 \ ,$$

where h_f represents the distance of the foundation mass center from the point G. Therefore, the equations of motion of the system are:

$$m_1\ddot{y}_1 + m_1 h_1\ddot{\phi} + K_1 y_1 - m_1 g\,\phi = - m_1\ddot{x}_g \tag{2.33}$$

$$I_\phi\ddot{\phi} + m_1 h_1\ddot{y} - m_1 g\, y_1 - g m_\phi\,\phi - M_g = - m_\phi\ddot{x}_g \tag{2.34}$$

where

$$I_\phi = (m_o\bar{h}_o^2 + I_c) + m_1\bar{h}_1^2 + (m_r\bar{h}_r^2 + I_r) + (m_s\bar{h}_s^2 + I_s) + (m_f h_f^2 + I_f)$$

$$m_\phi = m_o\bar{h}_o + m_1\bar{h}_1 + m_r\bar{h}_r + m_s\bar{h}_s + m_f h_f \ .$$

In many cases the ground/structure interaction is modeled by placing a rotational spring of stiffness k_f at the bottom of the tank, so that

$$M_g = - k_f\,\phi \ .$$

Then, the equations (2.33, 2.34) can be written in the following form:

$$M \ddot{\underset{\sim}{x}} + K \underset{\sim}{x} = -\ddot{x}_g(t) \ \underset{\sim}{f} \tag{2.35}$$

with

$$M = \begin{bmatrix} m_1 & m_1 h_1 \\ m_1 h_1 & I_\phi \end{bmatrix}, \qquad K = \begin{bmatrix} K_1 & -m_1 g \\ -m_1 g & k_f - g m_\phi \end{bmatrix}$$

$$\underset{\sim}{x} = \begin{bmatrix} y_1(t) \\ \phi(t) \end{bmatrix}, \qquad \underset{\sim}{f} = \begin{bmatrix} m_1 \\ m_\phi \end{bmatrix}.$$

Chapter 3

RESPONSE OF CYLINDRICAL LIQUID STORAGE TANKS UNDER BASE EXCITATION

3.1. Introduction.

A set of equations is derived here, which describes the dynamic behavior of cylindrical liquid storage tanks under horizontal ground excitation. In the present work, the structure consists of a flexible cylindrical tank with a roof and a bottom plate, resting on a flexible ground through a rigid foundation. Portion of the bottom of the tank may separate and lift off the foundation during ground motion.

In the next section the variables and parameters associated with the system response are defined. The third section is devoted to the introduction of the mathematical problem which describes the behavior of the real system. Then, in the fourth section, the method of approach is chosen and an outline of the procedure for the derivation of the equations for the coupled system is presented. In the fifth section, the various assumptions in modeling the behavior of each structural component are clearly stated. In the sixth section, Hamilton's Principle is employed and the formulation of the base uplift is completed. In the final three sections, the formulation of the liquid sloshing effects is performed and the equations of motion are explicitly derived and set in matrix form. A damping matrix is also appropriately chosen for the system.

3.2. Definition of System Parameters.

The system under consideration is shown in Figure 2.1. The tank has radius R, length L, thickness t_s and is partly filled with a liquid of density ρ_l, up to a level H. It is covered above by a rigid roof of mass m_r, centroidal moment of inertia I_r and centroid located at a height H_r from the horizontal plane z=0, and supported below by a thin flexible plate.

Ground motion is assumed to be aligned with the horizontal x-axis and to have a known displacement history $x_g(t)$. This motion is transferred to the tank through its foundation, which is assumed to be rigid but to rest on flexible ground. Apart from the point G, which is located along the vertical z-axis and purely translates by $x_g(t)$ with the ground, all the other points in the foundation rotate about G through the angle $\phi_f(t)$, in addition to the $x_g(t)$ translation. The foundation has mass m_f, centroidal moment of inertia I_f and its centroid is a vertical distance h_f above point G. Finally, h_g and h_b are the vertical distances of the plane z=0 and the bottom plate centroid above point G, while m_b and I_b represent the mass and the centroidal moment of inertia of the bottom plate, respectively.

Figure 3.1 illustrates the definition of the foundation rotation and the uplifting angles. Under dynamic excitation the foundation rotates through the angle $\phi_f(t)$ about the y-axis, in addition to the $x_g(t)$ translation. Also, part of the bottom plate may lift off and lose contact with the foundation. This is assumed to happen in such a way that the bottom periphery of the cylindrical part rotates an additional small angle $\phi_u(t)$ about the y-axis and simultaneously translates by $R\phi_u(t)$ along the z-axis. Therefore, the bottom section of the cylindrical part is assumed to rigidly translate by $[x_g(t) + h_g\phi_f(t)]$ along the x-axis and by $R\phi_u(t)$ along the z-axis, while it rotates through a total angle $\phi(t) = \phi_f(t) + \phi_u(t)$, about the y-axis. Finally, polar coordinates r, θ, z and time t are used for the description of the system variables and u_r, u_θ, u_z are the structural displacements in the radial, circumferential and axial direction, respectively.

3.3. Discussion of the Mathematical Formulation of the Coupled System.

For the considered system, the structural behavior drives and affects the liquid response, which in turn affects the structural response by developing and exerting on the structure appropriate hydrodynamic pressures. This coupling between the structural and the fluid response is reflected in the mathematical description of the system.

The equations of motion of the structure can be represented in short and convenient operational form as follows:

$$\underset{\sim}{N}(\underset{\sim}{u}) = \underset{\sim}{f}(\ddot{x}_g, P)$$

where $\underset{\sim}{u}$ is a vector containing the various structural displacements as components and $\underset{\sim}{f}$ is a forcing vector depending on the ground acceleration and the liquid pressure. This pressure P is found from the equations describing the liquid dynamic behavior, as presented in chapter 2. Obviously, this pressure depends on the structural motion, which in turn depends on the liquid pressure, as indicated by the above form of the structural equilibrium equations. To complete the mathematical formulation of the problem the various matching, boundary and initial conditions should also be considered.

Writing the equations of motion for the structure in operational form prevents one from seeing their difficult and non-cooperative nature even for completely linear formulations. What makes the problem really hard, though, is the fact that when the structure is allowed to lift off the foundation, the formulation becomes unavoidably nonlinear (contact problem). In addition, the deformation of the bottom plate during uplift can become so large that linear bending theory is no longer adequate in modeling the behavior of the bottom plate.

According to the above, the behavior of the system, in the general case, is rigorously governed by a nonlinear system of coupled partial differential equations. Then, if a theoretical approach is sought, one must employ approximate methods in developing and solving the governing equations. The choice of an appropriate method is the subject of the next section.

3.4. Choice and Outline of Method of Approach.

The most popular approximate techniques used for obtaining finite-dimensional field equations for the considered system are those employing finite element or other energy type methods. These methods take care of the difficulties associated with the geometry of the problem by appropriate spatial discretization. Then, the

only remaining independent variable - for the dynamic problem - is the time variable and consequently the initial system of partial differential equations is reduced to a more manageable system of a finite number of ordinary differential equations.

The basic difference between the finite element and the other commonly used energy methods lies in the form and use of the functions for the geometric discretization. In the finite element method these (trial) functions are confined into small portions of the domain while in the other energy methods they cover the whole domain. This implies that the finite element approach may generally result in larger and therefore more time consuming and expensive numerical systems. On the other hand, the other energy methods are more risky since the accuracy of their results depends more directly on how close the assumed displacements are to the real geometrical pattern. However, for the problem at hand, previous analytical and experimental investigations [20,26,29,37] have given fairly good ideas for the expected modes. Finally, the energy methods provide a better insight into the coupling of the various modes through the procedure of developing and solving the equations of the system.

In the present work, considering the above and also some important numerical difficulties (extra degrees-of-freedom, ill-conditioning of stiffness matrix and slow convergence) encountered in the solution of contact problems using current finite element formulations, an energy type method was chosen as most appropriate for the spatial discretization of the structural domain, while the equations in the fluid domain are solved analytically. This approach results in a compact system of equations, since the fluid degrees-of-freedom are thus eliminated from the formulation. The general solution procedure follows the next three steps:

a. First, the form of the structural displacements is assumed. These displacements contain the proper rigid body terms, as well as terms accounting for the shell flexibility and the uplifting motion of the tank. The flexible parts of these displacements are expanded in series forms as explained in the next section. Each

term of these series is a product of a term with assumed spatial dependence multiplied by a term of unknown time dependence. These time dependent functions then, together with the foundation rotation $\phi_f(t)$ and the uplifting rotation $\phi_u(t)$, when they are included, comprise the set of unknowns of the problem.

b. Using the assumed displacements as boundary conditions, the equations describing the fluid behavior are solved exactly and the corresponding hydrodynamic pressure is obtained in closed form by the methods of the previous chapter. This pressure is expressed in terms of the time dependent functions of the structural displacements. Then, the pressure on the wetted surface is treated as an external load to the structure, representing the liquid's action on the structure.

c. In the final step, Hamilton's Principle is applied in the structural domain and the system equations are generated in the classical matrix form. Solution of these equations results in the determination of the time dependent functions of the system, which then completes the solution for the coupled response problem, since the spatial dependence for both the structural and fluid variables is already known.

Having found the pressure distribution for a given base excitation history, one can directly predict possible buckling failure at the top of the tank, near the liquid free surface. Also, one can calculate the corresponding resultant loads at the base of the tank. However, prediction of failure at the bottom of the tank - which is the most frequently observed damage pattern for the tanks in the field - is still not an easy, straightforward task when uplifting occurs. In such a case, the failure at the tank bottom can only be predicted from a reasonable estimation of the stress distribution corresponding to the calculated base loads and the use of an appropriate failure criterion.

3.5. Behavior of the Structural Components.

Apart from the fundamental assumptions made for the behavior of the system, some additional assumptions are needed here. They are associated with the energy-based nature of the chosen approach and they refer to the form of the structural displacements. These assumptions are given next for each structural component.

3.5.1. *Displacement Form for the Cylindrical Shell.* The cylindrical shell is modeled as a thin shell whose middle surface displacements are of the following form:

$$u_r(\theta,z,t) = [x_g(t) + h_g\phi_f(t) + z\phi(t) + u_r^e(z,t)]\cos\theta \tag{3.1}$$

$$u_\theta(\theta,z,t) = -[x_g(t) + h_g\phi_f(t) + z\phi(t) + u_\theta^e(z,t)]\sin\theta \tag{3.2}$$

$$u_z(\theta,z,t) = R\phi_u(t) + [-R\phi(t) + u_z^e(z,t)]\cos\theta \tag{3.3}$$

The first three terms in u_r, u_θ and the first two terms in u_z represent the rigid body part of these displacements, as explained in section 3.2. The other terms in the above expressions represent the flexible part of the shell displacements.

Generally, the cylindrical shell displacements can be decomposed into appropriate modes in the circumferential and axial direction. Each of these geometrical patterns is characterized by two numbers (n,m), which represent the number of the full circumferential and half axial waves of the mode (Figure 3.2). Obviously, the axisymmetric n=0 shell modes - except for the rigid body translation $R\phi_u$ term in u_z - are not included in this formulation. These modes are primarily excited during vertical ground motion, which is not considered in this analysis. The effects of the $n>1$ modes are also neglected here, for the following reasons. First, using linear analysis for a perfect tank anchored on a rigid foundation it can easily be shown that these modes are not excited under horizontal base excitation. For unanchored and/or imperfect tanks, some of the $n>1$ modes may be excited but they produce no resultant base moment and shear. Thus, since the ultimate objective of this work is prediction of tank failure, which appears to be caused by loads which

mostly result from the n=1 modes [28,29], it is thought that the effect of the $n>1$ modes can be neglected.

As far as the flexible parts of the displacements are concerned, they are expanded in the following forms:

$$u_r^e(z,t) = \sum_{m=1}^{N1} [w_m(z)\, \psi_m(t)],\quad u_\theta^e(z,t) = \sum_{m=1}^{N2} [v_m(z)\, \xi_m(t)],\quad u_z^e(z,t) = \sum_{m=1}^{N3} [u_m(z)\, \varsigma_m(t)] \quad (3.4\text{-}6)$$

where N1, N2 and N3 are appropriately chosen integers, depending on the accuracy needed for each case. In the present work, the functions w_m, v_m and u_m are chosen based upon both experimental and theoretical observations and results provided by previous investigations on the subject [20,26,29,37]. What remains to be determined is the corresponding time functions ψ_m, ξ_m and ς_m.

Summarizing, the displacements of the cylindrical shell are chosen so that the initial continuous system is represented by an appropriate finite (N1+N2+N3) degree-of-freedom system. When $w_m\, \psi_m \neq v_m\, \xi_m$, the corresponding mode contains circumferential straining.

3.5.2. *Displacement Form for the Roof.* For the purposes of this investigation it is easy to include into the formulation the effects of a rigid roof. Based upon the displacements of the cylindrical shell, the corresponding displacements for the roof are immediately obtained:

$$\bar{u}_r(r,\theta,z,t) = [x_g(t) + h_g \phi_f(t) + z\phi(t) + u_r^e(L,t)] \cos\theta$$

$$\bar{u}_\theta(r,\theta,z,t) = -[x_g(t) + h_g \phi_f(t) + z\phi(t) + u_r^e(L,t)] \sin\theta$$

$$\bar{u}_z(r,\theta,t) = R\phi_u(t) + \frac{r}{R} [-R\phi(t) + u_z^e(L,t)] \cos\theta\ .$$

When the assumption of rigidity of the roof is not sufficiently accurate, the roof must also be modeled as a flexible component.

3.5.3. *Displacement Form for the Bottom Plate.* When the tank is not allowed to lift off its foundation the formulation of the bottom plate behavior is trivial. But, if uplifting effects are of concern, the formulation becomes much harder. This is so because of two fundamental reasons.

First, even for small amounts of uplift, one has to deal with a contact problem. To apply the correct boundary conditions one must first determine the amount of uplift, which changes in a nonlinear fashion with the applied loads. On the other hand, for relatively large amounts of uplift the deformations of the bottom plate become so large that its behavior cannot be adequately modeled by linear bending theory. The plate carries the external transverse loading partly by bending but mostly by in-plane membrane stresses [31]. This behavior is then analytically described by a coupled system of nonlinear partial differential equations.

To avoid the difficulties associated with the exact formulation of such a complex behavior, an approximate approach will be followed. According to this approach, the effects of the part of the bottom plate displacements which is due to uplift are modeled by placing a nonlinear rotational spring between the cylindrical shell and the foundation. Details on how this spring is chosen and how it fits within the formulation are given in subsection 3.6.4. Then, if the trial functions for the cylindrical shell are chosen so that:

$$w_m(0) = v_m(0) = u_m(0) = 0 \quad , \qquad m = 1, 2, \cdots$$

and the extra subscript u denotes the part of the displacements due to uplift, the total bottom plate displacements are given by:

$$\hat{u}_r(r,\theta,t) = [x_g(t) + h_b \phi_f(t)] \cos\theta + u_{ru}(r,\theta,t) \tag{3.7}$$

$$\hat{u}_\theta(r,\theta,t) = -[x_g(t) + h_b \phi_f(t)] \sin\theta + u_{\theta u}(r,\theta,t) \tag{3.8}$$

$$\hat{u}_z(r,\theta,t) = -r \phi_f(t) \cos\theta + u_{zu}(r,\theta,t) \tag{3.9}$$

3.5.4. *Ground/Structure Interaction.* It is well-known that the dynamic response of a structure supported on flexible ground can be significantly different from the response of the same structure supported on a rigid ground. However, the formulation of the general ground/structure interaction problem is still associated with considerable difficulties and uncertainties. Analytical solutions are available for some simple cases, in most of which a rigid circular or rectangular footing is considered to rest on a homogeneous, isotropic, linearly elastic, semi-infinite body which undergoes small strains [61-63]. Based on results of such solutions, the ground/structure interaction modes can be represented by discrete systems whose parameters, relating corresponding generalized forces and displacements, are functions of the frequency of excitation. Since this frequency dependence complicates the analysis, some studies examined the possibilities of approximating these functions by constant values within the frequency range of interest [e.g., 64]. This further approximation often may be justified since in real situations the shape of the foundation, the depth and conditions of embedment, the variations of the ground properties, the large strain ground behavior under strong earthquakes and other important parameters may depart significantly from the theoretical assumptions.

In the present study, the ground/structure interaction is modeled by placing two springs at the point G of the foundation. One of them is infinitely rigid and avoids any sliding of the foundation with respect to the ground along the x-axis. The other one is a rotational spring, allowing for rocking of the foundation and the whole structure by an angle $\phi_f(t)$ about the y-axis. It is believed that in this way, the important aspects of the ground/structure interaction are clearly modeled within the framework of this approach.

3.6. Equations of Motion for an Unanchored Fluid-Filled Tank.

After modeling the behavior of each component, the equations describing the dynamic behavior of the overall system can be derived by using Hamilton's Principle in the following form:

$$\delta T + \delta W = \delta U \tag{3.10}$$

where T is the kinetic energy, W is the work done by the "external" forces, and U is the strain energy of the system. Introducing displacements in the above, one can write:

$$\delta T = -\int_V \rho \ddot{\underline{u}} \cdot \delta \underline{u}\, dV \ , \quad \delta W = \delta W_v + \delta W_s \ , \quad \delta W_v = \int_V \underline{b} \cdot \delta \underline{u}\, dV \ , \quad \delta W_s = \int_S \underline{t} \cdot \delta \underline{u}\, dS \ .$$

Here, S represents the surface of the structure and V the corresponding enclosed volume. The δW_v term represents the virtual work due to the body forces, $\underline{b}$. This term is left out of the formulation since its contribution is usually negligible compared to that of the δW_s term, which represents the virtual work done by the external surface tractions $\underline{t}$ on the surface S. In the present case, these tractions result from the pressure exerted on the wetted surface of the structure by the contained liquid. Here, the radial displacement of the cylinder is of the form given by equation (3.1) while the vertical displacement of the bottom plate is expressed by equation (3.9). Therefore, the associated hydrodynamic pressure can be written as

$$P_d = P_x + P_f + P_u + \sum_{m=1}^{N1} P_m \ .$$

The component P_x is given by equation (2.17) - but with a time function $[x_g(t)+h_g\phi_f(t)]$ instead of simply $x_g(t)$ - and represents the hydrodynamic pressure due to rigid body translation of the tank along the x-axis. P_f is the pressure resulting from the rigid body rotation $\phi_f(t)$ about the y-axis, due to the ground flexibility. It is given by (2.19) but with $\phi_f(t)$ instead of $\phi(t)$ and with f_ϕ , $f_{\phi s}$ replaced by f_f and f_{fs}. The latter functions are obtained by setting $c=1$ in the expressions for f_ϕ and $f_{\phi s}$, respectively. The term P_u results from the uplifting motion of the structure and is determined as explained in the next subsection, while the last term represents the pressure due to the tank flexibility. The components P_m of the sum

are found from equation (2.14) for each flexible radial mode of the shell.

Next, due to the length of the resulting expressions, each term of (3.10) is examined and developed separately.

3.6.1. *Virtual Work.* Here, the virtual work done on the surface of the structure is

$$\delta W_s = \delta W_c + \delta W_b \ ,$$

where

$$\delta W_c = \int_o^H \int_o^{2\pi} P(R,\theta,z,t)\ \delta u_r(\theta,z,t)\ R d\theta\ dz$$

is the virtual work done on the wetted cylindrical part of the tank and

$$\delta W_b = -\int_o^R \int_o^{2\pi} P(r,\theta,0,t)\ \delta u_z(r,\theta,t)\ r d\theta\ dr$$

is the virtual work done on the wetted surface of the bottom plate.

At this point some difficulties arise, since the uplifting part u_{zu} of the bottom plate's vertical displacement is unknown. This has two important consequences. First, the virtual displacement δu_{zu} - which is part of the virtual displacement resulting in δW_b - is undetermined. Also, the pressure component P_u associated with the uplifting motion of the tank is unknown. In order to overcome these difficulties, it is first observed that in the above calculation for δW_c, only the $\cos\theta$ component of the total pressure P will survive the required θ-integration and will eventually contribute to δW_c, since the virtual displacement appearing in the corresponding integrand is proportional to $\cos\theta$. This implies that only the $\cos\theta$ component of P_u and therefore of u_{zu} is of importance in determining δW_c. A reasonable and convenient choice for this component of u_{zu} is

$$u_1(r,\theta,t) = -\ c\ r\phi_u(t)\ \cos\theta$$

where c is a constant. Clearly, c=1 means that the bottom plate participates completely in the rocking motion of the structure due to uplift, while c=0 means that

the bottom plate remains flat and only the shell undergoes the rocking motion due to uplift. What happens in reality is something in between these two extreme cases. Using the above assumption for the displacement u_{zu}, the hydrodynamic pressure due to uplift can be decomposed as

$$P_u = \bar{P}_u + \Delta P_u \quad ,$$

where $\bar{P}_u$ represents the $\cos\theta$ component and ΔP_u contains the rest of P_u. The $\bar{P}_u$ component is found from (2.19) but changing the notation from $\phi(t)$, $f_\phi(r,z)$, $f_{\phi s}(r,z)$ to $\phi_u(t)$, $f_u(r,z)$ and $f_{us}(r,z)$, respectively. These then allow the computation of δW_c, as follows:

$$\delta W_c = -\pi\rho_l R^2 \int_o^H \{ f_x(R,z)\,[\ddot{x}_g(t) + h_g\ddot{\phi}_f(t)] + f_f(R,z)\,R\ddot{\phi}_f(t) + f_u(R,z)\,R\ddot{\phi}_u(t) +$$

$$+ \sum_{m=1}^{N1}[\,f_m(R,z)\,\ddot{\psi}_m(t)] + \sum_{s=1}^{\infty}[\,\bar{f}_s(R,z)\,\bar{A}_s(t)]\}[(z+h_g)\delta\phi_f(t) + z\delta\phi_u(t) + \delta u_r^e(z,t)]\,dz \quad .$$

Next, using (3.9), the virtual work δW_b done at the bottom plate area S_b is further decomposed in two parts, as

$$\delta W_b = \delta W_f + \delta W_u$$

with

$$\delta W_f = \int_{S_b} P(r,\theta,0,t)\,[-r\delta\phi_f(t)\cos\theta]\,dS \qquad \text{and} \qquad \delta W_u = \int_{S_u} P(r,\theta,0,t)\,\delta u_{zu}(r,\theta,t)\,dS \quad ,$$

where S_u is the uplifted area of the bottom plate. For the calculation of the virtual work δW_f due to the rocking of the bottom by $\phi_f(t)$, only the $\cos\theta$ component of P - and therefore of P_u - is needed again. Using the previously assumed form for the $\cos\theta$ component of u_{zu}, it is then found that:

$$\delta W_f = -\pi\rho_l \int_o^R \{ f_x(r,0)\,[\ddot{x}_g(t) + h_g\ddot{\phi}_f(t)] + f_f(r,0)\,R\ddot{\phi}_f(t) + f_u(r,0)\,R\ddot{\phi}_u(t) +$$

$$+ \sum_{m=1}^{N1}[\,f_m(r,0)\,\ddot{\psi}_m(t)] + \sum_{s=1}^{\infty}[\,\bar{f}_s(r,0)\,\bar{A}_s(t)]\}\,r^2\,dr\,(R\delta\phi_f) \quad .$$

In the above expressions, the sloshing components of all the structural modes have been combined together in the form

$$P_{sl}(r,\theta,z,t) = -\rho_l R\cos\theta \sum_{s=1}^{\infty}[\bar{f}_s(r,z)\ \bar{A}_s(t)] \ ,$$

with

$$\bar{A}_s(t) = \omega_s \int_o^t \ddot{\eta}_s(\tau)\ \sin\omega_s(t-\tau)\ d\tau$$

$$\eta_s(t) \equiv x_g(t) + (h_g/R+c_{fs})R\phi_f(t) + c_{us}R\phi_u(t) + \sum_{m=1}^{N1}[c_{ms}\psi_m(t)] \ ,$$

where $c_{us} = c_{\phi s}$ and c_{fs} is obtained by setting c = 1 in the expression for $c_{\phi s}$. Also, from equation (3.4) it easily follows that:

$$\delta u_r^e(z,t) = \sum_{m=1}^{N1}[w_m(z)\ \delta\psi_m(t)] \ .$$

The virtual work δW_u done on the bottom plate due to uplift, can not be determined directly here, since the displacement u_{uz} which is required for this calculation, is unknown. This part of the virtual work is treated approximately as explained in section 3.6.4. Combining the components of the virtual work

$$\delta W_s = \delta W_c + \delta W_f + \delta W_u \tag{3.11}$$

3.6.2. *Kinetic Energy of the System.* Substituting the displacements of the cylindrical shell from equations (3.1-3.3), the virtual kinetic energy of the shell is found to be:

$$\delta T_c = -\pi R \int_o^L \rho_s t_s\ [(\ddot{x}_g + h_g\ddot{\phi}_f + z\ddot{\phi} + \ddot{u}_r^e)(h_g\delta\phi_f + z\delta\phi + \delta u_r^e) +$$

$$+ (\ddot{x}_g + h_g\ddot{\phi}_f + z\ddot{\phi} + \ddot{u}_\theta^e)(h_g\delta\phi_f + z\delta\phi + \delta u_\theta^e) +$$

$$+ (-R\ddot{\phi} + \ddot{u}_z^e)(-R\delta\phi + \delta u_z^e)]\ dz - m_s(R\ddot{\phi}_u)(R\delta\phi_u) \ .$$

The kinetic energy of the foundation is expressed by:

$$T_f = \frac{1}{2}\, m_f(\dot{x}_g + h_f\dot{\phi}_f)^2 + \frac{1}{2}\, I_f\dot{\phi}_f^2 \ .$$

Therefore,

$$\delta T_f = - m_f(\ddot{x}_g + h_f\ddot{\phi}_f)\frac{h_f}{R}(R\delta\phi_f) - \frac{I_f}{R^2}(R\ddot{\phi}_f)(R\delta\phi_f) \ .$$

Similarly, for the kinetic energy of the bottom plate, ignoring that of the uplifted part, it is found that:

$$\delta T_b = - m_b(\ddot{x}_g + h_b\ddot{\phi}_f)\frac{h_b}{R}(R\delta\phi_f) - \frac{I_b}{R^2}(R\ddot{\phi}_f)(R\delta\phi_f) \ .$$

Finally, the kinetic energy of the roof is represented by:

$$T_r = \frac{1}{2} m_r\{[\dot{x}_g + h_g\dot{\phi}_f + H_r\dot{\phi} + \dot{u}_r^e(L,t)]^2 + (R\dot{\phi}_u)^2\} + \frac{1}{2} I_r\dot{\phi}_r^2 \ ,$$

where

$$\phi_r = \frac{u_z(0,L,t) - u_z(\pi,L,t)}{2R} = \frac{1}{R}[-R\phi + u_z^e(L,t)] \ .$$

Therefore,

$$\delta T_r = - m_r[\ddot{x}_g + h_g\ddot{\phi}_f + H_r\ddot{\phi} + \ddot{u}_r^e(L,t)][h_g\delta\phi_f + H_r\delta\phi + \delta u_r^e(L,t] +$$

$$- m_r(R\ddot{\phi}_u)(R\delta\phi_u) - \frac{I_r}{R^2}[-R\ddot{\phi} + \ddot{u}_z^e(L,t)][-R\delta\phi + \delta u_z^e(L,t)] \ .$$

Since the kinetic energy of the system equals to the sum of the kinetic energy of its components:

$$\delta T = \delta T_c + \delta T_f + \delta T_b + \delta T_r \tag{3.12}$$

3.6.3. *Strain Energy of the System.* In this case, the total strain energy U of the system consists of three parts: the strain energy U_c of the shell, the strain energy U_u of the bottom plate due to uplift, and the energy U_f developed from the interaction between the foundation and the ground.

The strain energy for the cylindrical shell is obtained in Appendix C. Employing equations (3.1-3.3), it is then found that:

$$\delta U_c = \frac{\pi REt_s}{2(1-\nu^2)}\int_0^L [\frac{2}{R^2}(u_r^e - u_\theta^e)\delta(u_r^e - u_\theta^e) + 2\frac{\partial u_z^e}{\partial z}\delta(\frac{\partial u_z^e}{\partial z}) +$$

$$+ \frac{2\nu}{R}(u_r^e - u_n^e)\,\delta\left(\frac{\partial u_z^e}{\partial z}\right) + \frac{2\nu}{R}\,\frac{\partial u_z^e}{\partial z}\,\delta(u_r^e - u_\theta^e) +$$

$$+ (1-\nu)\left(\frac{u_z^e}{R} + \frac{\partial u_\theta^e}{\partial z}\right)\delta\left(\frac{u_z^e}{R} + \frac{\partial u_\theta^e}{\partial z}\right)\Big]\,dz +$$

$$+ \frac{\pi R E t_s^3}{12(1-\nu^2)} \int_0^L \left[\frac{\partial^2 u_r^e}{\partial z^2}\,\delta\left(\frac{\partial^2 u_r^e}{\partial z^2}\right) + \frac{1}{R^4}(u_r^e - u_\theta^e)\,\delta(u_r^e - u_\theta^e) +\right.$$

$$+ \frac{\nu}{R^2}(u_\theta^e - u_r^e)\,\delta\left(\frac{\partial^2 u_r^e}{\partial z^2}\right) + \frac{\nu}{R^2}\,\frac{\partial^2 u_r^e}{\partial z^2}\,\delta(u_\theta^e - u_r^e) +$$

$$\left. + \frac{2(1-\nu)}{R^2}\left(\frac{\partial u_r^e}{\partial z} - \frac{\partial u_\theta^e}{\partial z}\right)\delta\left(\frac{\partial u_r^e}{\partial z} - \frac{\partial u_\theta^e}{\partial z}\right)\right] dz \quad .$$

As expected, the rigid body terms have completely disappeared from the strain energy of the shell. According to the way the ground/structure interaction formulation was modeled in section 3.5.4, if M_f is the moment exerted between the foundation and the ground, then

$$\delta U_f = M_f\,\delta\phi_f \quad .$$

Lack of knowledge of the total displacements prevents the explicit calculation of the virtual strain energy of the bottom plate. This energy is approximately formulated and included in the following subsection. Obviously,

$$\delta U = \delta U_c + \delta U_f + \delta U_u \tag{3.13}$$

3.6.4. *Uplift Formulation and Static Tilt Tests.* As becomes clear through the procedure of applying Hamilton's Principle, some terms in the energy expressions can not be formulated directly. This is a consequence of the fact that the uplifting part of the displacements of the bottom plate is unknown. Those energy terms which have not been formulated yet include the virtual work δW_u done on the bottom plate area due to the uplifting motion, the virtual kinetic energy of the uplifted bottom plate and the virtual strain energy δU_u of the bottom plate. Although the kinetic energy of the uplifted part of the bottom plate seems to be negligible and can be ignored for the present case, the other two terms are thought to be important and are modeled approximately as explained below.

Using relations (3.10)-(3.13) and dropping the δW_v term, Hamilton's Principle can be expressed for the general dynamic case in the following form

$$\delta T + (\delta W_c + \delta W_f + \delta W_u) = (\delta U_c + \delta U_f + \delta U_u) \ .$$

However, this expression cannot generate the system equations yet, since the terms δW_u and δU_u are unknown. Collecting these two terms together and defining the virtual quantity δV_u by

$$\delta V_u \equiv \delta U_u - \delta W_u \tag{3.14}$$

the extended form of Hamilton's Principle can be rewritten as

$$\delta V_u = \delta T + (\delta W_c - \delta U_c) + (\delta W_f - \delta U_f) \tag{3.15}$$

Direct analytical calculation for the δV_u term in the above equation requires the solution of the contact problem at the base of the tank for any time instance. In that calculation, nonlinear strain-displacement relations should be used for the behavior of the bottom plate. These difficulties can be overcome here following approximate approaches. Namely, critical examination of experimental results [29,35,37] suggests that the uplifting behavior at the base of the tank may be described by placing an appropriate rotational spring between the bottom plate and the foundation. The characteristics of that nonlinear spring can actually be derived once and for all from static considerations, for example from static tilt tests, as explained below.

Since these tests are static, δT is absent for the case of the tilt tests. By assuming a rigid foundation, the δW_f and δU_f terms also disappear. Then, carrying the bar symbol as a distinction between the quantities corresponding to the static tilt tests and similar quantities for the dynamic case, equation (3.15) takes the form:

$$\delta \bar{V}_u = \delta \bar{W}_c - \delta \bar{U}_c \ .$$

From previously performed static tilt tests [35], it is found that the flexible components of the shell displacements are negligible compared to the corresponding rocking component due to uplift. If this is the case, then

$$\delta \bar{W}_c = \int_{S_c} \bar{P}_{st}(R,\theta,z)\ (z\delta\phi_u \cos\theta)\ dS$$

where $\bar{P}_{st}$ is the hydrostatic pressure exerted on the wetted cylindrical part, of surface S_c, of the tilted tank. If one defines the overturning moment with respect to the center of the bottom plate by

$$\bar{M}_c \equiv \int_{S_c} \bar{P}_{st}(R,\theta,z)\ z \cos\theta\ dS$$

and if $\delta \bar{U}_c$ is left out, then it follows that

$$\delta \bar{V}_u = \bar{M}_c\ \delta\phi_u \tag{3.16}$$

Finally, by assuming that

$$\delta V_u = \delta \bar{V}_u \tag{3.17}$$

and using (3.16), the equation (3.15) can be rewritten as

$$\bar{M}_c\ \delta\phi_u = \delta T + (\delta W_c - \delta U_c) + (\delta W_f - \delta U_f) \tag{3.18}$$

The equations (3.16) and (3.17) require that for the static tilt tests the shell flexibility effects should be negligible and that the pressure distribution and the deformation at the bottom plate should be close to those developed during the dynamic base excitation. The available information suggests that these assumptions are sufficiently accurate at least for tall tanks but there are no experimental results to support the above assumptions for broad tanks. Therefore, the validity of these assumptions should also be checked for the case of broad tanks and proper modifications must be imposed, if needed.

Knowledge of the relation between the moment $\bar{M}_c$ and the system parameters - especially the angle ϕ_u - allows one to proceed from (3.18) to generate the equations of motion of the system in matrix form. The required relation between the moment $\bar{M}_c$ and the uplifting angle ϕ_u can be obtained from static tilt tests or estimated analytically [31,32,41].

3.7. Governing Equations for the Coupled System.

Using the expressions developed in section 3.6 for the various terms of (3.10), the equations governing the behavior of the overall system can be set in the form:

$$M \ddot{\lambda} + K \lambda + \underset{\sim}{k}(\lambda) + \underset{\sim}{p}(t) = - \ddot{x}_g(t) \ f \tag{3.19}$$

where the vector λ contains the unknown time functions in the following order:

$$\lambda(t) = [\psi_1(t), \psi_2, \cdots, \psi_{N1}, \xi_1, \cdots, \xi_{N2}, \varsigma_1, \cdots, \varsigma_{N3}, R\phi_f, R\phi_u(t)]^T \ .$$

The above equations are first found in scalar form. The i^{th} scalar equation is obtained by assuming all the components of λ to have zero variation, except for the i^{th} component. Following common nomenclature, M is termed the mass matrix, K is the stiffness matrix and f multiplied by $-\ddot{x}_g(t)$ is the corresponding forcing vector. The vector $\underset{\sim}{k}(\lambda)$ has all of its components zero, except for the last two which depend on the rotational degrees-of-freedom. Finally, the vector $\underset{\sim}{p}(t)$ contains the sloshing terms, which are identified as those terms of the equations involving the spectral accelerations $\bar{A}_s(t)$ for time functions.

Following the classical notation used for the elements of matrices and vectors, the first subscript of each element indicates the row while the second subscript - when present - indicates the column in which the element belongs. The elements of the various matrices and vectors appearing in (3.19) are presented in Appendix D.

3.8. Sloshing Formulation.

As a consequence of the approach used, all the sloshing terms are isolated and included in the vector $\underset{\sim}{p}(t)$, as noted in the previous section. Since these terms contribute only to the hydrodynamic pressures and the variations in Hamilton's Principle apply only to the displacements, the sloshing formulation is not as straightforward as it is for the components of λ. In order to incorporate the sloshing effects, the definition of the spectral acceleration is used. For example, if the s^{th} sloshing mode is to be included in the analysis, an extra degree-of-freedom y_s should be introduced together with the additional equation:

$$\ddot{\eta}_s + \ddot{y}_s + \omega_s^2 y_s = 0 \ ,$$

where the time function $\eta_s(t)$ is defined in section 3.6.1. Then, since for $y_s(0)=0=\dot{y}_s(0)$ the associated spectral acceleration can be expressed by:

$$\bar{A}_s(t) = \ddot{\eta}_s(t) + \ddot{y}_s(t) \ ,$$

the corresponding terms of $p(t)$ are appropriately added into the mass matrix of the system.

3.9. Choice of Damping Matrix.

After modeling the sloshing effects, an appropriate damping matrix D is chosen as explained in Appendix E and the behavior of the system is finally found to be governed by the following matrix equation:

$$M \ddot{\underset{\sim}{x}} + D \dot{\underset{\sim}{x}} + K \underset{\sim}{x} + \underset{\sim}{k}(\underset{\sim}{x}) = -\ddot{x}_g(t) \ \underset{\sim}{f} \qquad (3.20)$$

where

$$\underset{\sim}{x} = [\Delta \ , \ \underset{\sim}{x}_{sl}]^T$$

and the vector $\underset{\sim}{x}_{sl}$ contains the included sloshing degrees-of-freedom. The matrices M, K and the vectors $\underset{\sim}{k}$ and $\underset{\sim}{f}$ contain the same elements as the corresponding ones in (3.19) plus the added components due to sloshing.

In the case of a nonlinear system, a damping matrix is chosen according to the analysis presented in Appendix E, after appropriate linearization of the vector $\underset{\sim}{k}$ in equation (3.20).

Chapter 4

RESULTS FOR ANCHORED TANKS

4.1. Introduction.

The subject of this chapter is the investigation of the dynamic response and buckling of anchored tanks. Special consideration is given to the ground/structure interaction problem, which has not yet received much attention. For the response problem, the analysis developed in the previous chapter is used; it is only necessary to exclude the uplifting degree-of-freedom ($\phi_u \equiv 0$). In all the cases examined it is assumed that

$$w_m(z) = v_m(z) = u_m(z) = \sin[(2m-1)\frac{\pi z}{2L}] \tag{4.1}$$

which is suggested by previous investigations [20,26].

As a first step, the free vibration analysis is performed for two tanks (one broad and one tall), for which there are results provided by previous studies. Of special interest is the chosen form of the shell displacements, as given by (4.1). Secondly, the sloshing effects are considered and the coupling between the various sloshing modes and the structural modes is examined. Next, the effects of a rigid roof and the ground/structure interaction are studied. More results are presented in the sixth section, where buckling phenomena observed at the top of fluid-filled tanks are explained. This explanation uses analytical results applied to a previously tested model tank. The exact modeling of this specific tank required a nonlinear ground/structure interaction formulation. The nonlinear formulation led to some interesting new results, as far as the long-time response of the system is concerned. These results are presented in the last section of this chapter.

4.2. Free Vibration of Anchored Tanks.

For linear analyses, knowledge of the frequencies and modes of a structure allows the complete determination of its response to any excitation. For this reason, calculation of frequencies represents a reasonable first step in investigating the dynamic characteristics of a structure.

In many cases, a continuous structure is discretized into a finite degree-of-freedom system, for which only the lowest frequencies are predicted correctly. Depending on the frequency content and the spatial distribution of the excitation one then has to choose the required number of modes to be considered for any case of interest. For a liquid storage tank designed to withstand earthquake loads, usually only the first few modes contribute significantly to the overall tank response and therefore the highest modes are not of concern.

In this section, the lowest three frequencies are obtained for two tanks examined previously by other investigators [11,14-16,24]. Both tanks are assumed to be anchored on rigid ground. These tanks are made of steel, with Elasticity modulus $E= 3\times10^7\ lb/in^2$, Poisson ratio $\nu= 0.3$, density $\rho_s= 0.733\times10^3\ lbsec^2/in^4$ and thickness $t_s= 1\ in$. The first one has radius R= 60 ft and length L= 40 ft (broad), while the second one is a tall tank with R= 24 ft and L= 72 ft. In all cases, water is the contained liquid.

First, a check on the accuracy of the assumed spatial form of the shell modes is performed. From computer experiments it is found that the best accuracy for each case is obtained by choosing N1=N2=N3=$\bar{N}$. Results for the dependence of the first three frequencies on $\bar{N}$ are shown in Table 4.1 for the broad tank full of water. It is observed that a good estimate for ω_1 is obtained even for $\bar{N}$=1 and that the convergence of the other two frequencies is rapid as $\bar{N}$ is increased. In the last row of that table, the corresponding results of reference [24] are presented. Those results were obtained using 48 degrees-of-freedom and compare well with the results of the present analysis, using 15 degrees-of-freedom.

Table 4.1 Frequency Convergence for the Full Broad Tank

[Hz]

$\bar{N}$	ω_1	ω_2	ω_3
1	7.40	80.78	114.19
2	6.35	13.43	79.83
3	6.29	11.45	17.39
4	6.20	11.39	15.17
5	6.18	11.22	15.16
Ref.[24]	6.18	11.28	15.10

In Table 4.2, a comparison is made between the results of the present analysis ($\bar{N}$=5) and those of reference [24] again, for different H/L values and for the broad tank. Table 4.3 shows similar results, but for the tall tank. Clearly, good agreement is obtained in all the cases examined. It is noted that favorable comparison between the results of other investigations [11,14-16] is also reported in [24]. All these comparisons verify the validity and effectiveness of the method presented here. In addition, these comparisons indicate that the assumed spatial modes of the shell (modes of a shear beam of same length L, as the tank) are probably very close to the exact ones, at least for the case of anchored tanks. Finally, the data of Tables 4.2 and 4.3 also demonstrate another standard characteristic of anchored fluid-filled tanks. That is, the higher the level of the liquid the lower the system frequencies. This may not be necessarily true for the case of unanchored tanks.

4.3. Sloshing/Structural and Sloshing/Sloshing Coupling.

The sloshing formulation is discussed in section 3.8. The s^{th} sloshing frequency of any single structural mode can be computed from the formula

$$\omega_s^2 = \frac{gk_s}{R} \tanh(k_s \frac{H}{R}) \tag{4.2}$$

which is derived in section 2.3. When more than one tank mode is present some coupling occurs, which changes the sloshing frequencies.

Table 4.2 Frequency Comparison for the Broad Tank

	ω_1 [Hz]		ω_2 [Hz]		ω_3 [Hz]	
H/L	Present Analysis	Refer. [24]	Present Analysis	Refer. [24]	Present Analysis	Refer. [24]
1.0	6.18	6.18	11.22	11.28	15.16	15.10
0.8	7.19	7.24	12.93	12.96	16.93	17.07
0.6	8.74	8.79	15.16	15.37	23.19	20.05

Next, the coupling between the sloshing modes themselves as well as between the sloshing and the structural modes is investigated. Numerical results are presented in Table 4.4 for the case of the tall tank examined in the previous section, but with shell thickness $t_s = 0.43$ *in.* and $H = 72$ *ft* (for sloshing to occur assume here that L>H). Then, comparison with similar results presented in [24] can again be made.

The first four modes, listed in the first column of Table 4.4, represent sloshing modes, while the last two modes correspond to the two lowest structural modes. In the second column the values of the first four sloshing frequencies, obtained from (4.2), are shown. The next two columns contain the two lowest structural frequencies of the system according to results from the present analysis with $\bar{N}=3$ and similar results from reference [24], with 48 degrees-of-freedom. The last two columns present the frequencies of the coupled system as obtained by applying the present analysis and as presented in [24], respectively.

First, comparing the results of the present analysis and those of [24] good agreement is again observed. Also, at least for this case (tall tank, anchored on rigid ground) the coupling between the sloshing and the structural frequencies seems to be negligible. This is expected because of the large difference between the sloshing and structural frequencies and is in support of those analyses which consider separately the structural and sloshing responses in similar cases. Qualitatively similar results are also obtained for the forced vibrations of a tall tank but

Table 4.3 Frequency Comparison for the Tall Tank

	ω_1 [Hz]		ω_2 [Hz]		ω_3 [Hz]	
H/L	Present Analysis	Refer. [24]	Present Analysis	Refer. [24]	Present Analysis	Refer. [24]
1.0	5.39	5.31	15.69	15.64	23.50	23.24
0.8	7.12	7.05	18.85	18.76	27.08	26.99
0.6	9.72	9.64	22.46	22.45	31.45	30.57

anchored on a flexible foundation, examined in section 4.6.

Some numerical difficulties arise when the sloshing modes are included. According to the formulation presented in section 3.8 these modes introduce nonsymmetries in the mass matrix. Also, a problem arises from the fact that the frequencies of the sloshing modes are very small compared to the frequencies of the structural modes. Because the more structural degrees-of-freedom included, the higher the highest eigenvalues, the code used in the present work for the extraction of the eigenvalues presented problems after inclusion of a critical number of structural modes.

4.4. Roof Effects.

The analytical formulation of the effects of a rigid roof at the top of the shell is presented in section 3.5.2. Here, some numerical results are obtained for the case of the la1 model tank whose dimensions and material properties are given in Table 4.5. In all the examples $\bar{N}$=3 is chosen and the first three frequencies of the system, including water up to a height H= 0.8 L, are shown in Table 4.6 for various values of the roof mass m_r and the roof centroidal moment of inertia I_r.

The obtained results indicate that the larger the roof the lower the frequencies of the system, as expected.

Table 4.4 Sloshing Effects on System Frequencies [Hz]

Mode	Eqn. (4.2)	No Sloshing		Coupled System	
		Present Analysis	Reference [24]	Present Analysis	Reference [24]
1	0.2501	-	-	0.2540	0.2497
2	0.4256	-	-	0.4189	0.4254
3	0.5385	-	-	0.5436	0.5384
4	0.6306	-	-	0.6289	0.6307
5	-	3.654	3.559	3.658	3.557
6	-	10.580	10.450	10.582	10.433

4.5. Linear Ground/Structure Interaction.

Generally, the response of a structure supported rigidly can be quite different from the response of the same structure when mounted on flexible ground. To examine when the ground flexibility is important for fluid-filled tanks, a parametric study is carried out for a specific tank. The tank data are found in Table 4.5 for the la1 model. In this study the rotational spring which is used in formulating the ground/structure interaction problem - as explained in section 3.5.4. - is assumed to have a linear moment versus rotation relationship of the form

$$M_f = k_f \, \phi_f \ .$$

First, by choosing N1=2 and N2=N3=1 the frequencies ω_i of the system are found for the case where the tank is anchored on a rigid ground (ϕ_f=0). Then, the rotational degree-of-freedom ϕ_f is introduced into the formulation and the new frequencies ω'_i of the system are found for various values of the stiffness k_f. The results from this study are shown in Figure 4.1, in which the vertical axis represents the frequencies ω'_i, for a range of values of the parameter

$$\bar{\omega}_f = \sqrt{k_f / I_f}$$

which appear on the horizontal axis. In all the calculations the value of the centroidal moment of inertia of the foundation is kept constant (I_f= 0.037 Kgm^2). A small number of degrees-of-freedom was chosen here to avoid lengthy

Table 4.5 Dimensions and Material Properties of Model Tests [Ref. 28, 29]

Elasticity Modulus, E	$5.07 \times 10^9\ N/m^2$
Poisson's Ratio, ν	0.3
Shell Radius, R	6.35 cm
Shell Length, L	26.67 cm
Thickness of Shell Wall I	0.0051 cm
t_s II	0.0076 cm
Thickness of Bottom Plate a	0.0051 cm
t_b b	0.0076 cm
Density, ρ_s	1390 Kg/m^3
Roof Mass, m_r	0.0085 kg
Roof Moment of Inertia, I_r	$8.6 \times 10^{-6}\ kg/m^2$
Foundation Moment of Inertia, I_f	0.037 kg m^2
Distance between Foundation Centroid and Tank Bottom, h_g	0.013 m

The classification of tank models:

Tank # Ia1 means: t_s = 0.0051 cm; t_b = 0.0051 cm; Ring #1

Tank # IIb2 means: t_s = 0.0076 cm; t_b = 0.0076 cm; Ring #2

computations. As a result, only the first frequency is expected to be calculated correctly and therefore the frequencies of the higher modes are studied in a qualitative sense only.

Figure 4.1.b shows details near the point A of Figure 4.1.a. Considering the behavior of ω'_i as $\bar{\omega}_f$ varies, it is observed that for i>1 and for $\bar{\omega}_f < \omega_{i-1}$, it is $\omega'_i \sim \omega_{i-1}$, while for $\bar{\omega}_f > \omega_i$, $\omega'_i \sim \omega_i$. For intermediate values of $\bar{\omega}_f$, the frequency ω'_i changes rapidly between the two limiting values ω_{i-1} and ω_i. The distribution of ω'_i and ω'_{i+1} when $\bar{\omega}_f \sim \omega_i$ is similar to that obtained for a two degree-of-freedom system in which the oscillators have a large difference in their "masses." Finally, for the lowest mode (i=1) the frequency increases from 0 and tends to ω_1 as $\bar{\omega}_f$ becomes greater than ω_1.

Table 4.6 Roof Effect on System Frequencies [Hz]

m_r [Kg]	0	8.5×10^{-3}	0.085	0.425
I_r [Kgm^2]	0	10^{-5}	10^{-4}	10^{-3}
ω_1	42.1	41.8	39.5	31.4
ω_2	127.8	127.1	117.7	87.8
ω_3	346.3	295.9	178.5	146.5

By looking at the variation of the rocking component of the eigenvectors as $\bar{\omega}_f$ varies, the following points are observed. For the first mode when $\bar{\omega}_f \sim 0$, the rocking component dominates but decreases as $\bar{\omega}_f$ increases. For the i^{th} mode (i>1), the rocking component increases very slightly as $\bar{\omega}_f$ is increased from 0 to ω_{i-1}. Then it increases rapidly in the transition region of ω_i, up until $\bar{\omega}_f \sim \omega_i$; for larger values of $\bar{\omega}_f$ it again starts decreasing. So, every mode attains a maximum rocking component in the transition region of the corresponding frequency. This rocking component decreases progressively as i increases and becomes negligible - for large i - compared to the other elements of the eigenvectors.

Since the first two modes are the most important in determining the response of the structure, clearly if $\bar{\omega}_f < \omega_2$ the ground flexibility is going to affect the response of the system considerably. The effects are substantially greater in the case where $\bar{\omega}_f < \omega_1$. In many cases of practical importance, the frequency range of excitation is also less than ω_1.

4.6. Buckling at the Top of a Tank.

The purpose of this section is to provide an explanation for the cause of the earthquake induced damage observed at the top of liquid storage tanks which has a pattern similar to that shown in Figure 4.2. Damage of this type has been thought to be caused by fluid sloshing. Applying the analytical procedures developed in chapter 3 shows that this type of damage is due to a net external pressure, which causes local buckling at the top of the tank.

Under static conditions, the stresses in the tank wall are dominated by the hoop stress caused by the hydrostatic pressure. During ground motion, combination of the constant hydrostatic pressure and the hydrodynamic pressure can produce a negative resultant pressure over part of the tank area near the free surface of the fluid. This can then result in local buckling of the tank under sufficiently large ground acceleration.

Next, analytical results are obtained for a case where such damage was observed during experiments. For that case the required data are available and therefore comparison can be made between the analytical and the experimental values. Using these results, the mechanism which causes buckling at the top of a liquid storage tank during ground excitation is explained.

4.6.1. *Test Data.* The tank tested was made of Mylar A sheet, with material properties and dimensions as appear in Table 4.5 for the la1 model, and contained water up to a height H= 0.8 L. The tank was anchored on the table of a 30 lb shaker which was supposed to produce a single directional, horizontal, harmonic excitation at the base of the tank, with acceleration of the form

$$\ddot{x}_g(t) = a_o \sin\omega t \ .$$

For the chosen test case, the acceleration amplitude at buckling was measured to be 0.38-0.40 g, while the forcing frequency was ω = 20 Hz. It must be pointed out here that if the prototype tank is fabricated from steel - which is the most common case - the geometry and the pressure of the prototype tank should be scaled by a factor of 41, the excitation level for the model and the prototype should be the same, while the periods of time should be scaled by 6.4. More details of the experimental set-up and results can be found in [28,29]. During the test, buckling occurred at the top - as well as at the bottom - of the tank. The observed pattern at the top of the tank consisted of one half wave in the axial direction and a short wavelength in the circumferential direction, as shown in Figure 4.2. This pattern suggested that the buckling was caused by external pressure at the tank wall. This hypothesis is

verified below, using the previously developed analysis.

4.6.2. *Explanation of Buckling Mechanism.* Since the tank top was open to the atmosphere, the pressure difference between the external and the wetted cylindrical surface of the tank wall can be written as

$$P_{EX} = \rho_l g(H-z) + P_d(R,\theta,z,t) \tag{4.3}$$

If a linear analysis is performed and only the impulsive fluid effects are included, then the hydrodynamic pressure at the tank wall can be generally expressed as

$$P_d(R,\theta,z,t) = - a_o\, F(z)\, \sin\omega t\, \cos\theta \tag{4.4}$$

where

$$F(z) = \rho_l R \{ f_x(R,z)(1 + \frac{h_g}{R}\, R\bar{\phi}_f) + f_f(R,z)\, R\bar{\phi}_f + \sum_{m=1}^{N1} [f_m(R,z)\, \bar{\psi}_m] \} \ .$$

The barred quantities are components of the vector $\underline{\bar{x}}$, which is determined from the solution of (3.20) and is defined by

$$\ddot{\underline{\bar{x}}}(t) = (a_0 \sin\omega t)\, \underline{\bar{x}} \ .$$

From equation (3.20), the m^{th} component of $\underline{\bar{x}}$ is found to be as follows

$$\bar{x}_m = \sum_{i=1}^{N} \left[\frac{(\underline{y}_i,\, M^{-1} \underline{f})}{(\underline{y}_i,\, \underline{x}_i)} \ \frac{(\underline{x}_i)_m}{(\omega_i/\omega)^2 - 1} \right] .$$

The total number of degrees-of-freedom of the problem is N and the notation (.,.) represents the ordinary Euclidean inner product in an N-dimensional vector space. The eigenvectors of the matrix $M^{-1}K$ and of its transpose, corresponding to the same eigenvalue ω_i^2, are denoted by $\underline{x}_i$ and $\underline{y}_i$, respectively. Obviously then, F is a function of z and is known for a given system and forcing frequency ω. Looking back at (4.3), it is observed that the first (hydrostatic) term of that equation depends on z only, while the amplitude of P_d depends linearly on the amplitude a_o of the ground acceleration. Therefore, it is seen that increasing a_o can cause the hydrodynamic pressure to overcome the hydrostatic pressure locally. This means that the external pressure P_{EX} can become negative on parts of the wetted tank wall

close to the liquid free surface, where the hydrostatic pressure is relatively small. Since such a pressure creates local compressive hoop stresses, it can then be expected that sufficiently large amplitudes of the ground acceleration will result in local buckling at those places of the tank.

4.6.3. *Comparison of Analytical and Experimental Results.* Initially, the analysis predicted the lowest structural frequency of the system to be 41.9 Hz, which is higher than the corresponding experimental value. This suggested the importance of the flexibility of the shaking table on the response of the system. To consider this effect, an equivalent, constant, rotational stiffness k_f is chosen for the conditions of the test, as follows. First, a value is assumed for k_f and a linear analysis is performed, yielding the lowest structural response frequency ω_1 for the corresponding system. Then, this value ω_1 is compared to the corresponding frequency from the experimental results, which was about 28 Hz [29]. Choosing k_f= 3000 *Nm*, $\bar{N}$=2 (so that the total number of included degrees-of-freedom of the system is N=7), the lowest structural frequency of the system is computed to be 27.6 Hz. For comparison purposes it is added here that choosing values of 2500 and 3500 Nm for k_f, produces values of 25.8 and 29 Hz for ω_1, respectively. From these calculations, k_f = 3000 Nm is chosen as the most reasonable equivalent stiffness for the case under consideration. Clearly, the effect of the base flexibility resulted in the reduction of ω_1, which is typical and expected in such cases. Some more results on the subject are presented in section 4.7.

Next, in order to determine the critical amplitude a_c of the ground acceleration which can buckle the top of the tank, the BOSOR5 computer code was used [65]. This code can determine the bifurcation buckling load for shells of revolution under arbitrary but axisymmetric loading. For the cases where this load is an external pressure, the number of waves of the buckling pattern is unknown in the circumferential direction only. Therefore, for the determination of the bifurcation load, an eigenvalue problem is set up in the form

$$[K(n) + \lambda_n K_G(n)]\, q_n = \underline{0} \tag{4.5}$$

where K is the stiffness matrix for the shell, K_G is the "load-geometric" matrix, λ_n is the eigenvalue and q_n the eigenvector corresponding to n circumferential waves.

For the present case, the critical acceleration amplitude a_c is determined for quasi-static buckling conditions. This means that the buckling time scale is assumed to be much smaller than the response time scale of the system, which implies that static buckling analysis is sufficient, although the loads on the structure are time-dependent. The critical value a_c is computed by iterations, as follows. A value is chosen for a_o and the external pressure P_{EX} is obtained from (4.3), at $\theta=0^o$. Then, this pressure, which is a function of z only, is applied as an axisymmetric external pressure and an eigenvalue problem is set up in the form of (4.5). Since the matrix K_G is computed for external pressure P_{EX} corresponding to the assumed a_o, the critical amplitude a_c is identified as that value of a_o which results in a minimum eigenvalue of unit magnitude. In this case, following suggestions of the code, P_{EX} is uniformly divided by one thousand, so that the calculations due to non-linear geometrical effects are kept to a minimum. Then, the a_c is chosen as that value of a_o which gives rise to a minimum eigenvalue with magnitude one thousand.

Results of such iterations are given in Figure 4.3. Using these results the critical ground acceleration amplitude is found to be a_c = 0.423 g, which compares favorably with the experimental value. The eigenvalues corresponding to a_0 = 0.42 g for different circumferential wave numbers n are shown in Table 4.7. Obviously, the minimum eigenvalue corresponds to n=13 waves. This result justifies the fact that axisymmetric loading was used for the buckling calculations, although the hydrodynamic part of P_{EX} varies as $\cos\theta$ in the circumferential direction. Clearly, in this case, the pressure can be considered as almost constant over the distance of one circumferential wavelength, which is enough for local buckling to occur. The corresponding normalized displacements of the computed buckling pattern are of the form shown in Figure 4.4. Comparing with Figure 4.5, it is seen that the largest amplitudes of the displacements occur near the free surface of the liquid, where P_{EX}

Table 4.7 Buckling Load vs. Circumferential Wave Number (a_o = 0.42 g)

n	12	13	14	15	16
λ	1058	1033	1035	1051	1078

is non-positive.

Another remark is associated with the choice of the appropriate boundary conditions for the buckling calculations. Since the tank was anchored to its foundation, the bottom end of the tank was assumed to be clamped, i.e.,

$$u_r = \frac{\partial u_r}{\partial z} = u_\theta = u_z = 0 , \quad at\ z = 0.$$

The top of the tested tank was fitted with a light-weight plastic plate in order to simulate a roof and there was some uncertainty in choosing the corresponding boundary conditions. The numbers in Table 4.7 are obtained for boundary conditions

$$u_r = \frac{\partial u_r}{\partial z} = N_{\theta z} = N_z = 0 , \quad at\ z = L$$

in the prebuckling state, while for the buckling analysis the $\partial u_r/\partial z=0$ condition at z=L is changed to $M_z=0$. Changing the chosen boundary conditions at the top to other reasonable sets, results in virtually no change in the numbers in Table 4.7.

Knowledge of the critical base acceleration amplitude allows for the direct calculation of the corresponding P_{EX} and its components. Figure 4.5a represents the distribution of P_{EX} at r=R and $\theta=0^o$, versus z. For small z the hydrostatic pressure dominates and results in a positive external pressure which is an almost linear function of z. However, near the free surface, the hydrodynamic component becomes dominant and creates negative external pressure, as expected. Between the free surface and the top of the tank the pressure is zero, since there is no liquid there. In Figure 4.5.b the impulsive components of the hydrodynamic pressure are plotted in the same manner. It is seen that the parts due to rigid body translation and rotation dominate the part which is due to the tank flexibility. The most dominant component results from the rigid body translation, but obviously the other

two components are not negligible at all in this case. The numerical results also indicate that from the flexible modes of the tank only the first one (m=1) contributes significantly to the hydrodynamic pressure.

To illustrate the effect of the liquid sloshing on the system, the first sloshing mode is included in the formulation and the computed results are compared to those obtained by neglecting the sloshing. In the first column of Table 4.8 the normalized amplitudes of the acceleration for the rocking mode and the m=1 flexible mode are given for the case where sloshing is not included in the computations. In the second column the same amplitudes are given, computed for the same system but including the first sloshing mode. Obviously, the effect of the sloshing on the structural modes tends to reduce P_{EX} but it is negligible in the considered case. The corresponding spectral acceleration of the sloshing mode - normalized by a_o, again - is also negligible. This is expected since the first sloshing frequency for the system is 2.68 Hz, which lies far away from both the forcing and the structural frequencies. In the third column of the Table 4.8, the same amplitudes are given after introducing 5% critical damping for all the modes. No significant change is observed since the forcing frequency is not close to any of the system frequencies. Finally, the amplitudes are given in the last column for the same system but including 25 ($\bar{N}$=8), instead of 7, degrees-of-freedom. The numbers show that the difference due to the extra degrees-of-freedom is not large, indicating that the chosen spatial dependence of the structural modes is quite satisfactory for the present case.

Table 4.8 Effect of Sloshing, Critical Damping and Total Number of Degrees-of-Freedom.

	N=7, ς=0	N=7, ς=0	N=7, ς=0.05	N=25, ς=0
	No Sloshing	Sloshing	No Sloshing	No Sloshing
$\ddot{\iota}_1/a_o$	0.678	0.671	0.671	0.769
$R\ddot{\theta}_f/a_o$	0.204	0.202	0.201	0.214
$\bar{A}_1/a_o$	-	- 0.040	-	-

4.7. Nonlinear Ground/Structure Interaction.

Use of linear analysis, when applicable, is convenient in clarifying and explaining various aspects of a phenomenon. This was the case for the problem attacked in the previous section. There, by modeling the tank/shaking table interaction using an appropriately chosen linear spring and utilizing a linear formulation for the fluid/structure interaction problem, it was eventually feasible to carry out a completely linear response analysis for the system. However, an attempt to measure the rotational stiffness of the shaking table, resulted in a nonlinear moment versus rotation relationship, as shown in Figure 4.6. This behavior is probably due to lack of good contact between the bearings of the table and their supporting shafts.

To examine the accuracy of the results obtained from the linear analysis and also to study possible qualitative changes in the response, the tank/table interaction was modeled by using a trilinear spring, whose characteristics are obtained from Figure 4.6 to be as follows:

$$M_f = \begin{cases} k_1\phi_f, & |\phi_f| \le \phi_c \\ k_2\phi_f + (k_1-k_2)\phi_c sgn(\phi_f), & |\phi_f| > \phi_c \end{cases}$$

with k_1= 0 Nm, k_2= 9400 Nm, and ϕ_c= 10^{-4} rad.

At first, the results from the nonlinear analysis were quite surprising. Namely, since the excitation is a harmonic function of time, one might expect the system to have a periodic steady-state response. Instead, a strange and complicated history was obtained for all the components of the system. Since the system is nonlinear, a direct time integration numerical scheme (backward differentiation of order 1 to 5) was employed in obtaining its response. For this reason, as a first step the possibility of an improper choice of the damping matrix was examined. This matrix is chosen according to section 3.9. Comparing the steady-state response of several linear cases, identical results were obtained from both the modal analysis and the direct time integration. Also, running the nonlinear case even for relatively large time periods (more than 250 forcing periods) did not produce a periodic steady-state response. These checks provided evidence that what was observed was not

due to improper choice of the damping matrix.

The behavior of the system was not well understood at the beginning. Since it was not clear if this kind of behavior was a result of a possible failure of the numerical scheme, or if it was something inherent and characteristic of the dynamics of the nonlinear system, it was decided to isolate and study more carefully the nonlinear component of the system alone. Some interesting observations from this study are presented in the next subsection. Then the results from the tank problem follow.

4.7.1. *Complicated Dynamics of a Simple Nonlinear Oscillator.* In this subsection, some unusual results are discussed, obtained from the study of a single degree-of-freedom oscillator whose behavior is described by the following equation:

$$\ddot{x} + 2\zeta\bar{\omega}\dot{x} + k(x) = A\sin\omega t \quad .$$

The restoring force of this oscillator has the general form:

$$k(x) = \begin{cases} \omega_1^2 x, & |x| \leq x_c \\ \omega_2^2 x + (\omega_1^2 - \omega_2^2) x_c \, sgn(x), & |x| > x_c \end{cases} \quad .$$

The nonlinearity of the restoring force takes the form of a piecewise linear function of x. This means that the system behaves as a different, but always linear, oscillator for $|x| \leq x_c$, $x > x_c$, and $x < -x_c$ and an analytical solution can be obtained for any of these three intervals. However, the complete response history cannot be obtained in closed form since the determination of the instances of time at which the displacement x takes the value x_c or $-x_c$ requires the solution of a transcendental equation. Therefore, the response of the system is obtained according to the following mixed analytical/numerical procedure. Any time the solution x crosses the x_c or $-x_c$ line in the x-t plane, the appropriate form of the oscillator equation is first chosen, depending on which x-interval the solution enters. Then, the corresponding values of x and $\dot{x}$ at the cross-point are used as initial conditions and the complete time history (homogeneous plus particular solution) is utilized in

closed form, just up until the next crossing of x and x_c or $-x_c$ happens. The value of t_c - and therefore of $\dot{x}_c$ - at each cross-point is iteratively obtained to a specified numerical accuracy.

After checking the adequacy and accuracy of this numerical scheme in linear cases ($\omega_1=\omega_2$), the nonlinear problem ($\omega_1\neq\omega_2$) was attacked. Several cases were examined by varying such parameters as ω_1, ω_2, $\bar{\omega}$, A, ζ, $\bar{\omega}$ and the initial conditions. Some of the observed interesting points are discussed next.

For cases with $\omega_1 \sim \omega_2$, relatively small or relatively large forcing amplitudes A and large ζ, a periodic steady-state was obtained, which could contain appropriate subharmonics and/or ultraharmonics, as typically expected for nonlinear systems. The most unusual behavior encountered for a system exhibiting a periodic steady-state response was that obtained for a system with ω_1 = 4 Hz, ω_2 = 65 Hz, $\bar{\omega}$ = 60 Hz, ζ = 0.05, x_c= 0.9×10^{-5} *m*, A= 5 m/s^2 and ω = 100 Hz. Experimenting numerically with that system it was found that depending on the initial conditions, the steady-state could have a symmetric or asymmetric form with a positive or negative offset. Of course, the dependence of the steady-state on the initial conditions is typical for nonlinear systems but the offset and the nonsymmetric response were not initially expected for the system under study. Partial explanation for this behavior is provided by the corresponding phase-planes of the system. Figure 4.7 shows the history of the displacement x and the phase-plane for the time between 0.5 and 1 sec for two cases with the only difference being in the initial displacement. In the first case x_o= -1.5×10^{-5} *m*, while in the second case x_o= 3.5×10^{-5} *m*. In both cases $\dot{x}_o$= 0. For the same system a symmetric steady-state response was also obtained for various other initial displacements x_o.

The response was even more complicated for cases with large differences between ω_1 and ω_2. From the results of numerical experiments it was found that keeping ω_2 constant at a sufficiently high value and decreasing ω_1 produced the same kind of strange behavior encountered previously in the solution of the

nonlinear tank response problem. This behavior was obtained after decreasing ω_1 below a critical value - usually well above zero. Also, for a fixed ω_1, increasing ω_2 resulted in strange long-time behavior above a critical minimum value for ω_2. Results for a specific case with parameters as given in the previous paragraph but with zero initial conditions, A= 1 m/s^2 and ω= 20 *Hz* are presented next. For ω_2= 65 *Hz* and for values of ω_1 greater than about 27 Hz a periodic steady-state was obtained. But for $\omega_1 < 26$ *Hz* no periodic steady-state could be obtained for the system, for the first 5 sec (100 forcing cycles.) On the other hand, for ω_1= 4 *Hz* a periodic steady-state was obtained for $\omega_2 \leq 56$ *Hz*. For higher ω_2 the observed response history - up to 100 forcing cycles, again - was non-periodic. It is worth mentioning here that the character of the long-time solution kept changing *gradually* from harmonic to periodic and eventually to non-periodic, by increasing the difference between ω_1 and ω_2. Also, the response history was found to depend largely on the initial conditions. Slight perturbations in the initial conditions resulted in very different forms of the solution. Another characteristic of the system was the numerical difficulty in obtaining the correct solution for such cases. The system considered in the general form satisfies all the theoretical requirements (continuity and Lipschitz condition) for the existence of a unique solution. But during the numerical experimentation some extra difficulties were experienced with this specific system. Namely, by changing the accuracy required of the numerical iterations in determining the crossing times, the form of the solution kept changing, even after complete exhaustion of the double-precision computing capabilities (calculations with 16 significant figures). The fact that the system was known to have a unique solution led to further experiments utilizing quadruple computing precision (33 significant figures). This numerical accuracy proved to be sufficient in finding a solution - in the examined time range - which did not change form with further increases in the required accuracy for the numerical calculations and iterations. This solution is shown in Figure 4.8.a. A period of two seconds (40 forcing cycles) was chosen, because it was thouhgt initially that this period of time would be long enough for a periodic steady-state solution to form, if one existed.

A complete analytical explanation for such complicated behavior does not seem to be straightforward. Only some qualitative arguments are presented next. By considering the stability of periodic solutions for the general system, the variation equation is found to resemble a Hill-Meisner equation. For the Hill-Meisner equation it is known that increasing the parameter $(\omega_1^2-\omega_2^2)/\omega^2$ increases the possibilities for loss of stability of an existent periodic solution, which is consistent with the observed phenomena during the numerical experimentation. Some characteristics of the solution such as the non-periodic long-time response and the large sensitivity to the initial conditions suggest that the system under consideration may experience what is called "*chaotic behavior*" for some combinations of its parameters. So far, such behavior has been observed experimentally and numerically for other systems [67-70]. Specifically, the case of chaotic behavior of an oscillator with a bilinear spring is examined in [66]. The results presented here are not extensive; they are meant to be only a source of information and stimulation for future studies on the subject.

Similar results were obtained by studying the one degree-of-freedom system with the numerical code which performs the direct integration for the structural system. Namely, in the cases with periodic steady-state solutions, identical results were obtained with the numerical scheme using the analytical solution. Also, loss of stability of a periodic solution was observed for about the same values of the parameters of the system. Of course, the solutions with no steady-state had different appearances in the two different methods because of the different implications of the imposed numerical accuracy for the two cases.

All these observations provide evidence that the observed strange behavior of the nonlinear system is something inherent in the system itself. Looking at the phase-plane of the system which exhibited non-periodic steady-state, as shown in Figure 4.8.b for the time period between the 3rd and 4th seconds of the excitation, one observes that although not periodic, the response is always of bounded amplitude and that it loosely follows some ordered pattern. The displacement history

corresponding to that period of time is shown in Figure 4.8.c. Similar behavior was encountered for even longer periods of time. Figure 4.8.d shows the Fourier spectrum for the response between 6 and 10 sec. The nonperiodicity of the solution in that time interval is indicated by the fact that the spectrum is distributed broadly over wide frequency bands. Over long periods of time, the trajectories densely fill the area of the phase-plane shown in Figure 4.8.b. If, instead of drawing the whole trajectory, one plots a single point of it on the phase-plane every forcing period, the so-called Poincare map is obtained. Figure 4.8.e shows the Poincare map for the system, for the time between 5 and 55 sec (100-1100 forcing cycles). This map provides an additional indication for the nonperiodicity of the long-time solution. What is nice about this map is that the shape of the obtained strange attractor was found to be independent of the initial conditions and the accuracy of the numerical calculations, which is not the case for the solution itself. Also, this map indicates the boundedness of the solution. Finally, it is worth mentioning that the same system exhibited a periodic steady-state for $\zeta = 0.15$.

Some additional interesting points are also stressed in the following subsection, where the structural system already examined in section 4.5 is restudied by performing nonlinear analysis. It is found that the various components of the response, although non-periodic again, follow simpler patterns than the response of the similar one degree-of-freedom system examined in the present subsection.

4.7.2. *Nonlinear Response Analysis and Buckling.* The study of the one degree-of-freedom oscillator, presented in the previous subsection, provided confidence in the appropriateness of the numerical scheme chosen to perform direct time integration in obtaining the nonlinear response of the structural system. This allowed the analysis for the structural system examined in section 4.5 to be taken further, by incorporating the nonlinear tank/shaking table interaction behavior.

First, the time histories for ψ_1, $\dot{\psi}_1$ and $\ddot{\psi}_1$ are shown in Figure 4.9 for the time period between 2.5 and 3 seconds (50-60 forcing periods). A subharmonic of order 4 and an ultraharmonic of order 5 dominate these response histories and the solution does not seem to be far away from being periodic. However, it is not periodic, which can be readily seen by looking at the phase-planes for the ψ_1, ψ_2 and $R\phi_f$ degrees-of-freedom, as shown in Figures 4.9.d-f. These were obtained by plotting the corresponding displacement and velocity values for the time between 2.5 and 3 seconds. The subharmonic and ultraharmonic components in the response are clearly present in these figures. The motion for each degree-of-freedom seems to follow very close patterns but the fact that the trajectories in the phase-planes are thick, dense lines illustrates that the motion is not periodic; it does not repeat itself exactly. Similar phase-planes were obtained for time periods up to 15 seconds (300 forcing cycles). The above results were obtained for $\bar{N}$=2 and for ground acceleration a_o = 0.42 g. This was the critical value obtained in section 4.5 for buckling at the top of the tank. The pressure distribution in the area with negative P_{EX} was also found for this case and the results are shown in Table 4.9 and compared to the corresponding results from the linear analysis. This comparison indicates that the constant value for the stiffness of the rotational spring modeling the shaking table flexibility is quite satisfactory in this case. The history of P_{EX} at r=R, z= 0.92 H and θ= 0^o is shown in Figure 4.10.a. Similar patterns were obtained for all the other points considered.

Finally, the history of the moment at the tank bottom, resulting from the pressure from the fluid on the cylindrical shell is shown in Figure 4.10.b. It is important to note that the value of the moment which results from assuming the shell to be a flexural beam, with maximum bending stress equal to the classical buckling value for the considered shell, is computed to be 1.6 N/m^2.

Table 4.9 External Pressure P_{EX} [N/m^2] versus z / H

z/H	Linear Analysis	Nonlinear Analysis
0.96	-85.8	-85.0
0.94	-97.7	-94.4
0.92	-98.4	-94.3
0.90	-94.2	-87.0
0.88	-84.0	-73.9
0.86	-65.0	-56.2
0.82	-20.9	-9.6
0.78	31.4	48.6

Chapter 5

RESULTS FOR UNANCHORED TANKS

5.1. Introduction.

Most of the analytical studies performed on the behavior of fluid-filled tanks during base excitation have focused on the response of anchored tanks. On the other hand, most of the storage tanks encountered in the field are essentially unanchored. Even when some type of anchoring is provided, the connection between the base of the tank and its foundation is usually insufficient to prevent tank lift-off during strong earthquakes. This fact has repeatedly been made clear in reports of earthquake response [1-3]. In these cases, the connections or the tank foundation itself cannot resist and support earthquake loads of the order of magnitude of those loads which cause buckling at the bottom of an anchored tank. Simple analysis shows that the connections usually provided will fail under much lower loads than those causing buckling, giving rise to tank uplift before tank buckling can occur.

For an unanchored tank the analytical modeling of its behavior during base excitation is inherently nonlinear and as a result of the associated difficulties, not much analytical work has been reported on the subject so far. However, experimental studies have shown that an unanchored tank develops much greater axial membrane stresses at the bottom than an anchored one under the same loading conditions. Results presented in [29] showed that in some cases the buckling at the bottom of an unanchored tank can appear for amplitudes of the ground acceleration an order of magnitude less than those for an anchored tank. This is due to the different mechanisms by which the earthquake loads are developed, carried through and resisted by anchored and unanchored tanks. Since the overall behavior is more complicated for unanchored tanks, special care should be taken in their design.

The complete problem for the behavior of unanchored tanks under base excitation can be split into three parts. The first one is the determination of the response and the developed loads, the second deals with the calculation of the resulting stresses in the structure and the third problem is associated with the choice of an appropriate failure criterion. Each of these parts requires a much more elaborate and sophisticated analysis than that required for an anchored tank.

In this chapter, the analysis developed in the second and third chapters of this thesis is applied to cases examined previously experimentally. There are no analytical results available for comparison. In the following section, results from static tilt tests are obtained in order to derive the characteristics of the rotational spring modeling the uplift behavior of unanchored tanks, as presented in section 3.6. Then, the dependence of the dynamics of an unanchored tank on the stiffness of this spring is examined parametrically. In the fourth and fifth sections some preliminary results are obtained for the structural and the sloshing behavior of an unanchored tank, by using a linearized spring for the uplift formulation. Some useful results are obtained before the full nonlinear analysis is applied. In the last two sections, analytical results are obtained and compared with available experimental data, for unanchored tanks with harmonic or transient base excitation.

5.2. Static Tilt Tests with Unanchored Tanks.

Studying the experimental results presented in [29] one observes that the behavior of the same tank can be very different depending on the fixity of its base. As a specific instance, it is revealed that for the tank IIb2 (see Table 4.5) the lowest n=1 frequency is reduced from about 32 Hz in the anchored case to about 8 Hz for the unanchored case and for base accelerations resulting in buckling. Such a dramatic change in the fundamental frequency is observed also in simpler but similar structures, by changing the base fixity. For example, consider a flexural beam, which is free at the top and is supported by a rotational spring at the bottom. Performing the corresponding eigenanalysis (see Appendix F), it is found that the dependence of the first eigenvalues on the spring stiffness parameter κ is as shown

in Figure 5.1. For relatively large κ the beam frequencies do not change very much with κ and they are very close to those of a clamped/free beam, while for κ=0 the eigenvalues of a simply-supported/free beam are obtained, as expected. For intermediate values of the stiffness κ there is some effect in all the frequencies, which is very pronounced for the fundamental frequency. Clearly, for small values of κ, a great change in the fundamental frequency of the beam can result from changing the stiffness of the spring.

Results of static tilt tests indicated that an increase in ϕ_u results in a substantial decrease of slope in the relationship between the moment $\bar{M}_c$ and the uplifting angle ϕ_u, as shown in Figure 5.2. The data for this figure are taken from [37]. The relationship obtained in this case, together with the results of the eigenanalysis of the beam model discussed above, are in qualitative agreement with the results of the dynamic experiments. Also, the nonlinear relation between $\bar{M}_c$ and ϕ_u reflects the fact that the base uplifting is nonlinear in nature. These observations triggered the development of the present analytical model for the behavior of unanchored tanks.

To identify the system parameters important in obtaining the required relation between the base overturning moment $\bar{M}_c$ and the corresponding uplift angle ϕ_u from static tilt tests, some simple dimensional analysis is performed. Assuming a rigid roof, ignoring the bottom ring parameter and assuming that the whole tank structure is made of the same material, the following ten additional parameters seem to be important: E, ν, R, L, t_s, t_b, ρ_s, ρ_l, H, g. Then, according to Buckingham's π-theorem, there are 9 dimensionless, independent quantities required to express the relation among the system variables for static analysis. This relation may be written as follows:

$$F\left\{\frac{\bar{M}_c}{\rho_l g R^2 H^2}, \phi_u, \nu, \frac{H}{R}, \frac{L}{R}, \frac{t_s}{R}, \frac{t_b}{R}, \frac{\rho_s}{\rho_l}, \frac{E}{\rho_l g H}\right\} = 0$$

If all these parameters have the same values in both the scale model and the corresponding prototype, then the response of the prototype can be exactly predicted by the observed results of the scale model test. However, it is not possible to obtain general results for the $\bar{M}_c/\phi_u$ relationship by conducting simple experiments. For the purposes of the present work and in order to obtain analytical results for the dynamics of the IIb2 tank, static tilt tests were performed for this specific tank. During these experiments the tank was filled with water up to given levels (7.5, 8.5 and 9.5 in) and the uplifting displacement δ - see Figure 3.1 - was measured for various tilting angles. The results of these experiments are shown in Figure 5.3.

During the course of this work, a companion study was concerned with the analytical formulation of the static response of unanchored tanks with lateral loads caused by setting the tank on a tilted plane [31,32]. That study, as well as [41], can provide the required $\bar{M}_c/\phi_u$ curve analytically, which then implies that the complete response behavior can be obtained analytically for any case of interest.

5.3. Uplift Spring and Tank Dynamics.

A parametric study was carried out to examine the dependence of the frequencies of an unanchored tank on the equivalent stiffness $\bar{k}_u$ of the rotational spring modeling the uplift behavior. Using the IIb2 tank as a model, with water height H=3R, N1=2 and N2=N3=1, the frequencies ω_i (i=1 to 4) are first computed. Then, the uplift degree-of-freedom was introduced into the analysis by assuming a linear relation between $\bar{M}_c$ and ϕ_u. That is

$$\bar{M}_c = \bar{k}_u \, \phi_u \quad .$$

This formulation does not model exactly the behavior of an unanchored tank, since the real resistance to uplift does not possess constant stiffness. Also, due to the small number of the included degrees-of-freedom in this case, only the first frequency is expected to be computed correctly. However, some preliminary studies can be performed this way and an insight into the physics of the real problem can be gained before the complete nonlinear analysis is attempted.

The frequencies of the new system - including uplift - are denoted by ω_i' (i=1 to 5) and the results of the parametric study are presented in Figure 5.4. The most important characteristics of the system are the dramatic dependence of the lowest frequency on $\bar{k}_u$, for relatively small values of $\bar{k}_u$ and also the fact that $\omega_i' \rightarrow \omega_i$ as $\bar{k}_u \rightarrow \infty$. The transition in the values of the first three frequencies is similar to what is observed in Figure 5.1 and is quite different from what is shown to happen in Figure 4.1. This is expected here, since in the present case there is no "mass" associated with the bottom spring, while for the case presented in Figure 4.1 there was.

At least for the system examined, the real values of the rotational spring stiffness (30-500 Nm) are found to lie in the range where the fundamental structural frequency is drastically affected by changes in the stiffness $\bar{k}_u$. Thus, one may expect this to have an important effect on the dynamics of the system, for excitations with a typical frequency content. This is shown to be the case in sections 5.6 and 5.7.

5.4. Shell Flexibility Effects in Unanchored Tanks.

Some preliminary results are discussed here, referring to the free and forced vibrations of an unanchored tank. The IIb2 tank is again used as model in obtaining these results.

Table 5.1 gives the two lowest structural frequencies of the system for three different water levels. Constant values are used for the stiffnesses of the springs modeling the uplift of the tank and linear analysis is performed. For a given water level two values are chosen for $\bar{k}_u$, these are the highest and lowest stiffnesses measured from Figure 5.3. The calculations are done including the degree-of-freedom due to the ground flexibility, with $\bar{k}_f = 3000\ Nm$. Also, the degrees-of-freedom accounting for the shell flexibility are included ($\bar{N}$=3) or exluded ($\bar{N}$=0) from the formulation. A considerable difference is observed in the computed values of the fundamental frequency ω_1, by using the lowest or the highest value of $\bar{k}_u$. Comparing the computed and experimental values [29], it is observed that - at

least for the case H=3R, for which the frequency range between 2-20 Hz was examined during the tests - the lowest frequency resulting from the lowest $\bar{k}_u$ comprises a lower bound for the range of the resonant frequencies of the structure. Next, it is seen that the higher the fluid level H the lower the ω_1, which is in qualitative agreement to what happens with the anchored tanks. However, ω_2 remains almost constant with changes of H. Finally, by choosing zero or nonzero $\bar{N}$ no significant changes are observed in the values of ω_1 and ω_2. This indicates that the shell flexibility effects may be unimportant when considering the response of unanchored tanks of similar dimensions.

Table 5.1 Lowest Two Structural Frequencies for Various Water Levels H [in], Uplift Spring Stiffness k_u and Shell Flexibility dof

	Lowest k_u				Highest k_u			
H	$\omega_1[Hz]$		$\omega_2[Hz]$		$\omega_1[Hz]$		$\omega_2[Hz]$	
	$\bar{N}$=3	$\bar{N}$=0	$\bar{N}$=3	$\bar{N}$=0	$\bar{N}$=3	$\bar{N}$=0	$\bar{N}$=3	$\bar{N}$=0
7.5	6.23	6.27	45.55	45.56	18.27	19.20	48.69	49.24
8.5	5.24	5.27	45.53	45.55	15.69	16.54	48.65	49.25
9.5	4.63	4.67	45.54	45.56	15.17	16.21	49.69	50.78

Table 5.2 Normalized Acceleration Amplitudes for Different Water Levels H and Shell Flexibility Degrees-of-Freedom (ω = 10 Hz, Lowest k_u)

	H=7.5in		H=8.5in		H=9.5in	
	$\bar{N}$=3	$\bar{N}$=0	$\bar{N}$=3	$\bar{N}$=0	$\bar{N}$=3	$\bar{N}$=0
$R\ddot{\phi}_u/a_o$	0.894	0.910	0.668	0.677	0.549	0.558
$R\ddot{\phi}_f/a_o$	0.011	0.012	0.009	0.009	0.008	0.008
$\ddot{\psi}_1/a_o$	0.029	-	0.024	-	0.023	-

To investigate further the validity of the above finding, the response of the same tank to harmonic base excitation with amplitude a_o and forcing frequency ω was examined. For forcing frequencies typically expected, it was again found that the shell flexibility has no substantial effect on the dynamics of the unanchored tank.

Results from an example of such behavior are shown in Table 5.2. The values of the relative acceleration associated with the uplift, ground flexibility and the first radial shell mode, obtained for critical damping ratio 0.05 and normalized by a_o, are shown in this table, for various water levels. The forcing frequency for this particular example is $\omega = 10$ *Hz*, while the lowest value is used for $\bar{k}_u$ in each case. Clearly, the uplifting degree-of-freedom is completely dominant in all the cases presented. Also, the results are almost unaffected by consideration of the shell flexibility. The same behavior is also observed after performing a nonlinear analysis for the system, as explained in sections 5.6 and 5.7.

5.5. Sloshing and Structural Coupling.

In this section, the coupling occurring between the structural and the sloshing modes of an unanchored tank is examined. The analysis developed is applied to the IIb2 tank, partially filled with water up to a level H= 7.5 in. The various sloshing modes are incorporated into the formulation according to the relevant analysis presented in section 3.8. Results for this case are shown in Table 5.3. In this case the degrees-of-freedom due to the uplift and the ground flexibility are included with equivalent spring constants $\bar{k}_u$ = 30.8 and $\bar{k}_f$ = 3000 Nm, respectively. The lowest two sloshing and structural frequencies are obtained. The second column of Table 5.3 contains the first sloshing frequencies as computed by equation (4.2), while the third column contains the first two structural frequencies when no sloshing mode is included in the formulation. Finally, in the last column the same frequencies are shown after including in the formulation both the sloshing and the structural modes together.

These results are similar in nature to those obtained for the anchored tank examined in section 4.3. Namely - despite the fact that the lowest structural frequency is substantially reduced in an unanchored tank due to the uplift effect - there is very little coupling between the sloshing and the structural modes. Again, it must be pointed out, however, that the examined tank is relatively tall.

Table 5.3 Frequencies [Hz] for H= 7.5 in and $\bar{k}_u$= 30.8 *Nm*

Mode	Eqn. (4.2)	No Sloshing	Coupled System
1	2.684	-	2.558
2	4.568	-	4.532
3	-	6.269	6.629
4	-	45.557	45.557

5.6. Harmonic Buckling Tests.

An explanation is provided here for the behavior of an unanchored tank during experiments reported in [29]. According to the results of those experiments the unanchored tanks appeared to respond in a rocking mode when subjected to base excitation. During the harmonic tests, resonance type phenomena were observed for much lower frequencies than the resonant frequency of the same tank but anchored.

Results obtained by applying the analysis to the case of the ilb2 tank with H=3R are discussed next. In interpreting the results for a real tank, the frequencies of the model tests should be divided by 6.4 in order to obtain the frequencies for a prototype tank made of steel. Values for the springs modeling the uplift and the ground/structure interaction derived from the experimental results are utilized, while c=1 is also chosen for all the cases examined here. First, using the experimental values for the ground acceleration amplitude a_o, as presented in Figures 5.14 and 5.16 of [29], the corresponding moments at the bottom of the tank are computed for any forcing frequency ω. The results are shown in Figure 5.5. The broken horizontal line in that diagram represents the moment for which buckling started at the bottom of the tank during the static tilt tests presented in section 5.2. The continuous line represents the moment causing collapse of the tank. This last value is obtained from static tilt test results reported in [29]. Next, it is assumed that the buckling in the dynamic case starts at the tank bottom for the same value as in the static case (0.71 Nm here). Then, iterations are performed by changing the amplitude a_o until the computed moment at the tank bottom has an amplitude of

0.71 Nm, for any ω. The results of this procedure are shown in Figure 5.6. In that figure, the x's indicate the experimental data presented in [29], while the continuous line represents the computed results, using the present analysis. The broken line, which is apparent at the low frequencies only, represents the results obtained by the same analysis after excluding the sloshing modes from the formulation.

During the numerical iterations, for values of ω between 6 and 9 Hz, some jump phenomena were observed. Namely, small changes in a_o resulted in large differences in the moment amplitudes. This is expected for a soft nonlinear mode, such as the uplift mode, and provides the reason why the computed moments using the experimental a_o value are relatively inaccurate for those frequencies. Next, judging from the difference between the continuous and broken lines in Figure 5.6, it is observed that the sloshing effects are important only when the forcing frequency is very close to the sloshing frequency. Also, it becomes clear that the behavior of the system for $\omega > 4$ *Hz* is governed by the uplift and not the sloshing effects. Finally, although near the fundamental frequency the sloshing response cannot be captured and described by linear analysis, it seems that at least the bottom moment can be adequately computed. In the calculations only the fundamental sloshing mode was included, except for $\omega = 4$ *Hz* which is close to the frequency of the second sloshing mode, where this sloshing mode was also included for better accuracy.

All the above results were obtained by using only two structural degrees-of-freedom. These were the degrees-of-freedom modeling the uplift and the ground flexibility. Including degrees-of-freedom due to shell flexibility caused virtually no change in the results. This important feature of the behavior was also captured by the linearized analysis presented in section 5.3 and is in agreement with experimental observations, according to which the predominant response mode was rocking of the tank.

Examining in more detail the response histories of the system components, the sloshing effects are found to be important for ω = 2.5 to 5 Hz. In the range ω = 7 to 12 Hz, the uplift component is dominant, while for the rest of the frequencies the acceleration $R\ddot{\phi}_u$ was always important and comparable to a_o. Furthermore, the strange behavior observed during the nonlinear ground/structure interaction, discussed in section 4.7, shows up in this case also. Figure 5.7 shows the time histories of $R\ddot{\phi}_u$ and $R\ddot{\phi}_f$ for the case with ω = 20 Hz, a_o = 2.06 g and for the time period between 2.5 and 3 sec. The phase-planes corresponding to these degrees-of-freedom are also presented in Figures 5.7.c-d. However, in this case and for 5% critical damping, a periodic steady-state was obtained, after about 100 forcing cycles. For 2% critical damping, a periodic steady-state was obtained after about 200 forcing periods. Next, trying to simulate better the experimental procedure, the analysis was run for the same case but with a ground acceleration amplitude of the form $a_o(1-e^{-3t})$. This means that the base amplitude increases gradually and reaches the value $0.95a_o$ after the first second of excitation. The phase-planes for this case are shown in Figure 5.7.e-f, while the moment at the bottom of the tank is shown in Figure 5.7.g.

Comparing the analytical and experimental results, good agreement is observed over all the frequency range examined, indicating the applicability and the effectiveness of the present analytical model. The largest discrepancy is observed for ω > 17 Hz. However, the values of the overturning moments which are computed by using the experimental values for the critical base accelerations are not significantly different from the critical moment which results in buckling of the shell bottom under static conditions. For example, the moment calculated with the experimental a_o value for ω = 20 Hz is 0.60 Nm, which is not far from the measured statical critical value of 0.71 Nm. One possible reason for the difference between the experimentally and analytically determined critical base accelerations might be the different stress concentration developed at the bottom of the tank for various forcing frequencies. By assuming the shell to behave as a flexural beam with

maximum stress equal to the classical buckling value for the shell, the critical moment at the bottom is found to be 3.56 Nm. This value is 5 times larger than the experimentally measured buckling moment, indicating a large stress concentration at the bottom of an unanchored tank, even in the static case.

5.7. Transient Buckling Tests.

Results on the behavior of unanchored tanks subjected to transient base excitation are also presented in [29]. These results are similar in nature to those presented in the previous section for the harmonic case and show once again that the behavior of the same tank can be quite different depending only on the base fixity.

Using the same model tank (IIb2) and the analytical procedures of the previous section, results are obtained for a base excitation with acceleration history as shown in Figure 5.8. These results are presented in Figure 5.9. The x's in Figure 5.9 indicate the experimental values obtained for an unanchored tank, from [29] , while the nearby continuous line represents the results by application of the present analysis. The dots indicate experimental results from [29] again but refering to the anchored case, while the nearby continuous line represents analytical results obtained by [24] for that case, using the classical buckling criterion. Comparing the results for the anchored and unanchored case a large difference is again observed. As explained in the previous section, two important factors are believed to be responsible for this. First, the base loads result from a different response mechanism which causes different pressure distribution on the tank walls. The other reason is the large stress concentration which is expected for unanchored tanks, due to partial contact of the tank bottom with the ground.

The results obtained by the present analysis are again in good agreement with the experimental data. Including sloshing in the formulation does not have any important effects in the case considered. The amplitude of the critical ground acceleration was found to be virtually unaffected by inclusion of the sloshing

modes in the formulation. Figure 5.10 shows the computed history for the moment at the bottom of the tank for the case of H= 7.5 in and ground amplitude a_o= 2.5 m/s^2. The maximum moment for this case occurs at a time when the amplitude of the base acceleration is also close to its maximum. However, this is not the general case. In some cases the peak in the moment occurred well before the acceleration peak. It is also observed that although the excitation is transient - with most of its energy content concentrated between 0-20 Hz - the tank responds in a frequency which is close to its resonant frequency. That is about 9 Hz, as deduced from Figure 5.6. Finally, the effects of shell flexibility, which were neglected for these calulations, seem once more to play no significant role.

Chapter 6

SUMMARY AND CONCLUSIONS

Fluid-filled tanks (oil, water, wine, etc.) are extensively used structures, which sustain effectively the loads caused by their contents during static conditions, but they are subjected to severe loading during strong earthquakes. This can lead to stress or buckling failures and subsequent loss of contents. In order to design such structures properly, the response of the tank and its contents under base excitation must be known. Most of the previous studies on the subject have focused on the response of tanks which are anchored to their foundation. However, the proper anchoring of a tank is expensive and most of the tanks in the field are essentially unanchored. This complicates the analysis, since the bottoms of these tanks usually separate from and lift off their foundations during ground motion, before failure occurs.

The objective of the present work is to create an analytical model which describes the dynamic response of unanchored tanks and predicts the hydrodynamic loads developed by the motion of the system. This analysis includes the effects due to the flexibility (both membrane and bending) of the shell wall, the liquid sloshing and also the base rocking that occurs in the field as well as in experimental simulations, due to ground flexibility. In developing this analysis, the physics of real tank behavior is first critically examined, through results and observations of previous investigations. The nonlinearities of the system, due to loss of contact and due to the large displacements developed at the base of the tank during uplift, are then appropriately modeled in an approximate but simple way. Also, the fluid response problem is solved in closed form, resulting in a compact system of equations of motion, which includes only structural and sloshing degrees-of-freedom as unknowns.

This analysis is used to determine the hydrodynamic loads acting on the structure, during various base excitation conditions matching experimental work, in which buckling occurred. First, buckling observed at the top of an anchored fluid-filled tank is examined. It is found that the induced hydrodynamic pressure may overcome the hydrostatic component and produce a negative resultant pressure in areas near and below the fluid free surface. This negative pressure produces compressive hoop stresses which can lead to local buckling, during sufficiently strong ground accelerations. It is also found in this case that ground flexibility results in a reduction of the response frequencies of the system. Good correlation between the analytical and the experimental results is obtained.

Next, buckling observed at the bottom of an unanchored tank is examined. Once again, the analytical results agree favorably with the experimental data. These results show that there is a dramatic change in the dynamic characteristics of an unanchored fluid-filled tank compared to the same tank with anchoring. The effective stiffness of the beam-type deflection of the tank is substantially reduced when the tank is allowed to lift off its foundation. This reduces the frequency of the predominant response mode of the system, which in turn affects significantly the hydrodynamic pressure distribution through the fluid/structure coupling mechanism. When the tank is anchored and subjected to typical base excitation, the hydrodynamic pressures are mostly due to the rigid body translation of the tank and partly due to the shell flexibility. For an unanchored tank, however, it is found - for the ranges of the forcing frequencies considered - that in addition to the pressure due to the rigid body translation of the tank, there is a considerable pressure component resulting from the rocking of the tank due to the uplift, and practically no contribution from the shell flexibility. This - together with the fact that a large stress concentration is expected for the axial membrane stresses at the shell bottom - explains why there can be a tremendous difference between the ground acceleration causing buckling, depending on the anchorage. For example, in the low frequency range of the tests, where it is now known that the uplifting effects are

dominant, there is an order of magnitude difference between the values of a_o causing buckling in the same tank, depending on whether it is anchored or unanchored. This indicates how erroneous it can be to calculate hydrodynamic loads assuming the tank to be anchored and then use the same loads for the case where the tank is unanchored, as is done by the current seismic codes [48-50], or others [25,41].

As indicated by results obtained from harmonic and transient base excitation, the sloshing effects are important only when the excitation has frequencies close to the frequency of the fundamental sloshing mode. It is also found for the cases considered, that the effects of the shell flexibility were negligible. The rocking mode due to uplift dominates the response of the unanchored tank, which is in agreement with previous experimental observations [29,34]. If this is the general case, this result is, indeed, of practical value, since it implies that the behavior of an unanchored tank can be studied by ignoring the effects of shell flexibility, at least for some practical geometries. Then, simplified models can be developed, which will be useful for design purposes.

The agreement between the analytical and experimental results indicates the applicability and effectiveness of the analysis developed in this thesis. However, there is more to be done on the subject. For example, the available experimental data refer to tall tanks. Results of this analysis should also be obtained and compared with experimental results for broad tanks, where the shell-type vibrational modes - especially the n=2 modes - may have an effect on the dynamics of unanchored tanks. These modes produce no resultant loads (moment and shear) at the base of the tank, but they may contribute to them indirectly, through the nonlinear coupling with the beam-type modes of the structure. The choice of the rotational spring, modeling the base uplift, may also be more complicated for broad tanks.

Another topic of practical interest is the analytical consideration of the effects of the vertical component of the ground excitation for an unanchored tank. The uplifting motion of the tank results - apart from the rocking - in a vertical

displacement of the tank, also. This, together with possible coupling of the axisymmetric shell modes with the beam-type modes, may have some important effects on the response of the system. These effects are expected to be pronounced in cases where the vertical component of the base excitation is relatively large and contains energy in important frequency ranges.

Finally, a topic which deserves further attention is the effect of large changes of the stiffness, occurring at the base of the tank, on the dynamic behavior of the system. Large changes in the structural stiffness may result in chaotic behavior of the structure. Such stiffness changes were found to happen in this work, due to the rotational flexibility of the shaking table and due to base uplifting. Although the former reason is associated with specific conditions of the experimental work cited, the latter is expected to be the general case for unanchored tanks. For such tanks, apart from the effects of the dramatic reduction of the frequency of the predominant response mode, one should also investigate the effect on the response to a real earthquake of a structure which is characterized by the possibility of exhibiting chaotic behavior. It is of practical importance to find out if this effect appears within the duration of an earthquake and how large or small is this effect compared to other unknowns about the problem, including the frequency content of the excitation. The study of the one degree-of-freedom oscillator with trilinear stiffness may help in understanding and explaining at least some aspects of the response of an unanchored tank. Thus, more extensive and comprehensive analyses should be carried out for this problem, in order to determine combinations of parameters for which this system possesses at least one stable periodic solution, for harmonic excitation. Then, it would be interesting to investigate the characteristics of the instability, for other combinations of the parameters.

7. References

1. Rinne, J.E., "Oil Storage Tanks," *The Prince William Sound, Alaska Earthquake of 1964 and Aftershocks*, U.S. Dept. of Commerce, E.S.S.A., Coast and Geodetic Survey, Washington, DC, Vol. II, Part A, pp.245-252, 1967.
2. Hanson, R.D., "Behavior of Liquid-Storage Tanks," *The Great Alaska Earthquake of 1964 (Engr. Section)*, National Academy of Sciences, Washington, DC, pp. 331-339, 1973.
3. Jennings, P.C. (ed.), "Engineering Features of the San Fernando Earthquake," Report No. EERL 71-02, Caltech, Pasadena, CA, pp. 434-470, 1971.
4. Moore, T.A. and Wong, E.K., "The Response of Cylindrical Liquid Storage Tanks to Earthquakes," *Proc. 8th World Conf. Earthq. Engr.*, San Francisco, CA, Vol. 5, pp. 239-246, 1984.
5. Manos, G.C. and Clough, R.A., "Tank Damage During the May 1983 Coalinga Earthquake," *Earthq. Engr. Struct. Dyn., Vol. 13, pp. 449-466, 1985.*
6. Hoskins, L.M. and Jacobsen, L.S., "Water Pressure in a Tank Caused by a Simulated Earthquake," *Bull. Seism. Soc. America*, Vol. 24, pp. 1-32, 1934.
7. Jacobsen, L.S., "Impulsive Hydrodynamics of Fluid Inside a Cylindrical Tank and of a Fluid Surrounding a Cylindrical Pier," *Bull. Seism. Soc. America*, Vol. 39, pp. 189-204, 1949.
8. Housner, G.W., "Dynamic Pressures on Accelerated Fluid Containers," *Bull. Seism. Soc. America*, Vol. 47, No. 1, pp. 15-35, 1957.
9. Housner, G.W., "The Dynamic Behavior of Water Tanks," *Bull. Seism. Soc. America*, Vol. 53, No. 1, pp. 381-387, 1963.
10. Baron, M.L. and Skalak, R., "Free Vibrations of Fluid-Filled Cylindrical Shells," *J. Engr. Mech., ASCE*, Vol. 88, No. EM3, pp. 17-43, 1962.
11. Edwards, N.W., "A Procedure for the Dynamic Analysis of Thin Walled Cylindrical Liquid Storage Tanks Subjected to Lateral Ground Motion," *Ph.D. Dissertation*, Un. Michigan, Ann Arbor, 1969.
12. Arya, A.S., Thakkar, S.K. and Goyal, A.C., "Vibration Analysis of Thin Cylindrical Containers," *J. Engr. Mech. Div., ASCE*, Vol. 97, No. EM2, pp. 317-331, 1971.
13. Hsiung, H.C.H. and Weingarten, V.I., "Dynamic Analysis of Hydroelastic Systems Using the Finite Element Method," Dept. CE USC, Report No. USCCE 013, 1973.
14. Wu, C.I., Mouzakis, T., Nash, W.A. and Colonell, J.M., "Natural Frequencies of Cylindrical Liquid Storage Containers," Un. Mass.Report No. NSF-RA-E-75-134, Amherst, MA, 1975.
15. Shaaban, S.H. and Nash, W.A., "Finite Element Analysis of a Seismically Excited Cylindrical Storage Tank, Ground Supported and Partially Filled with Liquid," Un. Mass., Report No. GI 39644-3, Amherst, MA, 1976.
16. Balendra, T. and Nash, W.A., "Earthquake Analysis of a Cylindrical Liquid Storage Tank with a Dome by the Finite Element Method," Report No. UMASS-ENV-76-14833-1, Amherst, MA, 1978.

17. Daysal, H. and Nash, W.A., "Soil-Structure Interaction Effects on the Response of Cylindrical Tanks to Base Excitation," Un. Mass. Tech. Report to NSF, Amherst, MA, 1982.

18. Liu, W.K. and Lam, D., "Nonlinear Analysis of Liquid-Filled Tanks," *J. Engr. Mech., ASCE, Vol. 109, No. 6, 1983.*

19. Veletsos, A.S., "Seismic Effects in Flexible Liquid Storage Tanks," *Proc. 5th World Conf. Earthq. Engr.*, Rome, Italy, Vol. 1, pp. 630-639, 1974.

20. Yang, J.Y., "Dynamic Behavior of Fluid-Tank Systems," *Ph.D. Dissertation*, Rice University, Houston, TX, 1976.

21. Veletsos, A.S. and Yang, J.Y., "Dynamics of Fixed-Base Liquid Storage Tanks," *U.S.-Japan Seminar for Earthq. Engr. Res.*, Tokyo, Japan, 1976.

22. Veletsos, A.S. and Turner, J.W., "Dynamics of Out-of-Round Liquid-Storage Tanks," *Proc. 3rd ASCE Eng. Mech. Div. Spec. Conf.*, Austin, TX, pp. 471-474, 1979.

23. Veletsos, A.S. and Kumar, Ashok, "Dynamic Response of Vertically Excited Liquid Storage Tanks," *Proc. 8th World Conf. Earthq. Engr.*, San Francisco, CA, Vol. 7, pp. 445-452, 1984.

24. Haroun, M.A., "Dynamic Analyses of Liquid Storage Tanks," *Ph.D. Thesis*, Report No. EERL 80-04, Caltech, Pasadena, CA, 1980.

25. Haroun, M.A. and Housner, G.W., "Seismic Damage of Unanchored Oil Storage Tanks," *International Convention of ASCE, 1981.*

26. Haroun, M.A., "Vibration Studies and Tests of Liquid Storage Tanks," *Earthq. Engr. Struct. Dyn., Vol. 11, pp. 179-206, 1983.*

27. Haroun, M.A. and Tayel, M.A., "Dynamic Behavior of Cylindrical Liquid Storage Tanks under Vertical Earthquake Excitation," *Proc. 8th World Conf. Earthq. Engr.*, San Francisco, CA, Vol. 7, pp. 421-428, 1984.

28. Shih, C.F. and Babcock, C.D., "Scale Model Buckling Tests of a Fluid Filled Tank Under Harmonic Excitation," *ASME Century 2 PVP Conf.*, 80-C2/PVP-66, San Francisco, CA, 1980.

29. Shih, C.F., "Failure of Liquid Storage Tanks Due to Earthquake Excitation," *Ph.D. Thesis*, Report No. EERL 81-04, Caltech, Pasadena, CA, 1981.

30. Shih, C.F. and Babcock, C.D., "Buckling of Oil Storage Tanks in SPPL Tank Farm During the 1979 Imperial Valley Earthquake," *1984 PVP Conf. Expos.*, ASME paper No. 84-PVP-74, San Antonio, TX, 1984.

31. Peek, R., "Analysis of Unanchored Liquid Storage Tanks Under Seismic Loads," *Ph.D. Thesis*, Caltech, Pasadena, CA, 1986.

32. Peek, R., Jennings, P.C. and Babcock, C.D., "The Preuplift Method for "Anchoring" Fluid Storage Tanks," *Proc. 3rd U.S. Nat. Conf. Earthq. Engr.*, Charleston, SC, 1986.

33. Clough, D.P., "Experimental Evaluation of Seismic Design Methods for Broad Cylindrical Tanks," Un. of California, Berkeley, Report No. UCB/EERC-77/10, 1977.

34. Niwa, A., "Seismic Behavior of Tall Liquid Storage Tanks," Un. of California, Berkeley, Report No. UCB/EERC-78/04, 1978.

35. Clough, R.W. and Niwa, A., "Static Tilt Tests of a Tall Cylindrical Liquid Storage Tank," Un. of California, Berkeley, Report No. UCB/EERC-79/06, 1979.

36. Cambra, F.J., "Earthquake Response Considerations of Broad Liquid Storage Tanks," Un. of California, Berkeley, Report No. UCB/EERC-82/25, 1982.

37. Manos, G.C. and Clough, R.W., "Further Study of the Earthquake Response of a Broad Cylindrical Liquid Storage Tank Model," Un. of California, Berkeley, Report No. UCB/EERC-82/07, 1982.

38. Niwa, A. and Clough, R.W., "Buckling in Seismic Response of Cylindrical Liquid Storage Tanks," *Proc. 7th European Conf. Earthq. Engr.*, Athens, Greece, Vol. 6, pp. 223-232, 1982.

39. Marchaj, T.J., "Importance of Vertical Acceleration in the Design of Liquid Containing Tanks," *Proc. 2nd U.S. Nat. Conf. Earthq. Engr.*, Stanford, CA, 1979.

40. Fischer, D.F. and Rammerstorfer, F.G., "Stability of Liquid Storage Tanks under Earthquake Excitation," *Proc. 8th World Conf. Earthq. Engr.*, San Francisco, CA, Vol. 5, pp. 215-222, 1984.

41. Auli, W., Fischer, D.F. and Rammerstorfer, F.G., "Uplifting of Earthquake-Loaded Liquid-Filled Tanks," *1985 PVP Conf., ASME*, New Orleans, LA, 1985.

42. Ishida, K. and Kobayashi, N., "An Effective Method of Analyzing Rocking Motion for Unanchored Cylindrical Tanks Including Uplift," *1985 PVP Conf., ASME*, New Orleans, LA, 1985.

43. Kondo, H., "Axisymmetric Free Vibration Analysis of a Circular Cylindrical Tank," *Bull. JSME*, Vol. 24, No. 187, pp. 215-221, 1981.

44. Fujita, K., "A Seismic Response Analysis of a Cylindrical Liquid Storage Tank Including the Effect of Sloshing," *Bull. JSME*, Vol. 24, No. 195, pp. 1634-1641, 1981.

45. Zui, H. and Shinke, T., "Seismic Response Analysis of Cylindrical Tanks with Initial Irregularities on Side Walls," *1984 PVP Conf. Exhib.*, ASME paper No. 84-PVP-70, San Antonio, TX, 1984.

46. Guo, H. and Qin, N.-X., "Axisymmetric Uplift Mechanism of a Cylindrical Liquid Storage Tank," 1983 Int. Symp. Lifeline Earthq. Engr., *4th Nat. Congr. PVP Tech.*, Portland, OR, pp. 102-106, 1983.

47. Chen, G.-Q., "Why the "Elephant's Foot" Phenomenon of Liquid Storage Tank Happened," *Proc. 8th World Conf. Earthq. Engr.*, San Francisco, CA, Vol. 7, pp. 445-452, 1984.

48. Wozniak, R.S. and Mitchell, W.W., "Basis of Seismic Response Provisions for Welded Oil Storage Tanks," *API Convention*, Toronto, Canada, 1978.

49. Anon, "Welded Steel Tanks for Oil Storage," *API Standard 650*, 6th Edition, Revision 3, American Petroleum Institute, Washington, DC, 1979.

50. Anon, "AWWA Standard for Welded Steel Tanks for Water Storage," *ANSI/AWWA Standard D100-84*, American Water Works Association, Denver, CO, 1984.

51. Cooper, R.M., "Dynamics of Liquids in Moving Containers," *ARS J.*, Vol. 30, No. 8, pp. 725-729, 1960.

52. Abramson, H.N. (ed.), "The Dynamic Behavior of Liquids in Moving Containers," *NASA SP-106*, 1966.

53. Abramson, H.N., Chu, W.H. and Kana, D.D., "Some Studies of Nonlinear Lateral Sloshing in Rigid Containers," *J. Appl. Mech.*, pp. 777-784, 1966.

54. Kana, D.D., "Seismic Response of Flexible Cylindrical Liquid Storage Tanks," *Nucl. Engr. Des.*, Vol. 52, pp. 185-199, 1979.

55. Abramson, H.N., Chu, W.H. and Ransleben, Jr., G.E., "Representation of Fuel Sloshing in Cylindrical Tanks by an Equivalent Mechanical Model," *ARS J.*, Vol. 31, pp. 1697-1705, 1961.

56. Schmitt, A.F., "Forced Oscillations of a Fluid in a Cylindrical Tank Undergoing Both Translation and Rotation," *Convair Astronautics*, Report ZU-7-069, 1956.

57. Hutton, R.E., "An Investigation of a Resonant, Nonlinear, Nonplanar Free Surface Oscillations of a Fluid," *NASA TN D-1870*, 1963.

58. Bauer, H.F., "Fluid Oscillations in the Containers of a Space Vehicle and Their Influence upon Stability," *NASA TR R-187*, 1964.

59. Graham, E.W. and Rodriguez, A.M., "The Characteristics of Fuel Motion which Affect Airplane Dynamics," *J. Appl. Mech.*, Vol. 19, pp. 381-388, 1952.

60. Miles, J.W., "On the Sloshing of Liquid in a Flexible Tank," *J. Appl. Mech.*, Vol. 25, pp. 277-283, 1958.

61. Whitman, R.V. and Richart, F.E., Jr., "Design Procedures for Dynamically Loaded Foundations," *J. Soil Mech. Found. Div.*, ASCE, Vol. 93, No. SM6, pp. 169-193, 1967.

62. Richart, F.E., Jr., Hall, J.R. and Woods, R.D., "Vibrations of Soils and Foundations," *Prentice Hall, Inc.*, Englewood Cliffs, N.J., 1970.

63. Veletsos, A.S. and Wei, Y.T., "Lateral and Rocking Vibration of Footings," *J. Soil Mech. Found. Div.*, ASCE, Vol. 97, pp. 1227-1248, 1971.

64. Tsai, N.C., Niehoff, D., Swatta, M. and Hadjian, A.H., "The Use of Frequency-Independent Soil-Structure Interaction Parameters," *Nucl. Engr. Des.*, Vol. 31, No. 2, pp. 168-185, 1974.

65. Bushnell, D., "BOSOR5 - Program for Buckling of Elastic-Plastic Complex Shells of Revolution Including Large Deflections and Creep," *Computers and Structures*, Vol. 6, No. 3-E, pp. 221-239, 1976.

66. Thompson, J.M.T. and Ghaffari, R., "Complex Dynamics of Bilinear Systems: Bifurcational Instabilities Leading to Chaos," *Collapse*, Thompson, J.M.T. and Hunt, G.W. (eds), 1982 IUTAM Symposium, Cambridge Un. Press, Cambridge, pp. 161-174, 1983.

67. Holmes, P., "A Nonlinear Oscillator with a Strange Attractor," *Philosophical Transactions of the Royal Society of London*, Ser. A, Vol. 292, pp. 418-448, 1979.

68. Ott, E., "Strange Attractors and Chaotic Motions of Dynamic Systems," *Reviews of Modern Physics*, Vol. 53, No. 4, Part I, pp. 655-671, 1981.

69. Eckmann, J.P., "Roads to Turbulence in Dissipative Systems," *Reviews of Modern Physics*, Vol. 53, No. 4, Part I, pp. 643-654, 1981.

70. Dowell, E.H. and Pezeshki, C., "On the Understanding of Chaos in Duffing's Equation Including a Comparison with Experiment," *J. Appl. Mech.*, Vol. 53, pp. 5-9, 1986.

Appendix A

SOLUTION OF SET OF EQUATIONS (2.6)-(2.10)

A.1. Separation of Variables.

Seek solution of the form:

$$\Phi_n(r,z,t) = \bar{R}_n(r)\, Z_n(z)\, T_n(t) \quad .$$

Substituting in equation (2.6) it is found that:

$$\frac{1}{r\bar{R}_n}\frac{d}{dr}\left(r\frac{d\bar{R}_n}{dr}\right) - \frac{n^2}{r^2} + \frac{1}{Z_n}\frac{d^2Z_n}{dz^2} = 0 \qquad \text{(A.1)}$$

Since the last term depends only on z, while the first two terms are functions of r, the last term must be equal to a constant c_n, that is:

$$\frac{1}{Z_n}\frac{d^2Z_n}{dz^2} = c_n \quad .$$

Depending on the sign of this constant one must consider the following three cases:

a. $c_n=0$. Then,

$$Z_n(z) = A_n\, z + B_n$$

and equation (A.1) becomes:

$$\frac{d}{dr}\left(r\frac{d\bar{R}_n}{dr}\right) - \frac{n^2}{r}\bar{R}_n = 0 \quad ,$$

with solution:

$$\bar{R}_n(r) = E_n\, r^n + F_n\, r^{-n} \quad .$$

Requiring bounded solution at r=0, choose $F_n=0$.

b. $c_n = -\, l_n^2 < 0$. Then,

$$Z_n(z) = C_n \cos(l_n z) + D_n \sin(l_n z)$$

and equation (A.1) becomes

$$\frac{d}{dr}(r\,\frac{d\bar{R}_n}{dr}) - (l_n^2 r + \frac{n^2}{r})\bar{R}_n = 0 \ ,$$

with solution

$$\bar{R}_n(r) = G_n\, I_n(l_n r) + H_n\, K_n(l_n r) \ ,$$

where I_n and K_n are the modified Bessel functions of the first and second kind, respectively, of order n. Since K_n has a logarithmic singularity at r=0, choose H_n=0. Also, to make use of the orthogonality properties of the trigonometric functions in $0 \leq z \leq H$, choose: $l_n = \frac{\lambda_{ns}}{H}$, with $\lambda_{ns} = 2s\pi$ and s = 1 , 2 , ...

c. $c_n = k_n^2 > 0$. Then,

$$Z_n(z) = P_n \cosh(k_n z) + Z_n \sinh(k_n z)$$

and equation (A.1) becomes

$$\frac{d}{dr}\,(r\,\frac{d\bar{R}_n}{dr}) + (k_n^2 r - \frac{n^2}{r})\,\bar{R}_n = 0 \ ,$$

with solution

$$\bar{R}_n(r) = U_n\, J_n(k_n r) + V_n\, Y_n(k_n r) \ ,$$

where J_n and Y_n are the Bessel functions of the first and second kind, respectively, of order n. To avoid the logarithmic singularity of Y_n at r=0, choose V_n=0. Then,

$$\bar{R}_n(r) = U_n\, J_n(k_n r) \ .$$

Applying the boundary conditions (2.8), (2.9) in homogeneous form:

$$\begin{aligned} Z_n(0) = 0 \quad &\rightarrow \quad Z_n(z) = P_n \cosh(k_n z) \\ \bar{R}(R) = 0 \quad &\rightarrow \quad k_n\, J_n'(k_n R) = 0 \end{aligned}$$

So, if k_{ns} are the roots of $J_n'(\cdot) = 0$, it must be $k_n = \frac{k_{ns}}{R}$. Finally, assuming harmonic time dependence for the solution, i.e., $T_n(t) = W_n \sin(\omega_n t)$, it follows from (2.7) that:

$$\omega_n^2 = g\, k_n \tanh(k_n H) \quad .$$

Summarizing, after proper rearrangement of the constants - which in this case can be functions of time because of the form of the differential equation - the general solution of the set of equations (2.6-2.10) is written in the following form:

$$\Phi_n(r,z,t) = (\frac{r}{R})^n \left[a_n(t)\, \frac{z}{H} + b_n(t)\right] +$$

$$+ \sum_{s=1}^{\infty} \{J_n(k_{ns}\, \frac{r}{R}) \left[A_{ns}(t) \cosh(k_{ns}\, \frac{z}{R}) + B_{ns}(t) \sinh(k_{ns}\, \frac{z}{R})\right] +$$

$$+ I_n(\lambda_{ns}\, \frac{r}{H}) \left[C_{ns}(t) \cos(\lambda_{ns}\, \frac{z}{H}) + D_{ns}(t) \sin(\lambda_{ns}\, \frac{z}{H})\right]\} \qquad \text{(A.2)}$$

where

$$J_n'(k_{ns}) = 0$$
$$\lambda_{ns} = 2s\pi \qquad n=0,1,2,\cdots$$

$$\text{and} \quad \omega_{ns}^2 = \frac{g k_{ns}}{R} \tanh(k_{ns}\, \frac{H}{R}) \quad .$$

A.2. General Solution.

Before attempting to determine the unknowns in the expression for the general solution Φ_n, as given by (A.2), some appropriate changes are first performed. In order to associate all the sloshing effects with one term of the solution, it is found appropriate to substitute z by (z-H) in the argument of sinh. Also, in order to avoid any confusion - as it will become obvious when applying (2.9) - it is convenient to decompose the function h_n as:

$$h_n(z,t) = \alpha_n z + \bar{h}_n(z,t) \quad .$$

Finally, D_{ns} can be set equal to zero, by expanding $\bar{h}_n(z,t)$ evenly in [-H,0] and taking $\lambda_{ns}=s\pi$. Then, Φ_n can be rewritten as:

$$\Phi_n(r,z,t) = (\frac{r}{R})^n \left[a_n(t)\, \frac{z}{H} + b_n(t)\right] +$$

$$+ \sum_{s=1}^{\infty} \{J_n(k_{ns} \frac{r}{R}) [A_{ns}(t) \cosh(k_{ns} \frac{z}{R}) + B_{ns}(t) \sinh(k_{ns} \frac{z-H}{R})] +$$

$$+ I_n(\lambda_s \frac{r}{H}) C_{ns}(t) \cos(\lambda_s \frac{z}{H})\} \tag{A.3}$$

with $\lambda_s = s\pi$.

Application of (2.9), leads to the following equation:

$$\frac{n}{R}(a_n \frac{z}{H} + b_n) + \sum_{s=1}^{\infty} \left[\frac{\lambda_s}{H} I_n'(\lambda_s \frac{R}{H}) C_{ns} \cos(\lambda_s \frac{z}{H}) \right] = \alpha_n z + \bar{h}_n(z,t) \ .$$

Choosing

$$a_n(t) = \frac{\alpha_n RH}{n} \tag{A.4}$$

and using the orthogonality properties of the cosine function in [-H,H]:

$$b_n(t) = \frac{R}{nH} \int_o^H \bar{h}_n(z,t)\, dz \tag{A.5}$$

$$C_{ns}(t) = \frac{2}{\lambda_s I_n'(\lambda_s \frac{R}{H})} \int_o^H \bar{h}_n(z,t) \cos(\lambda_s \frac{z}{H})\, dz \tag{A.6}$$

for n = 1, 2, ... and

$$a_o(t) = b_o(t) = 0. \tag{A.7}$$

The need for decomposing h_n is now clear. Otherwise, there would be a problem in determining $a_n(t)$, since z has its own Fourier components in the $\{\cos(\lambda_s \frac{z}{H})\}$ sequence. Next, the boundary condition (2.8) is applied, which results in:

$$(\frac{r}{R})^n \frac{a_n}{H} + \sum_{p=1}^{\infty} \{J_n(k_{np} \frac{r}{R}) B_{np} \cos(k_{np} \frac{H}{R})\} = f_n(r,t) \ .$$

Then, making use of the following properties of the Bessel functions:

$$\int_o^R r\, J_n(k_{ns} \frac{r}{R}) J_n(k_{np} \frac{r}{R})\, dr = \begin{cases} \frac{R^2}{2}(1 - \frac{n^2}{k_{ns}^2}) J_n^2(k_{ns}), & \text{for } s = p \\ 0, & \text{for } s \neq p \end{cases}$$

$$\int_o^R r^{n+1} J_n(k_{ns} \frac{r}{R})\, dr = \frac{R^{n+2}}{k_{ns}^2}\, n\, J_n(k_{ns})$$

$$\int_o^R r^{n+1} I_n(k_{ns} \frac{r}{R})\, dr = \frac{R^{n+2}}{k_{ns}^2} [k_{ns}\, I_n'(k_{ns}) - n\, I_n(k_{ns})]$$

$$\int_o^R r\, J_n(k_{ns} \frac{r}{R})\, I_n(\lambda_p \frac{r}{H})\, dr = R^2\, J_n(k_{ns}) \frac{(\lambda_p \frac{R}{H})\, I_n'(\lambda_p \frac{R}{H})}{k_{ns}^2 + (\lambda_p \frac{R}{H})^2}$$

where $J_n'(k_{ns})=0$, it is found that:

$$B_{ns}(t) = 2R^2 \frac{b_{ns}(t) - a_n(t)\, J_n(k_{ns})}{k_{ns}\, (k_{ns}^2-n^2)\, J_n^2(k_{ns})\, \cosh(k_{ns} \frac{H}{R})} \tag{A.8}$$

$$b_{ns}(t) = (\frac{k_{ns}^2}{R^3}) \int_o^R r\, J_n(k_{ns} \frac{r}{R})\, f_n(r,t)\, dr \ .$$

Application of (2.7) results in:

$$(\frac{r}{R})^n\, (\ddot{a}_n + \ddot{b}_n + g\frac{a_n}{H}) + \sum_{p=1}^{\infty} \{J_n(k_{np} \frac{r}{R}) [\ddot{A}_{np} \cosh(k_{np} \frac{H}{R}) +$$

$$+ g\frac{k_{np}}{R} \sinh(k_{np} \frac{H}{R})\, A_{ns} + g\frac{k_{np}}{R}\, B_{np}] + (-1)^p\, I_n(\lambda_p \frac{r}{H})\, \ddot{C}_{np}\} = 0 \ .$$

Finally, applying the properties of the Bessel functions given above for $J_n'(k_{np}) = 0$, this equation can be rewritten as:

$$\ddot{A}_{ns} + \omega_{ns}^2 A_{ns} = \ddot{D}_{ns}(t) - \omega_{ns}^2 E_{ns}(t)$$

where,

$$E_{ns}(t) = \frac{2\, n\, a_n(t)}{\mu_{ns}\, (k_{ns}^2-n^2)\, J_n(k_{ns})\, \sinh(\mu_{ns})} + \frac{B_{ns}(t)}{\sinh(\mu_{ns})} \tag{A.9}$$

$$D_{ns}(t) = -\, 2\, \frac{n\, [a_n(t)+b_n(t)] + d_{ns}(t)}{(k_{ns}^2-n^2)\, J_n(k_{ns})\, \cosh(\mu_{ns})} \tag{A.10}$$

$$d_{ns}(t) = \sum_{p=1}^{\infty} \left[(-1)^p\, \frac{(\lambda_p \frac{R}{H})\, I_n'(\lambda_p \frac{R}{H})}{1+(\lambda_p/\mu_{ns})^2}\, C_{np}(t) \right] \quad \text{and} \quad \mu_{ns} = k_{ns} \frac{H}{R} \ .$$

Using the initial conditions (2.10), it is then found that:

$$A_{ns}(t) = D_{ns}(t) - \omega_{ns} \int_{o}^{t} [E_{ns}(\tau) + D_{ns}(\tau)] \sin\omega_{ns}(t-\tau)\, d\tau \qquad (A.11)$$

with,

$$\omega_{ns}^2 = \frac{gk_{ns}}{R} \tanh(\mu_{ns}) \quad , \quad \lambda_s = s\pi \quad \text{and} \quad J_n'(k_{ns}) = 0 \quad .$$

Therefore, the time functions in the form (A.3) of the general solution Φ_n are determined to be as given by equations (A.5-A.11).

Appendix B

EXPRESSIONS FOR TANK BASE MOMENT AND SHEAR

$$q_x = 1 - \sum_{s=1}^{\infty} q_{xs}\,, \quad q_{xs} = 2\frac{R}{H}\frac{\tanh(\mu_s)}{k_s\,(k_s^2-1)}$$

$$\beta_x = \frac{1}{2} - \sum_{s=1}^{\infty} \beta_{xs}\,, \quad \beta_{xs} = 2\left(\frac{R}{H}\right)^2 \frac{\mu_s \sinh(\mu_s) - \cosh(\mu_s) + 1}{k_s^2\,(k_s^2-1)\cosh(\mu_s)}$$

$$\gamma_x = \left(\frac{R}{2H}\right)^2 - \sum_{s=1}^{\infty} \gamma_{xs}\,, \quad \gamma_{xs} = \left(\frac{R}{H}\right)^2 \frac{2}{k_s^2\,(k_s^2-1)\cosh(\mu_s)}$$

$$q_\phi = \frac{H}{2R} + \frac{cR}{4H} - \sum_{s=1}^{\infty} q_{\phi s}\,, \quad q_{\phi s} = c_{\phi s}\, q_{xs}$$

$$\beta_\phi = \frac{H}{3R} + \frac{R}{4H} - 2\left(\frac{R}{H}\right)^2 \sum_{s=1}^{\infty}\left[\frac{(\mu_s^2-c-1)\sinh(\mu_s) + (c+2)\mu_s}{k_s^3\,(k_s^2-1)\cosh(\mu_s)}\right], \quad \beta_{\phi s} = c_{\phi s}\, \beta_{xs}$$

$$\gamma_\phi = 2\left(\frac{R}{H}\right)^2 \sum_{s=1}^{\infty}\left[\frac{(c+1)\sinh(\mu_s)-\mu_s}{k_s^3\,(k_s^2-1)\cosh(\mu_s)}\right], \quad \gamma_{\phi s} = c_{\phi s}\, \gamma_{xs}$$

$$q_m = \alpha_{mo} - \sum_{s=1}^{\infty} q_{ms}\,, \quad q_{ms} = S_{ms}\, q_{xs}$$

$$\beta_m = \frac{\alpha_{mo}}{2} + \sum_{s=1}^{\infty}\left[2\alpha_{ms} r_s(R)\frac{\cos\lambda_s - 1}{\lambda_s^2} - \beta_{ms}\right], \quad \beta_{ms} = S_{ms}\, \beta_{xs}$$

$$\gamma_m = \alpha_{mo}\left(\frac{R}{2H}\right)^2 + \sum_{s=1}^{\infty}\left[2\alpha_{ms}\frac{1-r_s(R)}{\lambda_s{}^2} - \gamma_{ms}\right], \quad \gamma_{ms} = S_{ms}\, \gamma_{xs}$$

The symbols appearing in the above expressions are defined in chapter 2.

Appendix C

STRAIN ENERGY OF A CIRCULAR CYLINDRICAL SHELL

The strain energy of a circular cylindrical shell is given by:

$$U_c = \frac{1}{2} \int_o^L \int_o^{2\pi} \int_{-t_s/2}^{t_s/2} (\sigma_z \epsilon_z + \sigma_\theta \epsilon_\theta + \sigma_{z\theta} \gamma_{z\theta}) \, dr \, R d\theta \, dz \ .$$

If the shell stresses are linearly related to the strains by Hooke's law, then,

$$\sigma_z = \frac{E}{1-\nu^2} (\epsilon_z + \nu \epsilon_\theta) \ , \quad \sigma_\theta = \frac{E}{1-\nu^2} (\epsilon_\theta + \nu \epsilon_z) \quad \text{and} \quad \sigma_{z\theta} = \frac{E}{2(1+\nu)} \gamma_{z\theta} \ .$$

The strains ϵ_z, ϵ_θ and $\gamma_{z\theta}$ in an element at a distance z from the middle-surface of the shell wall are related to the middle-surface principal strains ϵ_1, ϵ_2 and γ_{12} and to the changes of the curvatures and twist k_1, k_2 and k_{12} by the expressions:

$$\epsilon_z = \epsilon_1 + z k_1 \ , \quad \epsilon_\theta = \epsilon_2 + z k_2 \quad \text{and} \quad \gamma_{z\theta} = \gamma_{12} + 2 z k_{12} \ .$$

Then, assuming constant shell thickness t_s over the length L, the strain energy expression can be rewritten as:

$$U_c = \frac{REt_s}{2(1-\nu^2)} \int_o^L \int_o^{2\pi} (\epsilon_1^2 + \epsilon_2^2 + 2\nu \epsilon_1 \epsilon_2 + \frac{1-\nu}{2} \gamma_{12}^2) \, d\theta \, dz +$$

$$+ \frac{REt_s^3}{24(1-\nu^2)} \int_o^L \int_o^{2\pi} [k_1^2 + k_2^2 + 2\nu k_1 k_2 + 2(1-\nu) k_{12}^2] \, d\theta \, dz \qquad \text{(C.1)}$$

The first integral term in the above expression represents the stretching energy of the shell, while the second term represents the bending energy of the shell. Keeping only the linear terms in the formulae relating the middle-surface strains to the corresponding displacements one can write:

$$\epsilon_1 = \frac{\partial u_z}{\partial z} \ , \quad \epsilon_2 = \frac{1}{R} (\frac{\partial u_\theta}{\partial \theta} + u_r) \ , \quad \gamma_{12} = \frac{\partial u_\theta}{\partial z} + \frac{1}{R} \frac{\partial u_z}{\partial \theta} \ ,$$

$$k_1 = -\frac{\partial^2 u_r}{\partial z^2}\ , \quad k_2 = \frac{1}{R^2}\left(\frac{\partial u_\theta}{\partial \theta} - \frac{\partial^2 u_r}{\partial \theta^2}\right) \text{ and } \quad k_{12} = \frac{1}{R}\left(\frac{\partial u_\theta}{\partial z} - \frac{\partial^2 u_r}{\partial z \partial \theta}\right)\ .$$

Substituting into (C.1), the final form of the shell strain energy is found to be:

$$U_c = \frac{REt_s}{2(1-\nu^2)} \int_o^L \int_o^{2\pi} \left[\left(\frac{\partial u_z}{\partial z}\right)^2 + \frac{1}{R^2}\left(\frac{\partial u_\theta}{\partial \theta} + u_r\right)^2 + \right.$$

$$+ \frac{2\nu}{R}\frac{\partial u_z}{\partial z}\left(\frac{\partial u_\theta}{\partial \theta} + u_r\right) + \frac{1-\nu}{2}\left(\frac{\partial u_\theta}{\partial z} + \frac{1}{R}\frac{\partial u_z}{\partial \theta}\right)^2 \Big]\, d\theta\, dz +$$

$$+ \frac{REt_s^3}{24(1-\nu^2)} \int_o^L \int_0^{2\pi} \left[\left(\frac{\partial^2 u_r}{\partial z^2}\right)^2 + \frac{1}{R^4}\left(\frac{\partial^2 u_r}{\partial \theta^2} - \frac{\partial u_\theta}{\partial \theta}\right)^2 + \right.$$

$$\left. + \frac{2\nu}{R^2}\frac{\partial^2 u_r}{\partial z^2}\left(\frac{\partial^2 u_r}{\partial \theta^2} - \frac{\partial u_\theta}{\partial \theta}\right) + \frac{2(1-\nu)}{R^2}\left(\frac{\partial^2 u_r}{\partial z \partial \theta} - \frac{\partial u_\theta}{\partial z}\right)^2 \right] d\theta\, dz\ .$$

Appendix D

ELEMENTS OF MATRIX EQUATION (3.19)

The elements of the mass matrix of equation (3.19) are found, as explained in section 3.7, to have the following form:

$$m_{\psi_i\psi_j} = \rho_l R^2 \int_o^H w_i(z)\, f_j(R,z)dz + R \int_o^L \rho_s t_s w_i(z) w_j(z)dz + w_i(L)w_j(L)\frac{m_r}{\pi}$$

$$m_{\psi_i\phi_u} = \rho_l R^2 \int_o^H w_i(z)\, f_u(R,z)dz + \int_o^H \rho_s t_s z w_i(z)dz + w_i(L)\frac{m_r H_r}{\pi R}$$

$$m_{\psi_i\phi_f} = \rho_l R^2 \int_o^H w_i(z)\, f_f(R,z)dz + \rho_l h_g R \int_o^H w_i(z)\, f_x(R,z)dz +$$

$$+ \int_o^L \rho_s t_s (z+h_g) w_i(z)dz + w_i(L)\frac{m_r(H_r+h_g)}{\pi R}$$

$$m_{\psi_i\xi_j} = m_{\xi_j\psi_i} = m_{\psi_i\varsigma_j} = m_{\varsigma_j\psi_i} = m_{\xi_i\varsigma_j} = m_{\varsigma_j\xi_i} = 0$$

$$m_{\xi_i\xi_j} = R \int_o^L \rho_s t_s v_i(z) v_j(z)dz\ ,\quad m_{\xi_i\phi_f} = \int_o^L \rho_s t_s (z+h_g) v_i(z)dz$$

$$m_{\xi_i\phi_u} = \int_o^L \rho_s t_s z v_i(z)dz\ ,\quad m_{\varsigma_i\varsigma_j} = R \int_o^L \rho_s t_s u_i(z) u_j(z)dz + u_i(L)u_j(L)\ \frac{I_r}{\pi R^2}$$

$$m_{\varsigma_i\phi_u} = m_{\phi_u\varsigma_i} = m_{\varsigma_i\phi_f} = m_{\phi_f\varsigma_i} = -\ R \int_o^L \rho_s t_s u_i(z)dz - u_i(L)\frac{I_r}{\pi R^2}$$

$$m_{\phi_u\psi_i} = \rho_l R H^2 \beta_i + \int_o^L \rho_s t_s z w_i(z)dz + w_i(L)\frac{m_r H_r}{\pi R}$$

$$m_{\phi_f\psi_i} = m_{\phi_u\psi_i} + \rho_l R H^2 \gamma_i + h_g[\rho_l R H q_i + \int_o^L \rho_s t_s w_i(z)dz + w_i(L)\frac{m_r}{\pi R}]$$

$$m_{\phi_u\phi_f} = \rho_l H^2 (R\beta_f + h_g \beta_x) + \frac{2}{R}\int_0^L \rho_s t_s z(z+h_g)dz + R \int_o^L \rho_s t_s dz + \frac{m_r H_r(H_r+h_g)+I_r}{\pi R^2}$$

$$m_{\phi_f\phi_u} = \rho_l RH^2(\beta_u+\gamma_u+\frac{h_g}{H}q_u) + R\int_o^L \rho_s t_s dz +$$

$$+ \frac{2}{R}\int_o^L \rho_s t_s(z+h_g)zdz + \frac{m_r H_r(H_r+h_g)+I_r}{\pi R^2}$$

$$m_{\phi_f\phi_f} = \rho_l RH^2[\beta_f+\gamma_f+\frac{h_g}{R}(\beta_x+\gamma_x)+\frac{h_g}{H}(q_f+\frac{h_g}{R}q_x)] + R\int_o^L \rho_s t_s dz +$$

$$+ \frac{2}{R}\int_o^L \rho_s t_s(z+h_g)^2dz + \frac{m_f h_f^2+I_f+m_b h_b^2+I_b+m_r(h_g+H_r)^2+I_r}{\pi R^2}$$

$$m_{\phi_u\phi_u} = \rho_l RH^2\beta_u + \frac{2}{R}\int_o^L \rho_s t_s z^2dz + R\int_o^L \rho_s t_s dz + \frac{(m_s+m_r)R^2+m_r H_r^2+I_r}{\pi R^2} \quad .$$

The β, γ and q's are defined in section 2.5 and their explicit forms are given in Appendix B. The subscript f indicates quantities which are evaluated by letting c=1, while the subscript u indicates quantities evaluated for arbitrary c. Generally, the notation used in the above expressions and those that follow, is consistent with that adopted chapters 2 and 3.

The elements of the stiffness matrix K are similarly found to be:

$$k_{\psi_i\psi_j} = \frac{2R^2C+D}{R^3}\int_o^L w_i(z)w_j(z)dz + DR\int_o^L w_i''(z)w_j''(z)dz +$$

$$+ \frac{2(1-\nu)}{R}D\int_o^L w_i'(z)w_j'(z)dz - \frac{\nu}{R}D\int_o^L [w_i(z)w_j''(z)+w_i''(z)w_j(z)]dz$$

$$k_{\psi_i\xi_j} = -\frac{2R^2C+D}{R^3}\int_o^L w_i(z)v_j(z)dz + \frac{\nu D}{R}\int_o^L w_i''(z)v_j(z)dz - \frac{2(1-\nu)D}{R}\int_o^L w_i'(z)v_j'(z)dz$$

$$k_{\psi_i\kappa_j} = 2\nu C\int_o^L w_i(z)u_j'(z)dz$$

$$k_{\xi_i\xi_j} = \frac{2R^2C+D}{R^3}\int_o^L v_i(z)v_j(z)dz + (1-\nu)\frac{R^2C+2D}{R}\int_o^L v_i'(z)v_j'(z)dz$$

$$k_{\xi_i\kappa_j} = -2\nu C\int_o^L v_i(z)u_j'(z)dz + (1-\nu)C\int_o^L v_i'(z)u_j(z)dz$$

$$k_{\varsigma_i\varsigma_j} = 2RC\int_o^L u_i(z)u_j'(z)dz + (1-\nu)\frac{C}{R}\int_o^L u_i(z)u_j(z)dz \ .$$

In all the above, prime stands for differentiation with respect to z, while:

$$C = \frac{Et_s}{2(1-\nu^2)} \quad \text{and} \quad D = \frac{Et_s^3}{12(1-\nu^2)}$$

are parameters associated with the membrane and the bending rigidity of the shell, respectively. Clearly, for the elements of K, $k_{ij} = k_{ji}$.

Next, for the components of the vector $\underset{\sim}{k}$, it is found that: $k_i \equiv 0$, except for k_{ϕ_f} and k_{ϕ_u}, which are given by:

$$k_{\phi_f} = \frac{M_f}{\pi R} \quad \text{and} \quad k_{\phi_u} = \frac{\bar{M}_c}{\pi R} \ .$$

The sloshing vector $\underset{\sim}{p}(t)$ is expressed by:

$$\underset{\sim}{p}(t) = \rho_l R^2 H \sum_{s=1}^{\infty}[\bar{\underset{\sim}{p}}_s \bar{A}_s(t)] \ ,$$

where the components of the vector $\bar{\underset{\sim}{p}}_s$ are given by

$$(\bar{\underset{\sim}{p}}_s)_{\psi_i} = \frac{1}{H}\int_o^H \bar{f}_s(R,z)\, w_i(z)dz$$

$$(\bar{\underset{\sim}{p}}_s)_{\xi_i} = (\bar{\underset{\sim}{p}}_s)_{\varsigma_i} = 0$$

$$(\bar{\underset{\sim}{p}}_s)_{\phi_f} = (H\beta_{xs} + h_g q_{xs} + H\gamma_{xs}) \,/\, R$$

$$(\bar{\underset{\sim}{p}}_s)_{\phi_u} = \frac{H}{R}\,\beta_{xs}$$

where β_{xs}, γ_{xs} and q_{xs} are defined in section 2.5 and the spectral acceleration $\bar{A}_s(t)$ in section 3.6.1.

Finally, the components of the forcing vector can be written as:

$$f_{\psi_i} = \rho_l R^2 \int_o^H f_x(R,z)w_i(z)dz + R\int_o^L \rho_s t_s w_i(z)dz + w_i(L)\frac{m_r}{\pi}$$

$$f_{\xi_i} = R\int_o^L \rho_s t_s v_i(z)dz \ , \quad f_{\varsigma_i} = 0$$

$$f_{\phi_f} = \rho_l R H^2(\beta_x+\gamma_x+\frac{h_g}{H}q_x) + 2\int_o^L \rho_s t_s(z+h_g)dz + \frac{m_f h_f+m_b h_b+m_r(h_g+H_r)}{\pi R}$$

$$f_{\phi_u} = \rho_l R H^2\beta_x + 2\int_o^L \rho_s t_s z dz + \frac{m_r H_r}{\pi R} \quad .$$

Clearly, the assumed spatial functions (w_m, v_m, u_m) appear only in the expressions of those elements in the equations of motion which are associated with the corresponding degrees-of-freedom ψ_m, ξ_m and ς_m.

Appendix E

DAMPING MATRIX FOR: $M \ddot{\underset{\sim}{x}} + K \underset{\sim}{x} = \underset{\sim}{f}$

For this system, a damping matrix D is chosen here in such a way that normal modes are preserved in the linear case, when the mass matrix M is not symmetric ($M \neq M^T$), but nonsingular, so that the matrix

$$A = M^{-1} K$$

can be defined. Then, if $\underset{\sim}{x}_i$, $\underset{\sim}{y}_i$ are the eigenvectors of A and its transpose A^T, respectively, corresponding to the same eigenvalue $\lambda_i=\omega_i^2$ and if the ordinary Euclidean inner product is used, it is found that

$$(A \underset{\sim}{x}_i, \underset{\sim}{y}_j) = \lambda_i(\underset{\sim}{x}_i, \underset{\sim}{y}_j) = (\underset{\sim}{x}_i, A^T \underset{\sim}{y}_j) = \lambda_j(\underset{\sim}{x}_i, \underset{\sim}{y}_j) \quad .$$

These imply that

$$(\lambda_i-\lambda_j)(\underset{\sim}{x}_i, \underset{\sim}{y}_j) = 0$$

and so, for the case of distinct eigenvalues

$$Y^T X = C \tag{E.1}$$

where X and Y are matrices containing as columns the eigenvectors $\underset{\sim}{x}_i$ and $\underset{\sim}{y}_i$, respectively, while C is a diagonal matrix with diagonal elements

$$c_i = (\underset{\sim}{x}_i, \underset{\sim}{y}_i) \quad .$$

Using the definition

$$A \underset{\sim}{x}_i = \lambda_i \underset{\sim}{x}_i$$

it is easily found that

$$K X = M X \Lambda \tag{E.2}$$

where Λ is the diagonal matrix containing the eigenvalues λ_i in its diagonal. Next, letting

$$\underset{\sim}{x} = X \, \underset{\sim}{q}(t) \, , \quad Y = M^T \, Z \, ,$$

choosing

$$D = M \, X \, \bar{D} \, X^{-1} \tag{E.3}$$

multiplying both sides of

$$M \, \ddot{\underset{\sim}{x}} + D \, \dot{\underset{\sim}{x}} + K \, \underset{\sim}{x} = \underset{\sim}{f}$$

by Z^T and using (E.1), (E.2) it is finally obtained that

$$M \, X \, [\ddot{\underset{\sim}{q}} + \bar{D} \, \dot{\underset{\sim}{q}} + \Lambda \, \underset{\sim}{q}] = \underset{\sim}{f} \, .$$

Clearly then, if $\bar{D}$ is chosen as a diagonal matrix, the last matrix equation can be decomposed into a system of uncoupled, scalar, second order ordinary differential equations.

Appendix F

FREE VIBRATIONS OF A BEAM ON A ROTATIONAL SPRING

Consider a flexural beam with length L, constant cross-section of area A and moment of inertia I with respect to the y-axis, Elasticity modulus E and mass density ρ. The beam displacement in the transverse z-direction is denoted by w(x,t), where x is the longitudinal axis and t stands for time. If this beam is supported at the end x=0 by a rotational spring of constant stiffness k and is free at the other end x=L, the equation of motion and the corresponding boundary conditions for no external load are as follows:

$$EI\,\frac{\partial^4 w}{\partial x^4} = -\rho A\,\frac{\partial^2 w}{\partial t^2} \tag{F.1}$$

$$w(0,t) = \frac{\partial^2 w}{\partial x^2}(L,t) = \frac{\partial^3 w}{\partial x^3}(L,t) = 0 \quad , \quad EI\,\frac{\partial^2 w}{\partial x^2}(0,t) = k\,\frac{\partial w}{\partial x}(0,t) \quad .$$

Employing separation of variables, a solution for (F.1) is obtained in the following form:

$$w(x,t) = [A\sin(\beta x) + B\cos(\beta x) + C\sinh(\beta x) + D\cosh(\beta x)]\, e^{i\omega t}$$

where A, B, C, D are constants and $\beta^4 = \frac{\rho A}{EI}\,\omega^2$.

Applying the boundary conditions it is eventually found that the following equation must be satisfied for a nontrivial solution w to exist:

$$\kappa[1 + \cos(p)\cosh(p)] + p[\cos(p)\sinh(p) - \sin(p)\cosh(p)] = 0 \tag{F.2}$$

where

$$\kappa = k/\bar{k}\,, \qquad p = (\omega/\bar{\omega})^{0.5}\,, \qquad \bar{k} = EI/L\,, \qquad \bar{\omega} = \frac{1}{L^2}\left[\frac{EI}{\rho A}\right]^{0.5} \quad .$$

Then, the eigenvalues ω of the system are found from (F.2) for every k.

Figure 1.2 Elephant-Foot-Bulge Buckling Mode (Ref. [3])

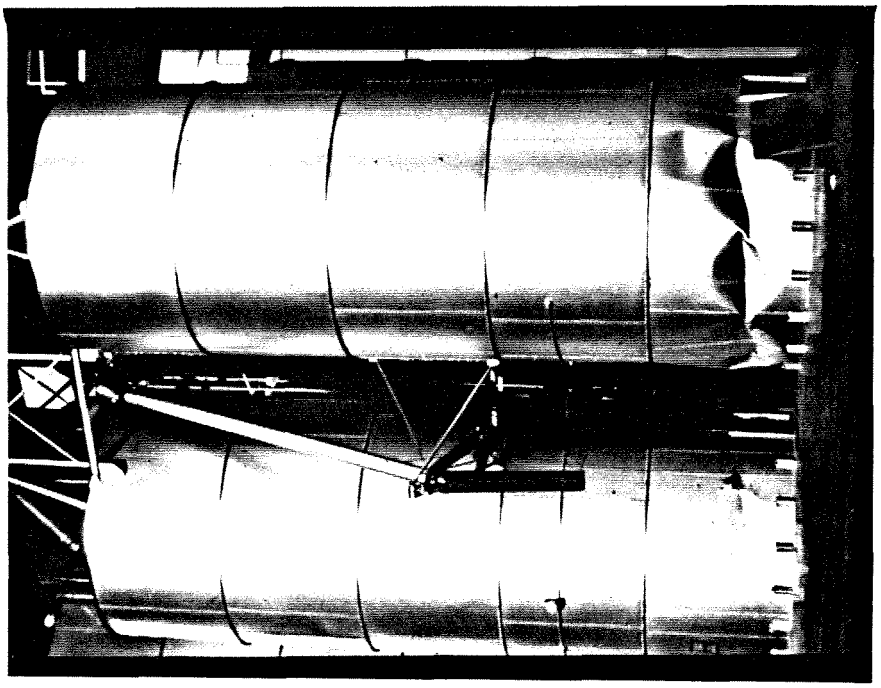

Figure 1.1 Diamond-Shaped Buckling Mode

Figure 1.3 Buckling at a Middle Section of a Tank

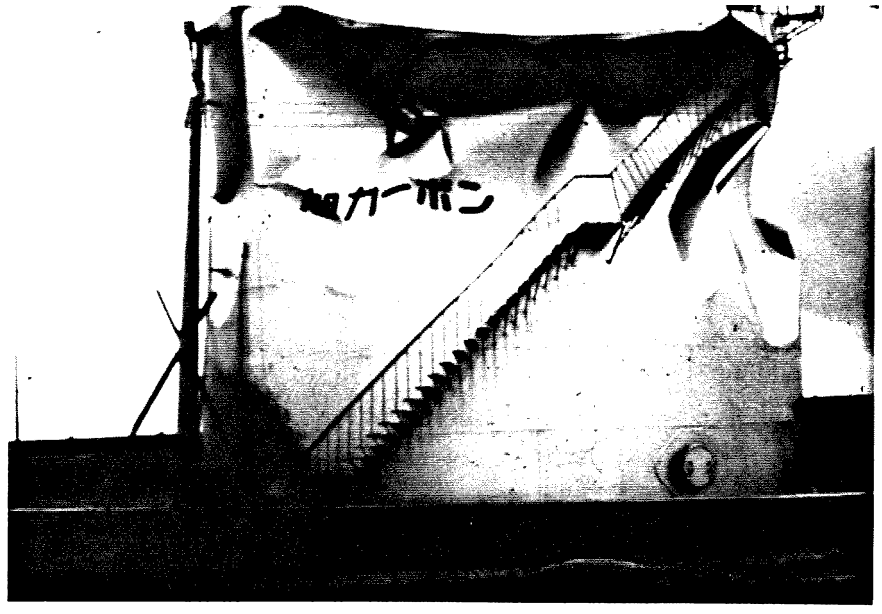

Figure 1.4 Buckling at the Top of a Tank (Niigata, Japan, 1964)

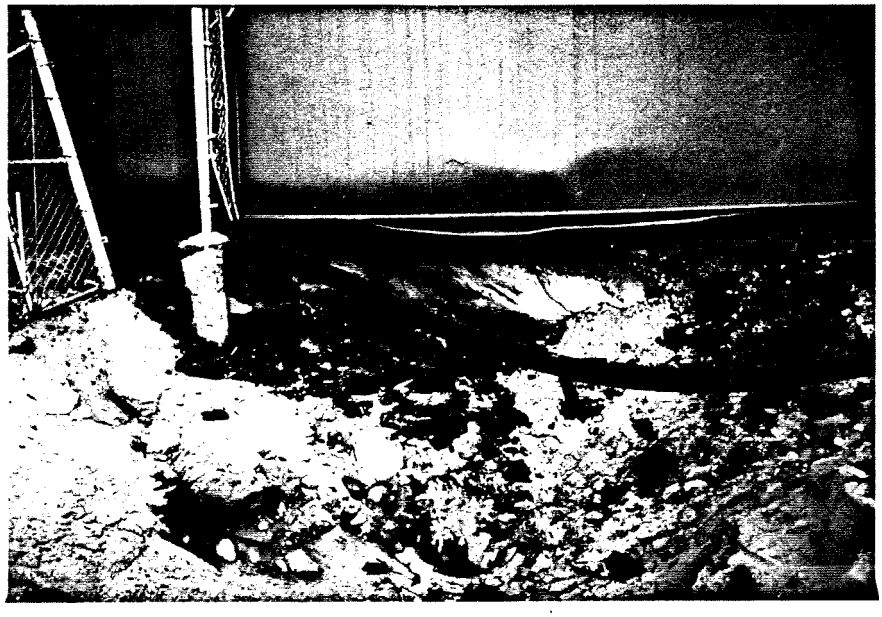

Figure 1.5 Rupture at the Shell / Bottom Plate Joint

Figure 1.6 Uplift at the Tank Bottom (San Fernando, 1971, Ref. [3])

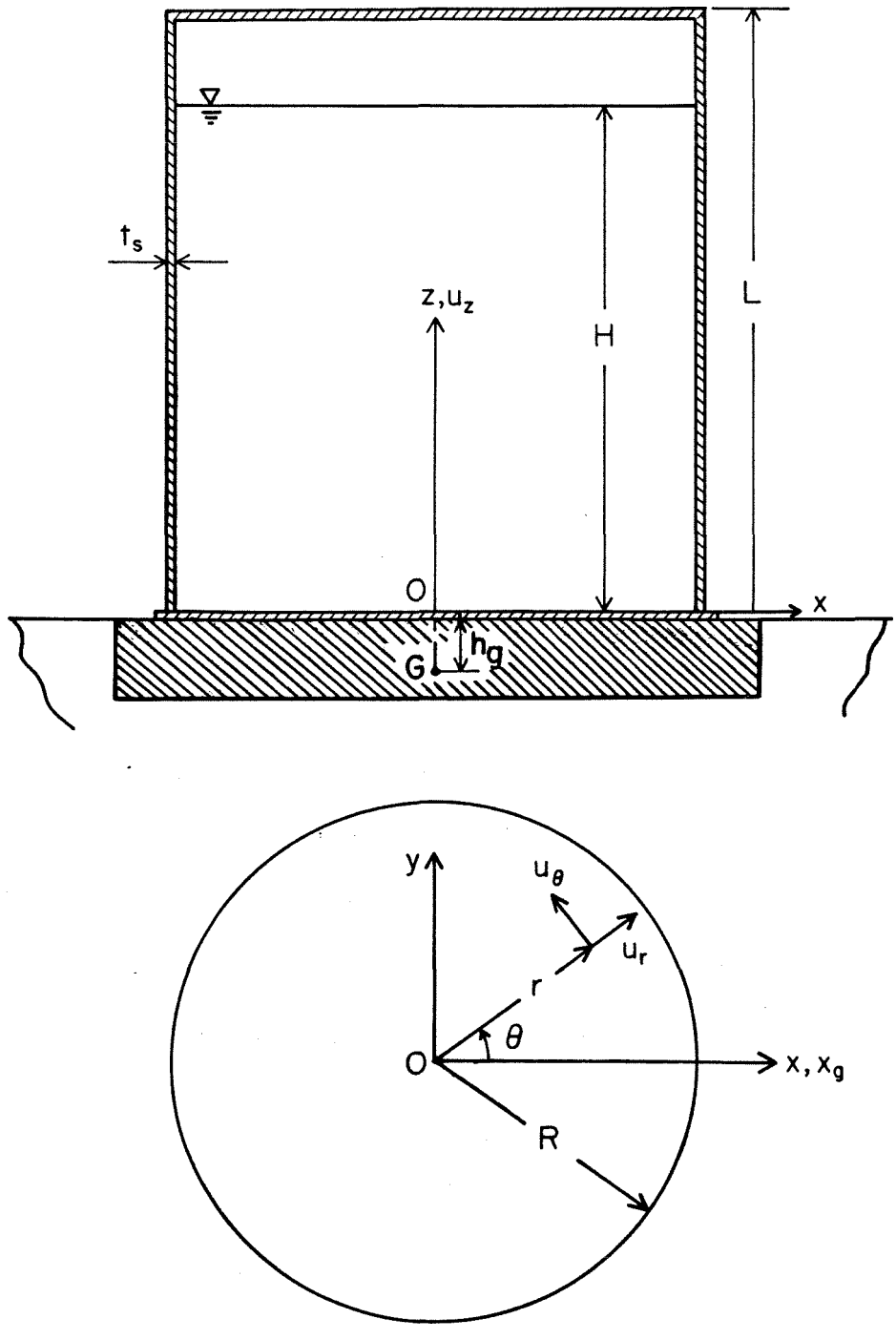

Figure 2.1 Coordinate System for a Cylindrical Tank

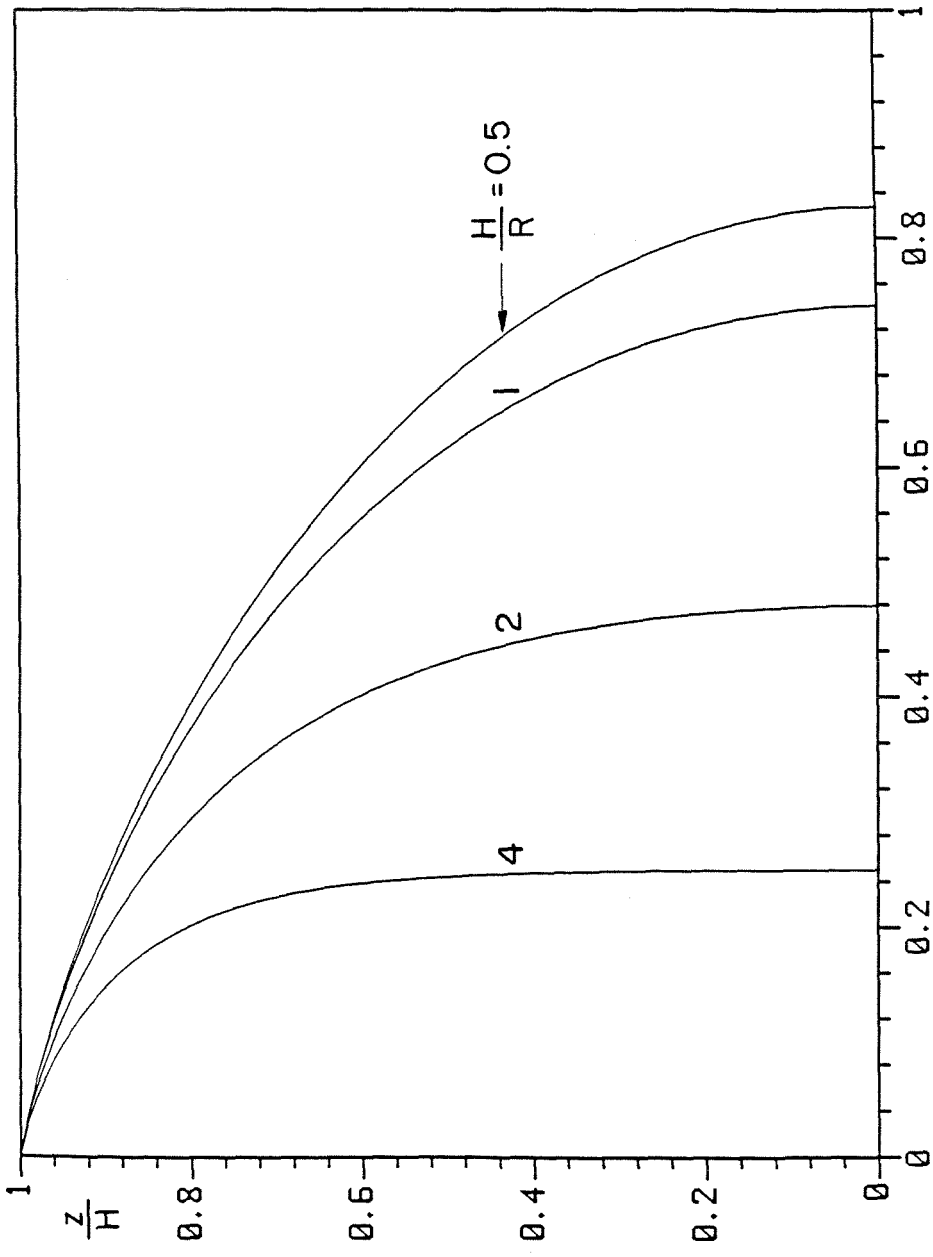

Figure 2.2.a Impulsive Pressure on Tank Wall (Translation)

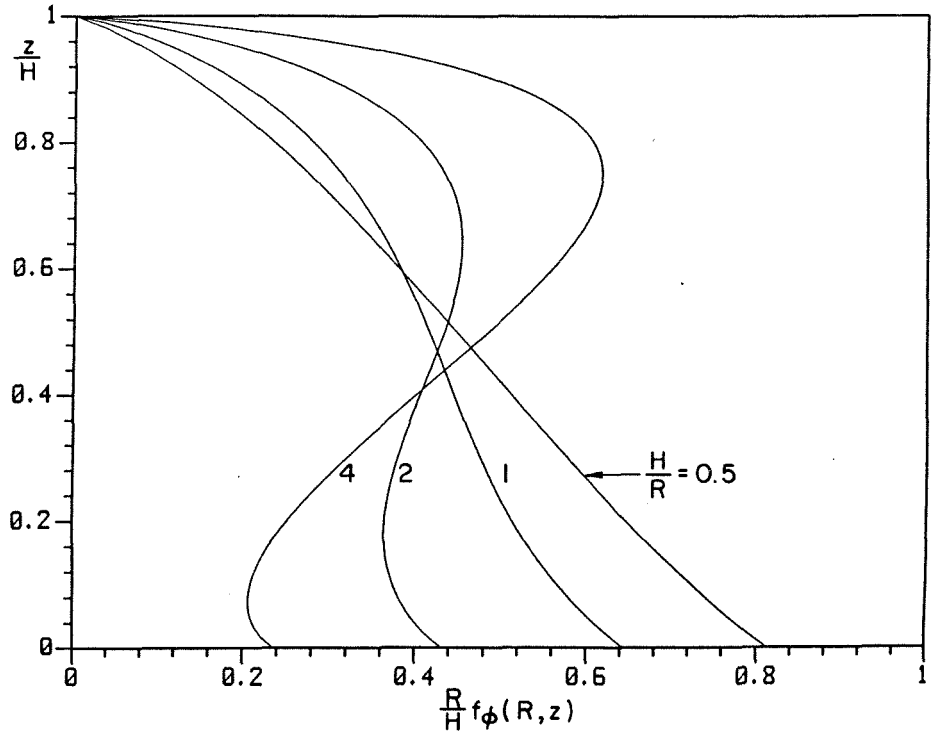

Figure 2.2.b Impulsive Pressure on Tank Wall (Rocking)

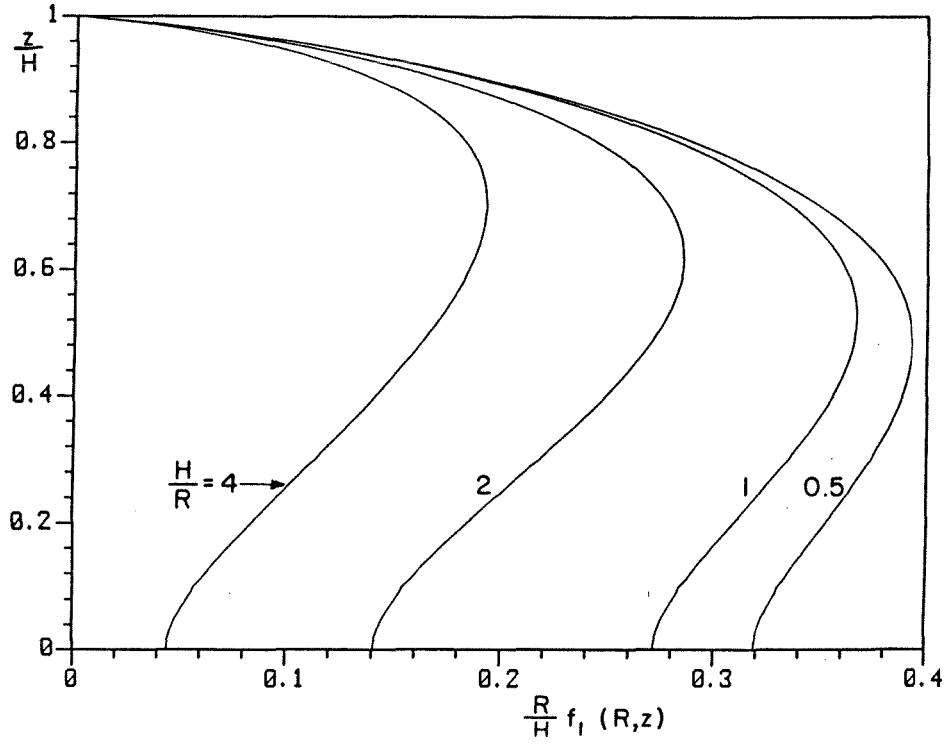

Figure 2.2.c Impulsive Pressure on Tank Wall (n=m=1 Shell Mode)

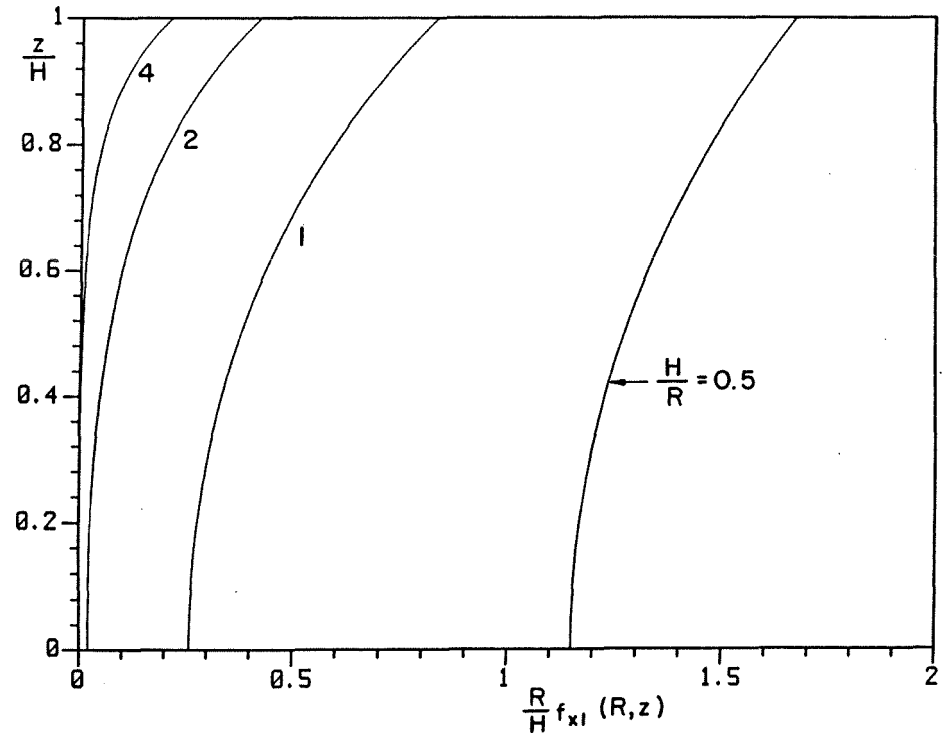

Figure 2.3.a Convective Pressure on Tank Wall (Translation, s=1)

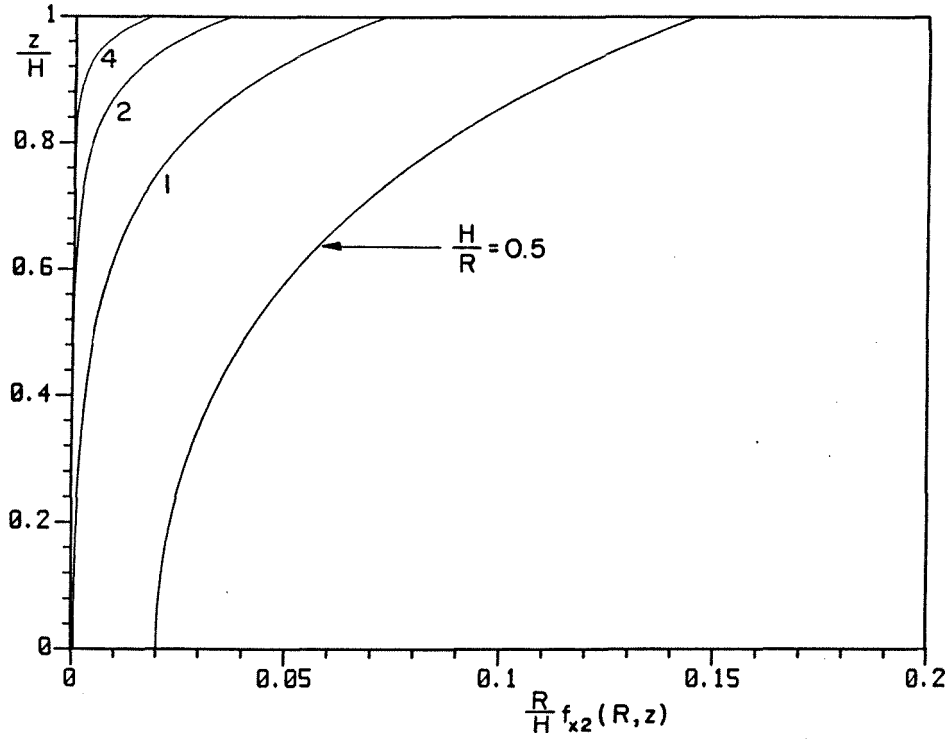

Figure 2.3.b Convective Pressure on Tank Wall (Translation, s=2)

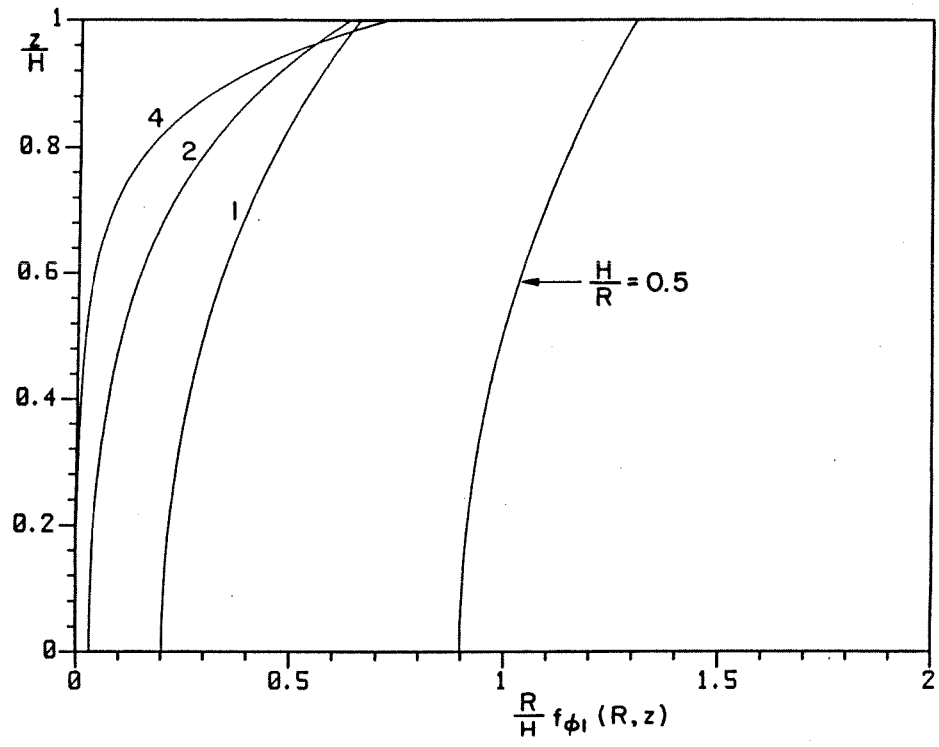

Figure 2.3.c Convective Pressure on Tank Wall (Rocking, s=1)

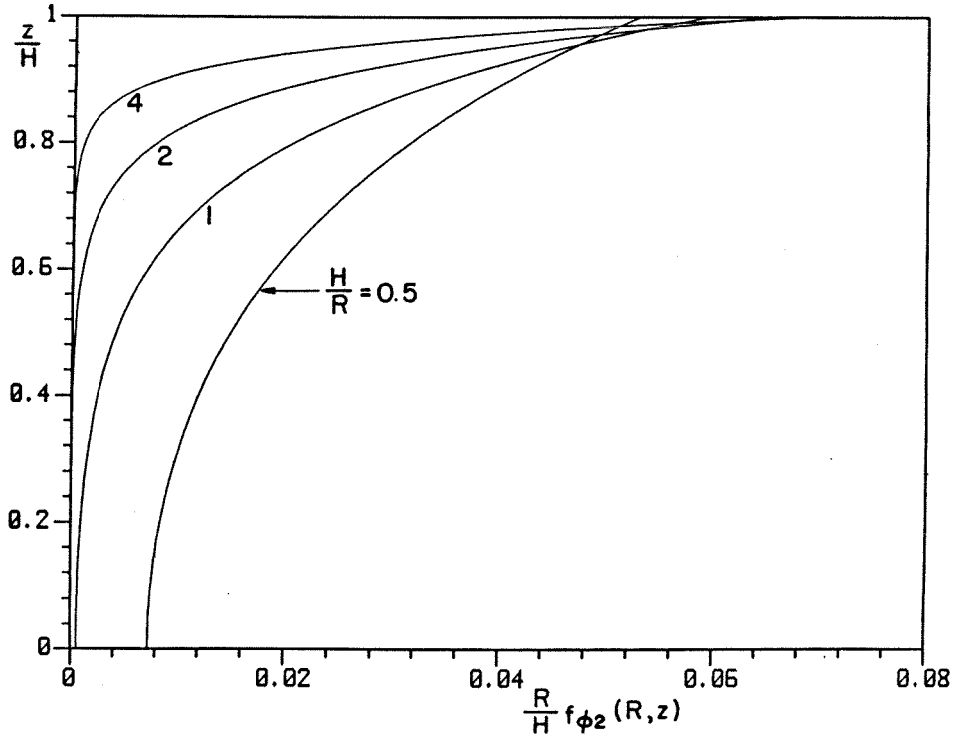

Figure 2.3.d Convective Pressure on Tank Wall (Rocking, s=2)

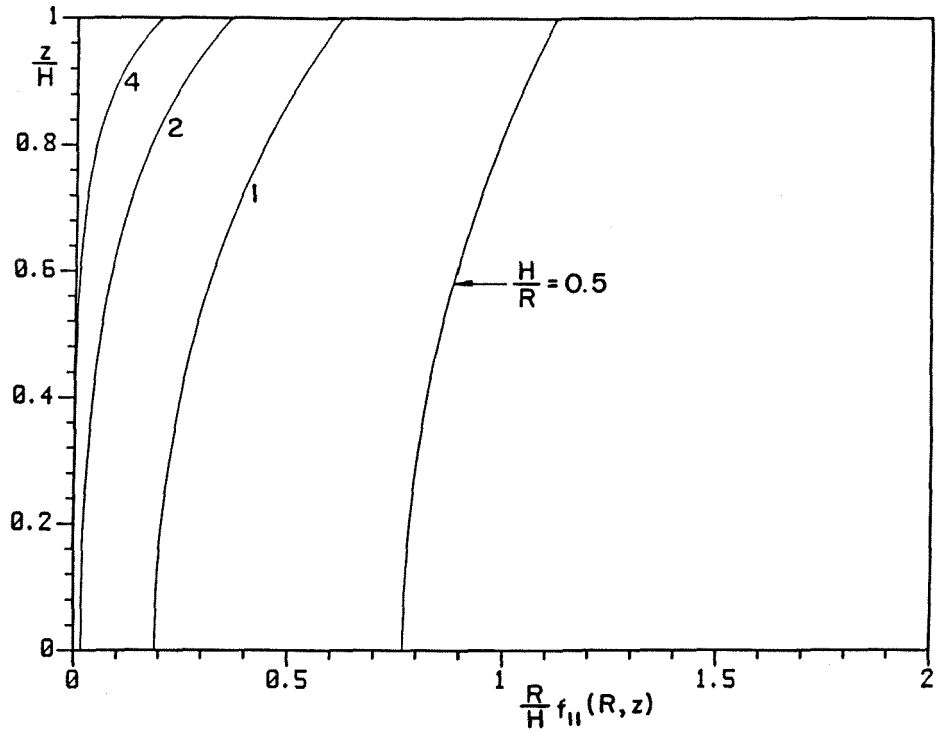

Figure 2.3.e Convective Pressure on Tank Wall (n=m=1 Shell Mode, s=1)

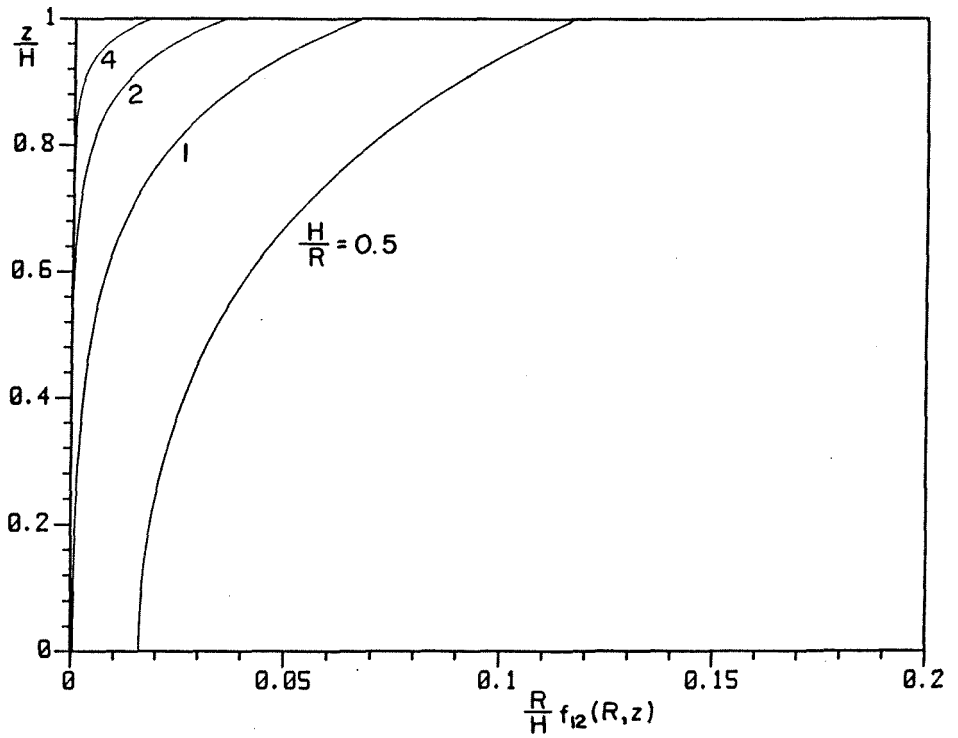

Figure 2.3.f Convective Pressure on Tank Wall (n=m=1 Shell Mode, s=2)

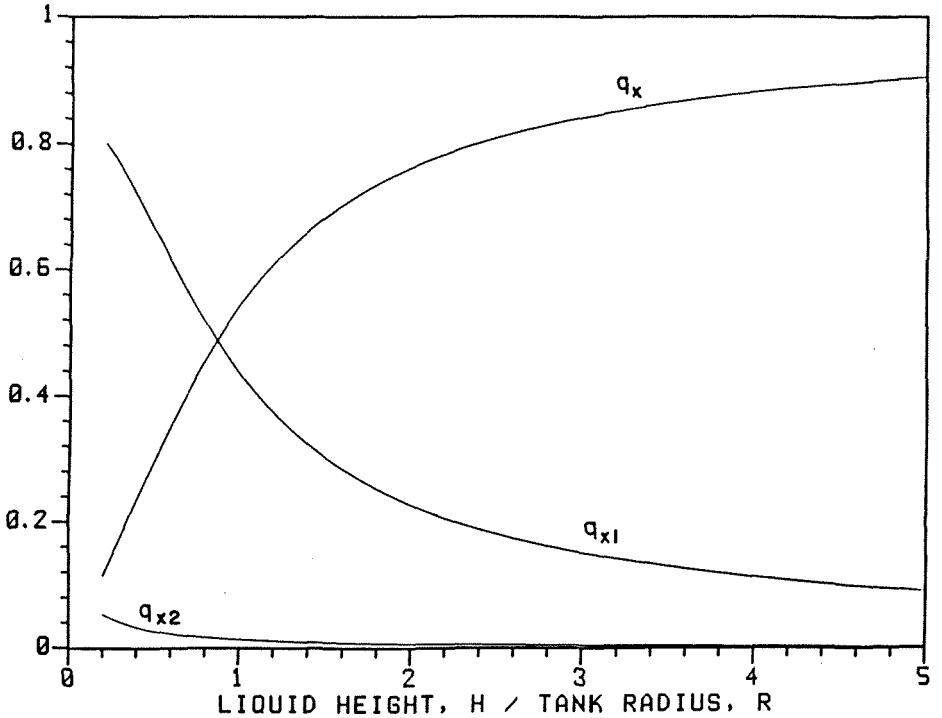

Figure 2.4.a Normalized Base Shear vs H/R (Translation)

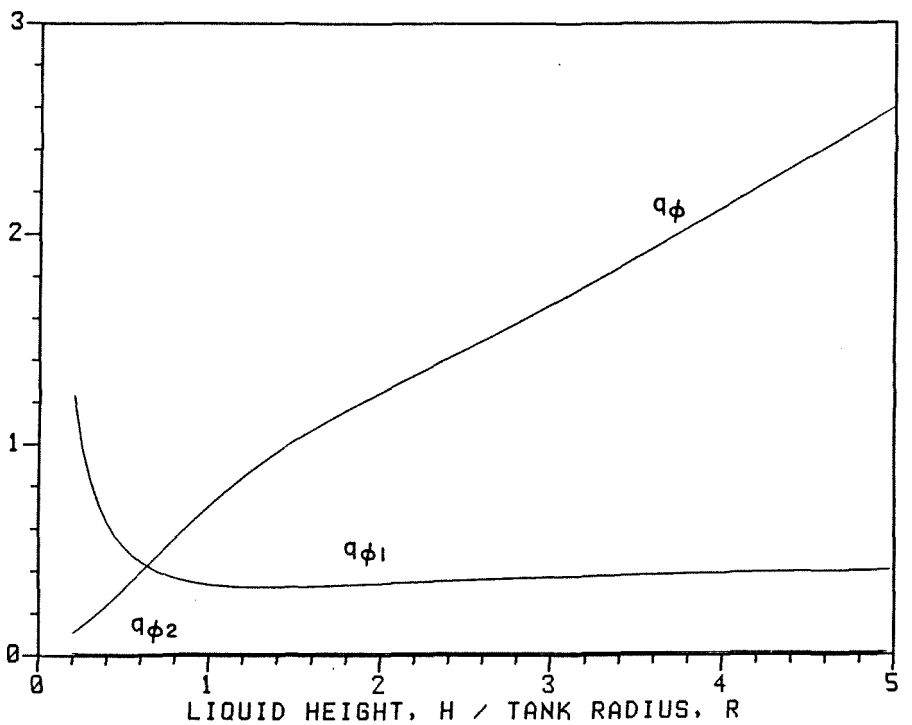

Figure 2.4.b Normalized Base Shear vs H/R (Rocking)

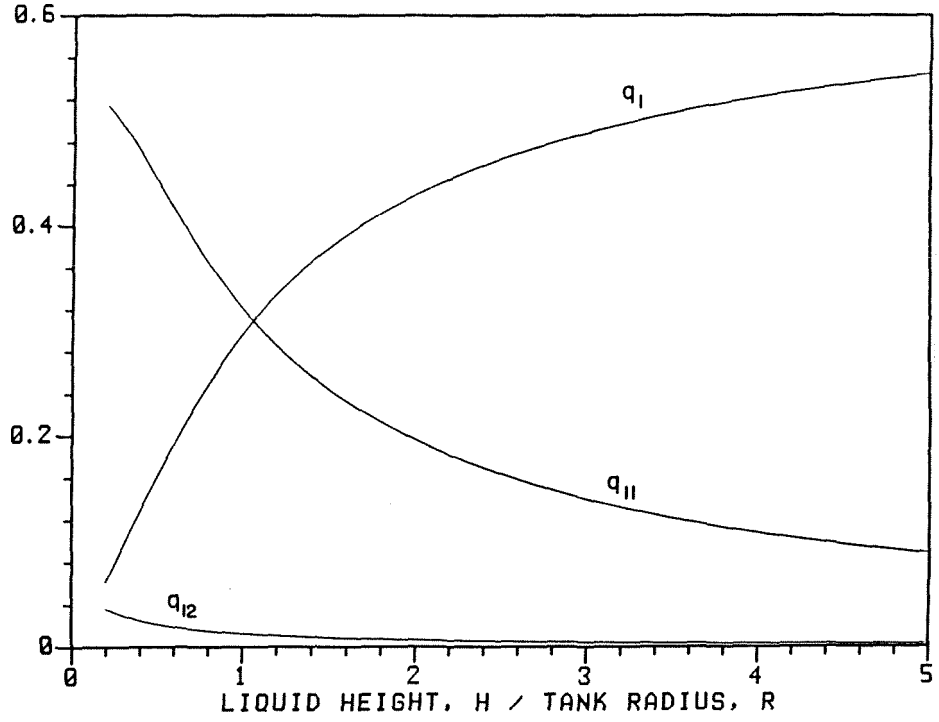

Figure 2.4.c Normalized Base Shear vs H/R (m=1 Shell Mode)

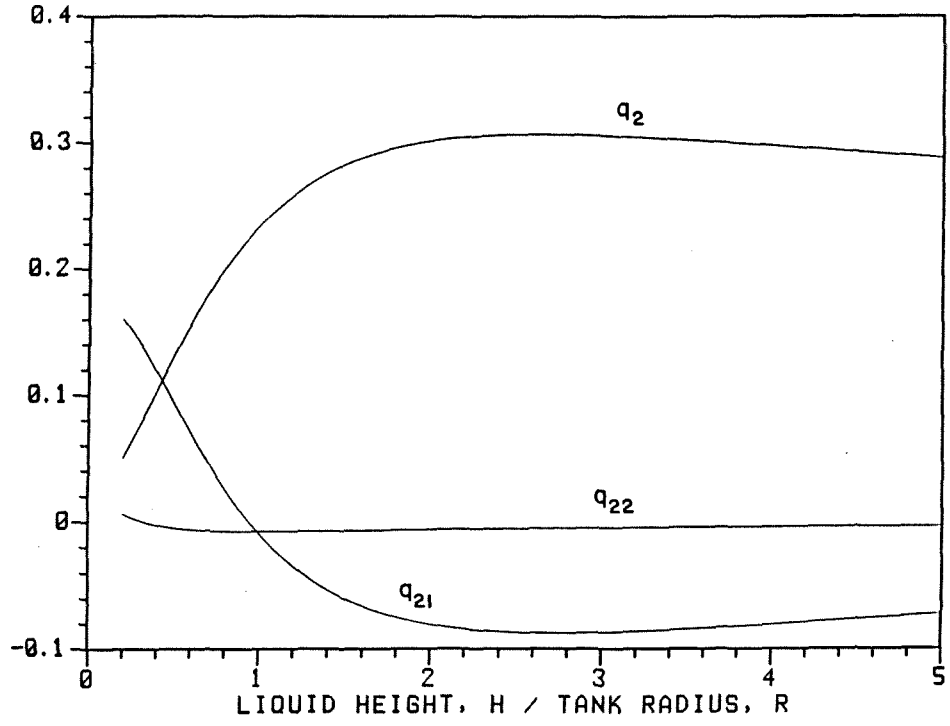

Figure 2.4.d Normalized Base Shear vs H/R (m=2 Shell Mode)

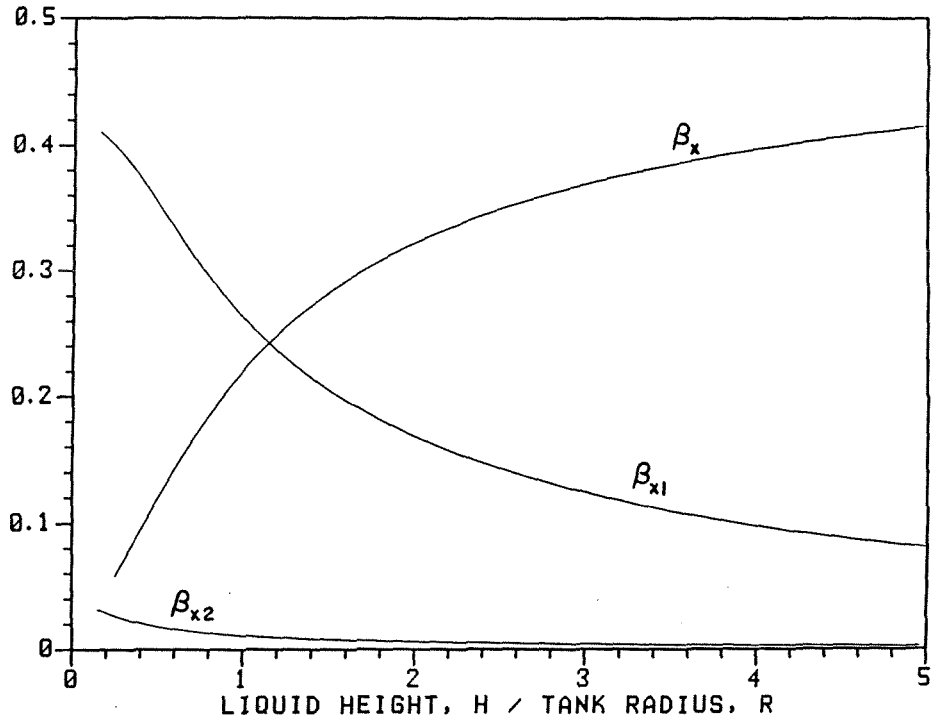

Figure 2.5.a Normalized Base Moment at Shell Wall vs H/R (Translation)

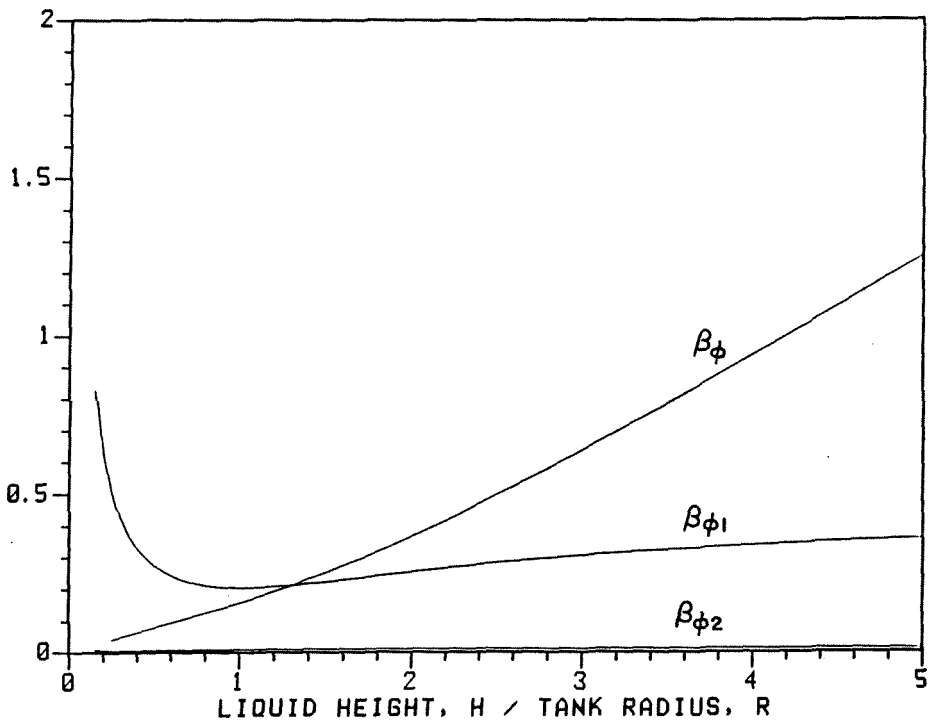

Figure 2.5.b Normalized Base Moment at Shell Wall vs H/R (Rocking)

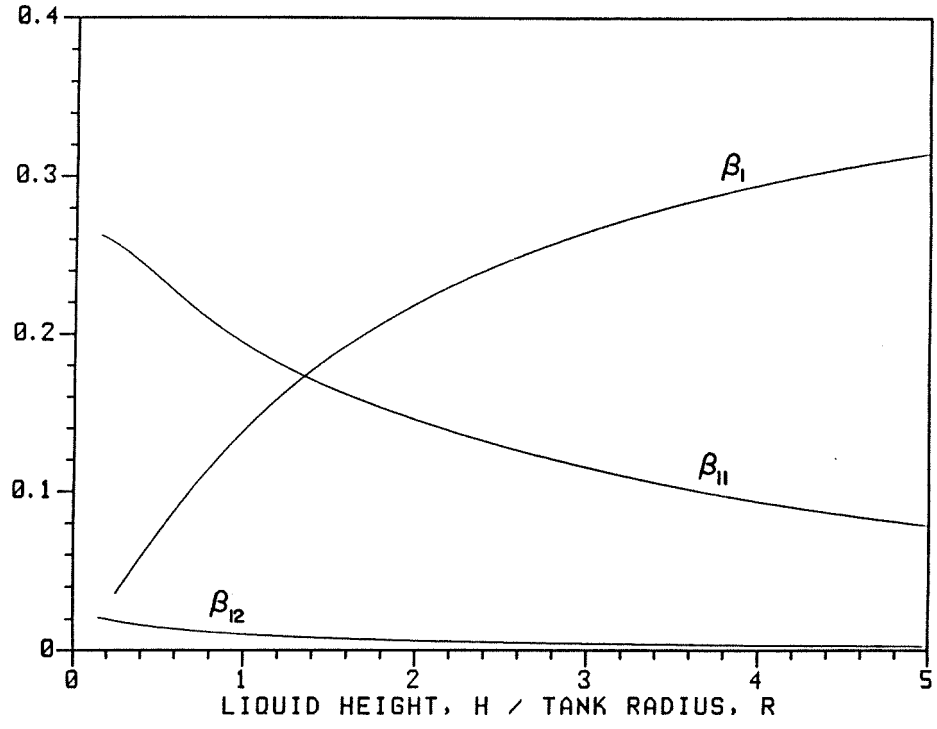

Figure 2.5.c Normalized Base Moment at Shell Wall vs H/R (m=1 Shell Mode)

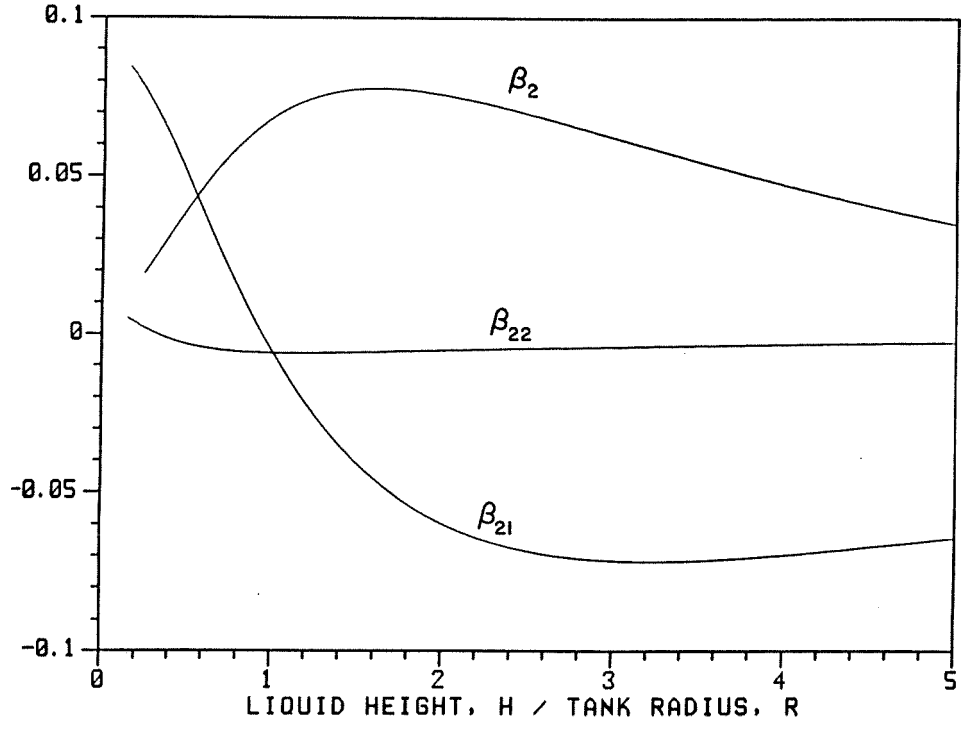

Figure 2.5.d Normalized Base Moment at Shell Wall vs H/R (m=2 Shell Mode)

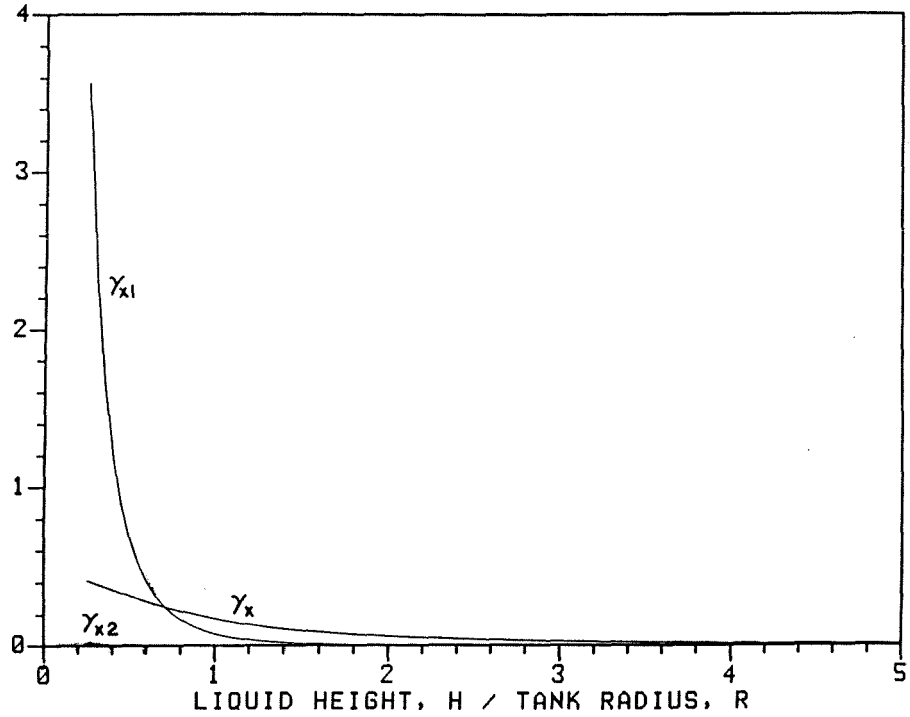

Figure 2.6.a Normalized Base Moment at Tank Bottom vs H/R (Translation)

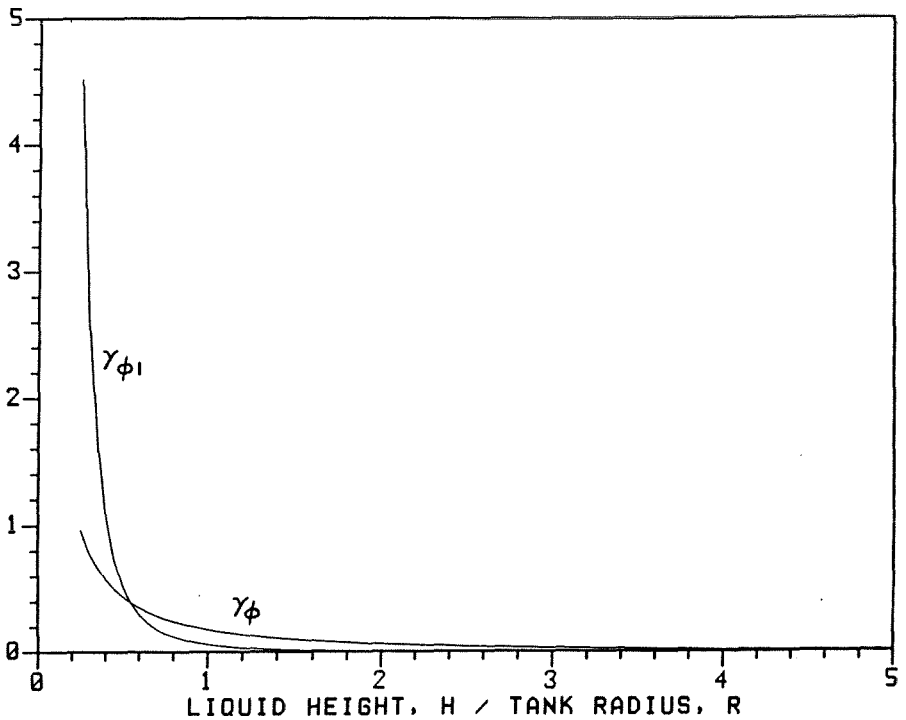

Figure 2.6.b Normalized Base Moment at Tank Bottom vs H/R (Rocking)

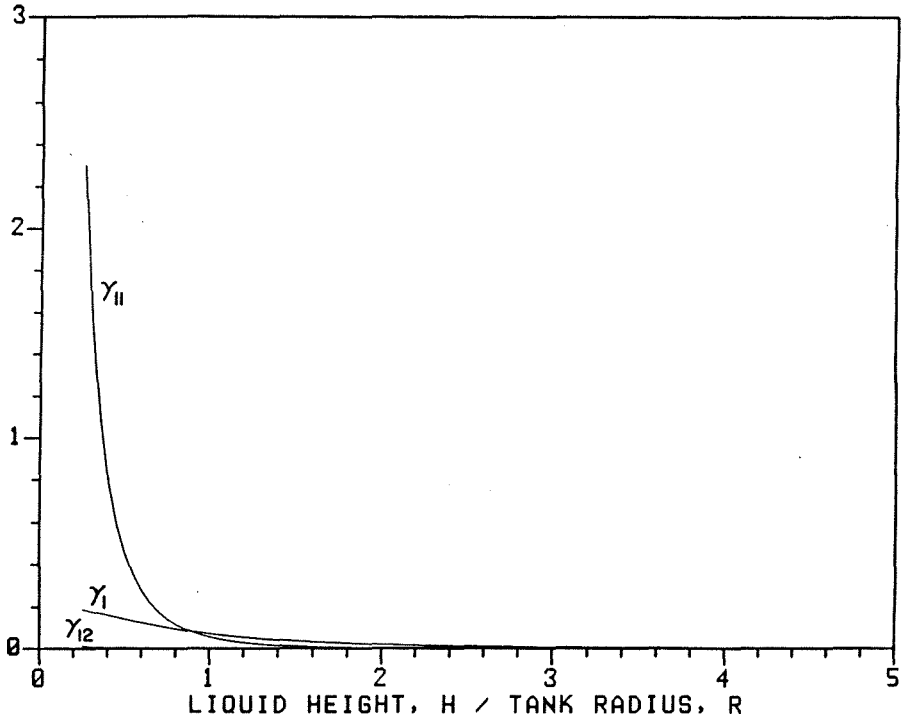

Figure 2.6.c Normalized Base Moment at Tank Bottom vs H/R (m=1 Shell Mode)

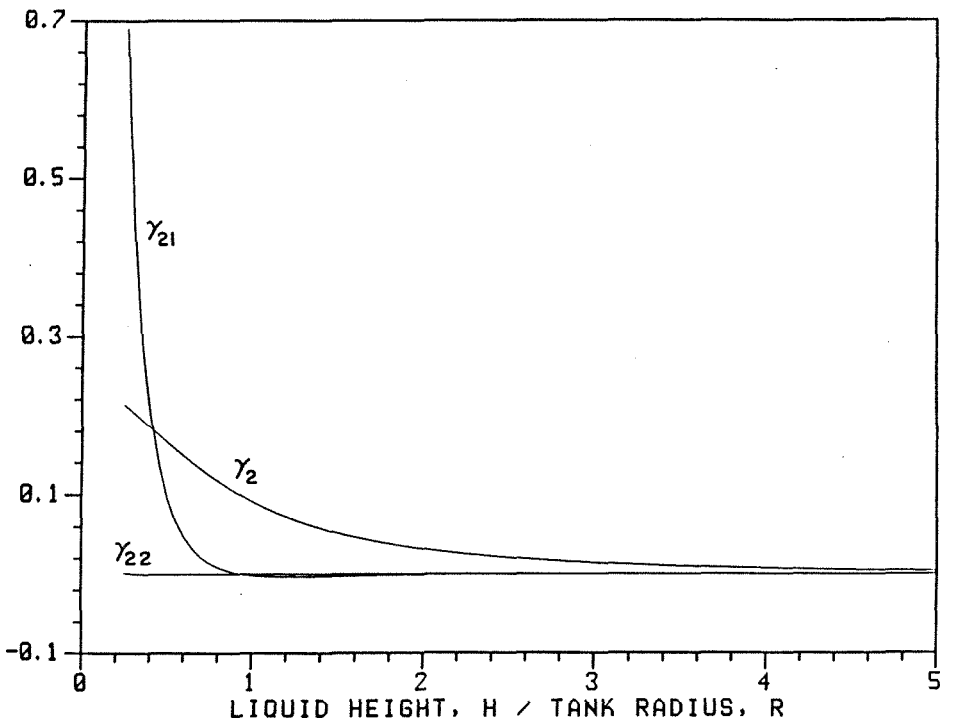

Figure 2.6.d Normalized Base Moment at Tank Bottom vs H/R (m=2 Shell Mode)

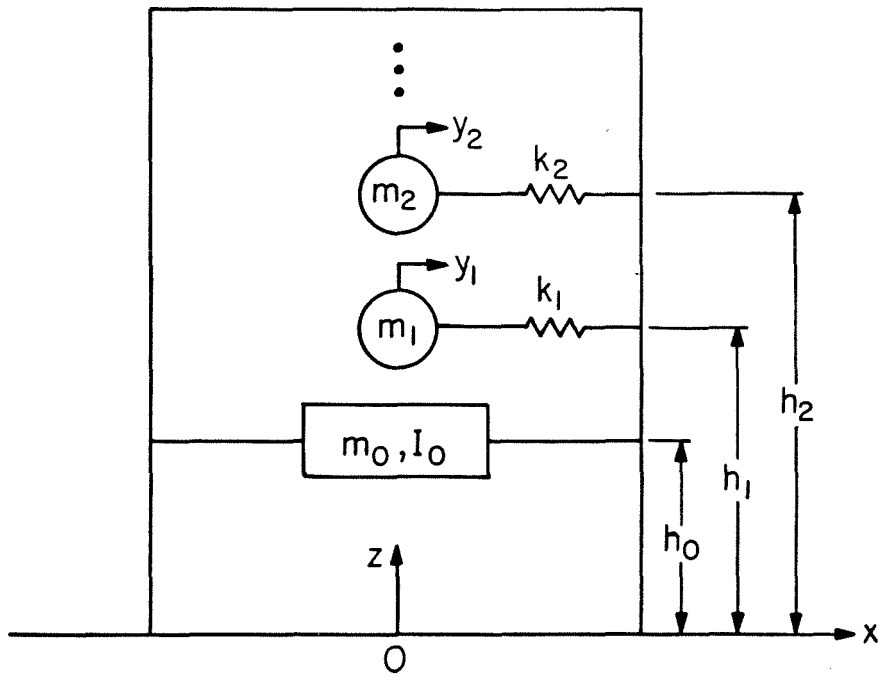

Figure 2.7 Equivalent Mechanical Model

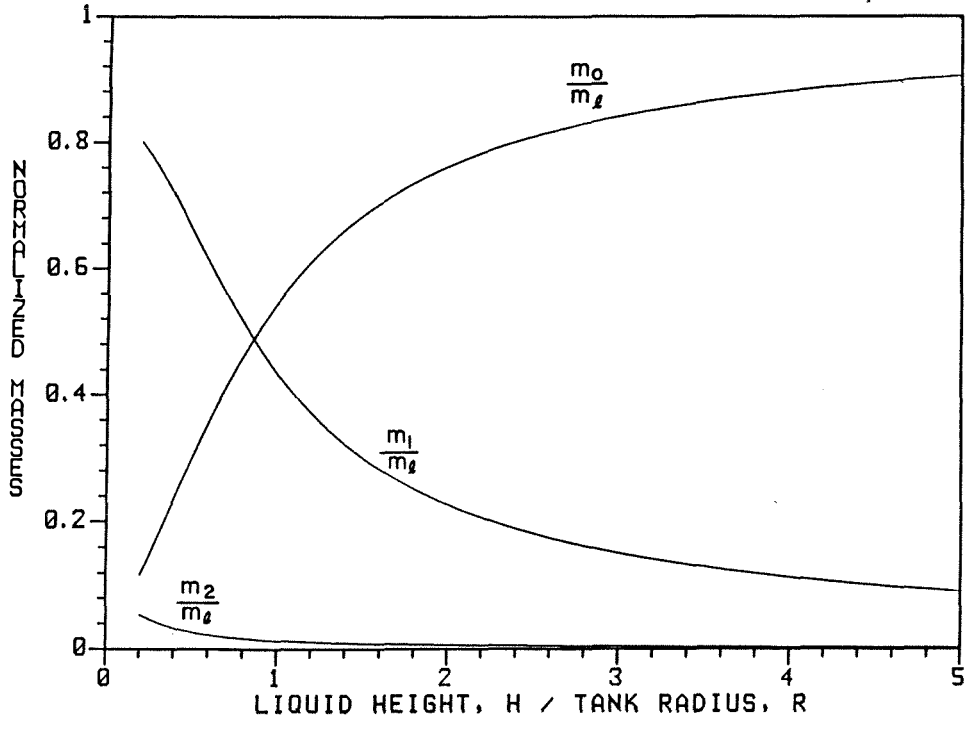

Figure 2.8.a Normalized Masses of Equivalent Model vs H/R

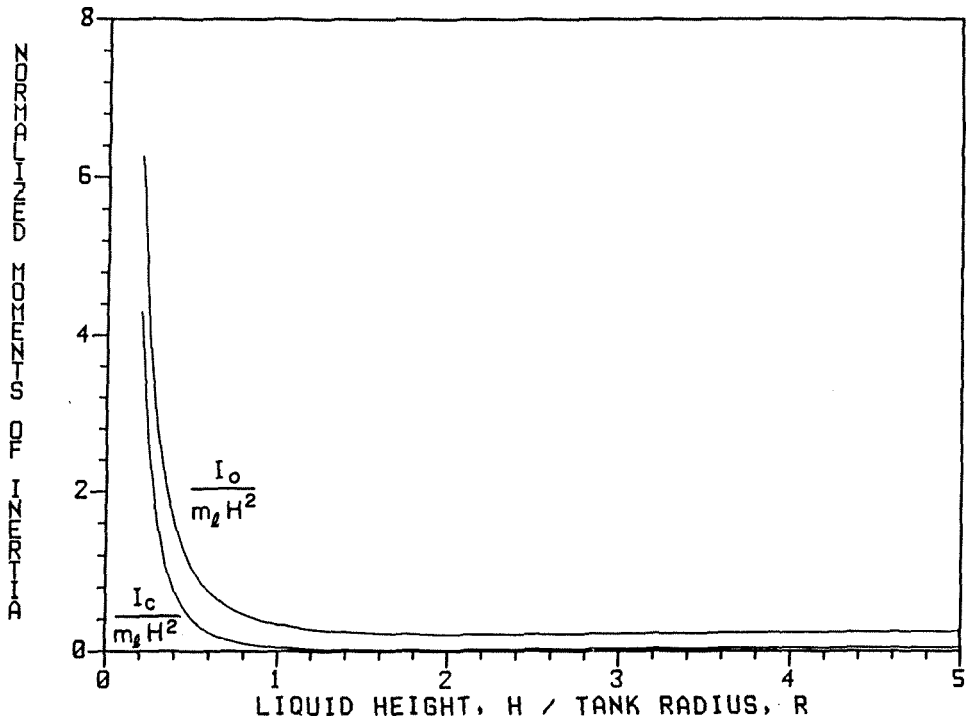

Figure 2.8.b Normalized Moment of Inertia of Equivalent Model vs H/R

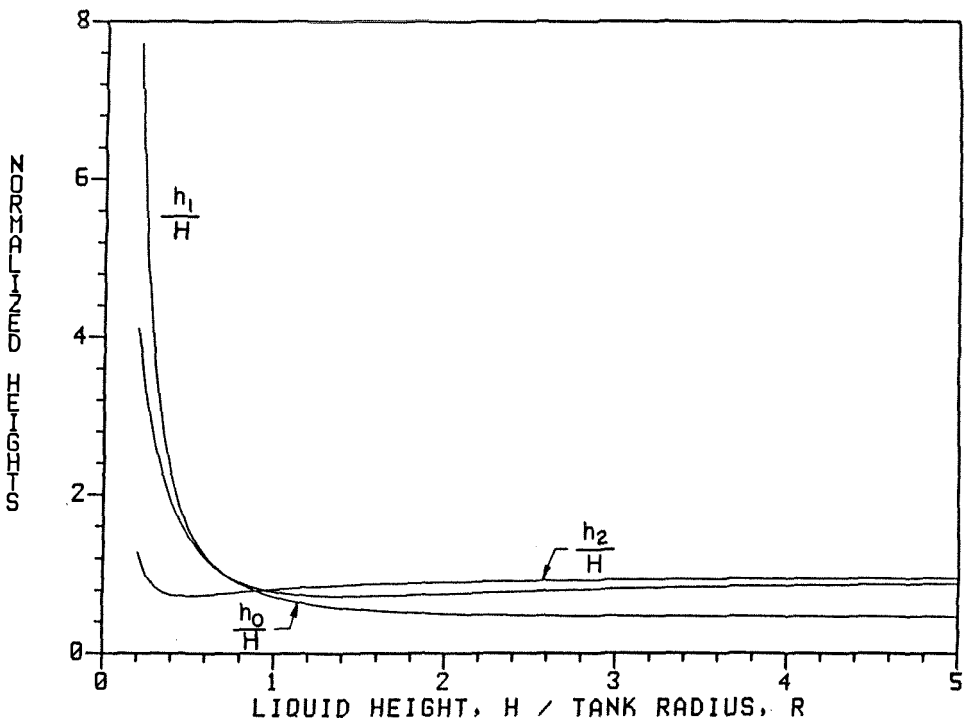

Figure 2.8.c Normalized Heights of Equivalent Model vs H/R

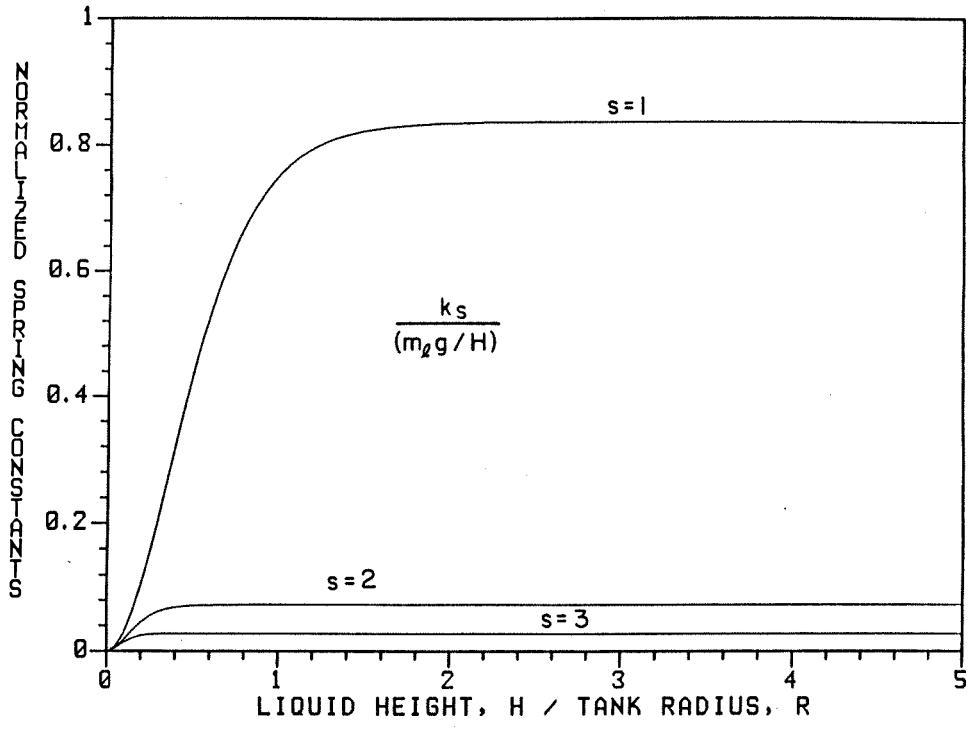

Figure 2.8.d Normalized Stiffnesses of Equivalent Model vs H/R

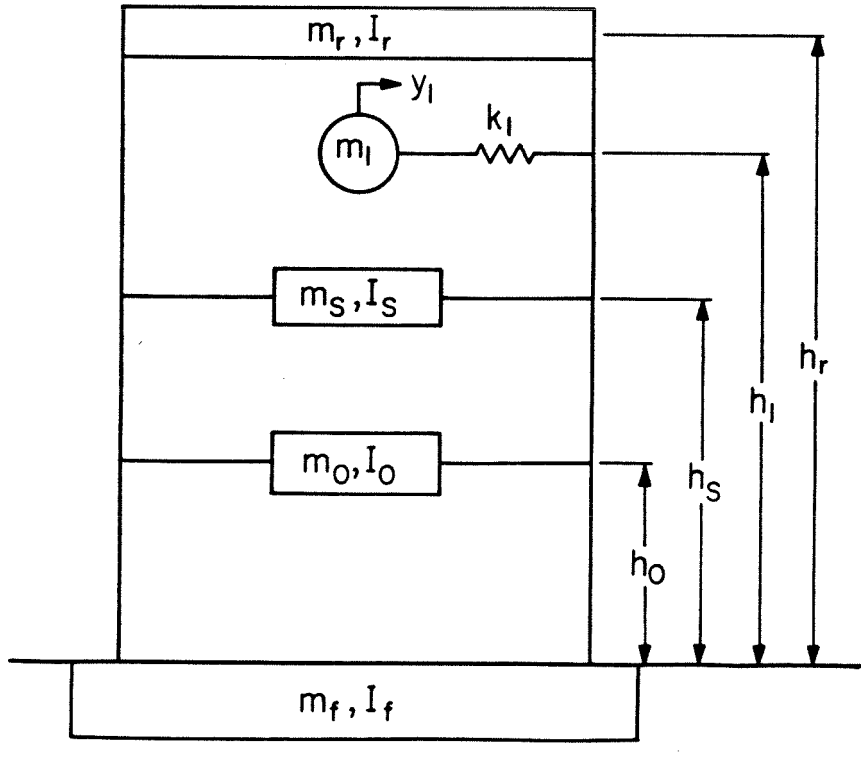

Figure 2.9 Simplified Model for a Fluid-Filled Tank

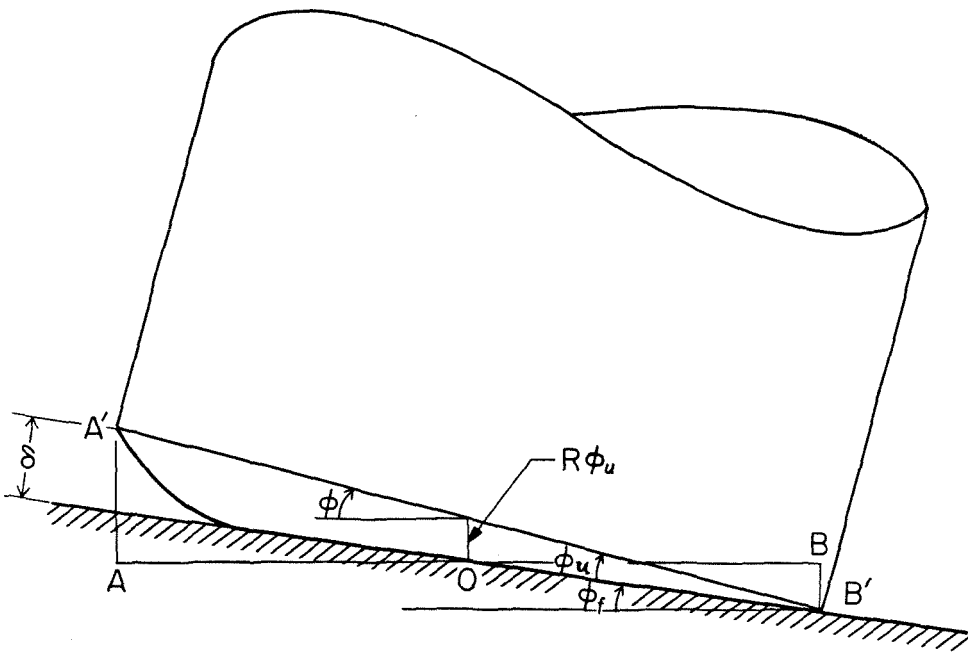

Figure 3.1 Definition of Uplifting and Foundation Rocking Angles

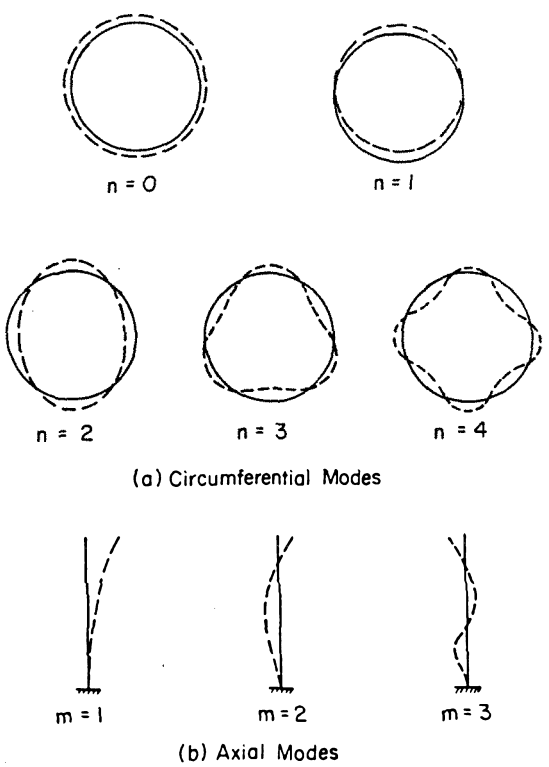

Figure 3.2 Vibrational Modes of a Cantilever Cylindrical Shell

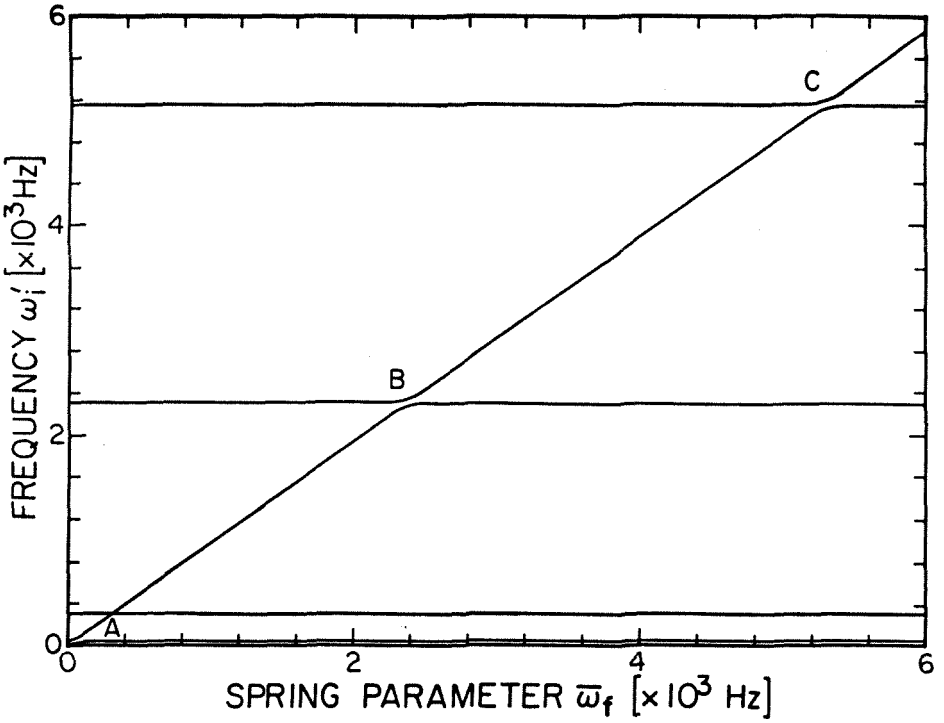

Figure 4.1.a Frequencies vs Foundation Stiffness Parameter

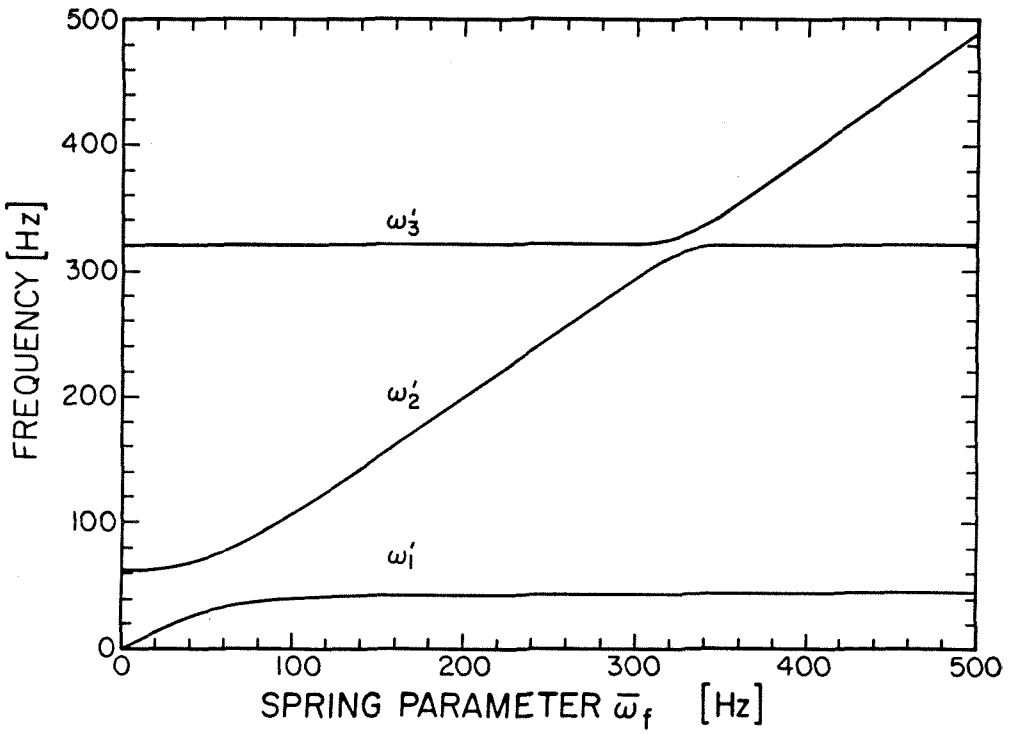

Figure 4.1.b Magnification of Area A in Figure 4.1.a

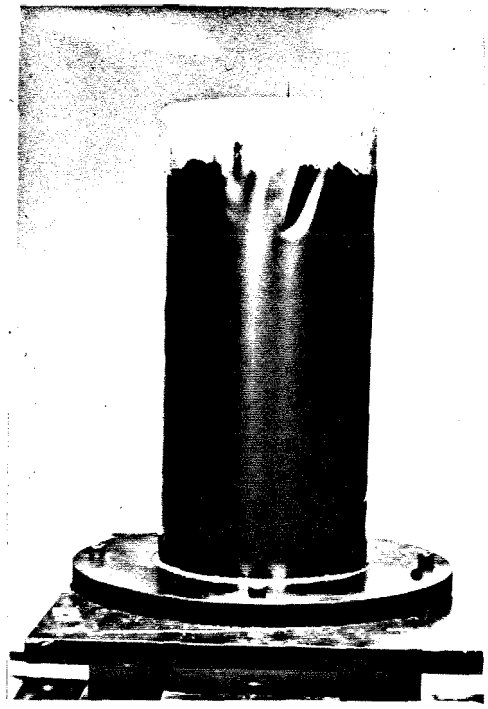

Figure 4.2 Buckling at the Top of a Model Tank (Ref. [28,29])

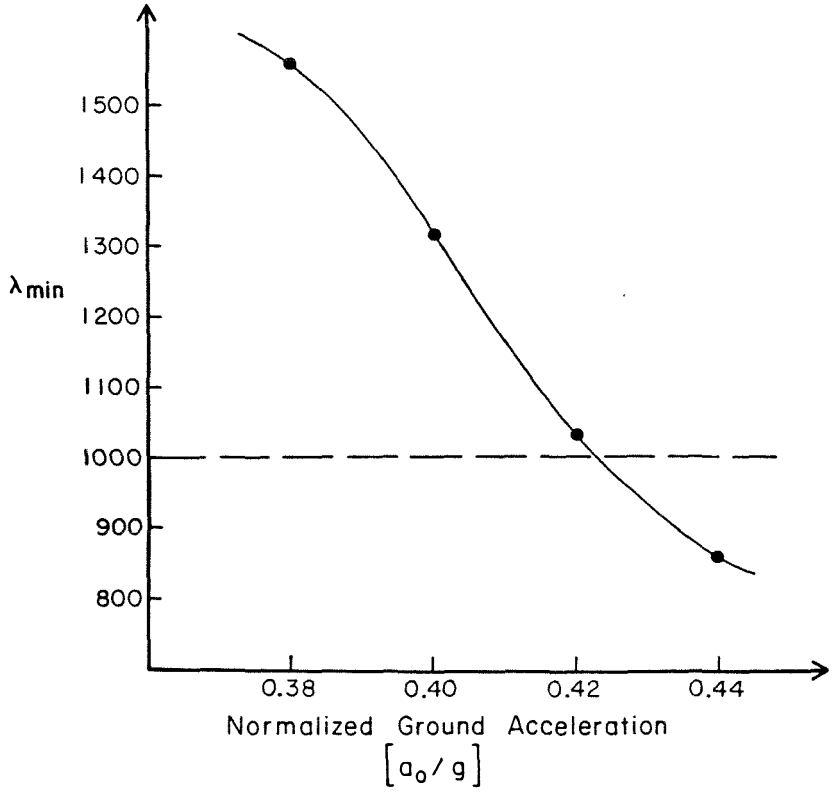

Figure 4.3 Normalized Ground Acceleration vs Minimum Eigenvalue, λ_{min}, as Predicted by BOSOR5

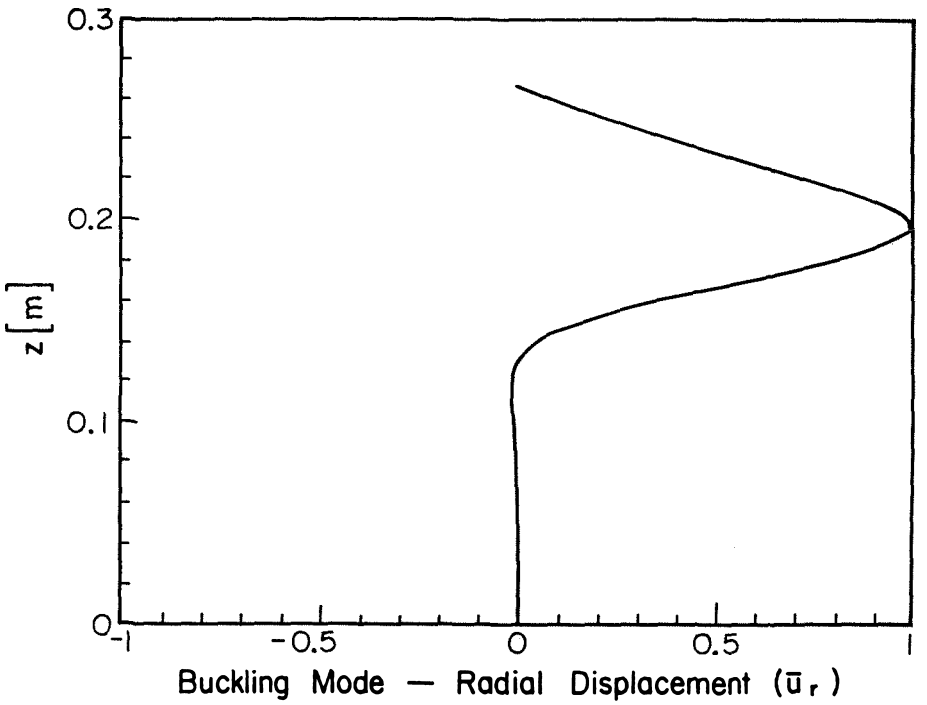

Figure 4.4.a Buckling Mode, Radial Displacement vs Distance along the Shell Length

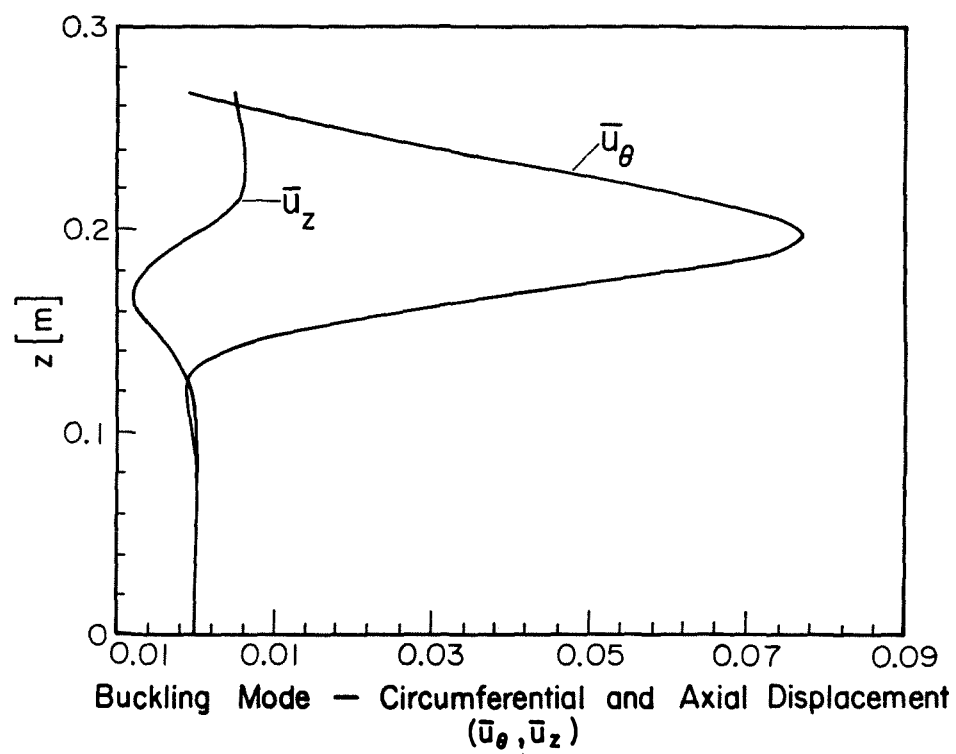

Figure 4.4.b Buckling Mode, Circumferential and Axial Displacement vs Distance along the Shell Length

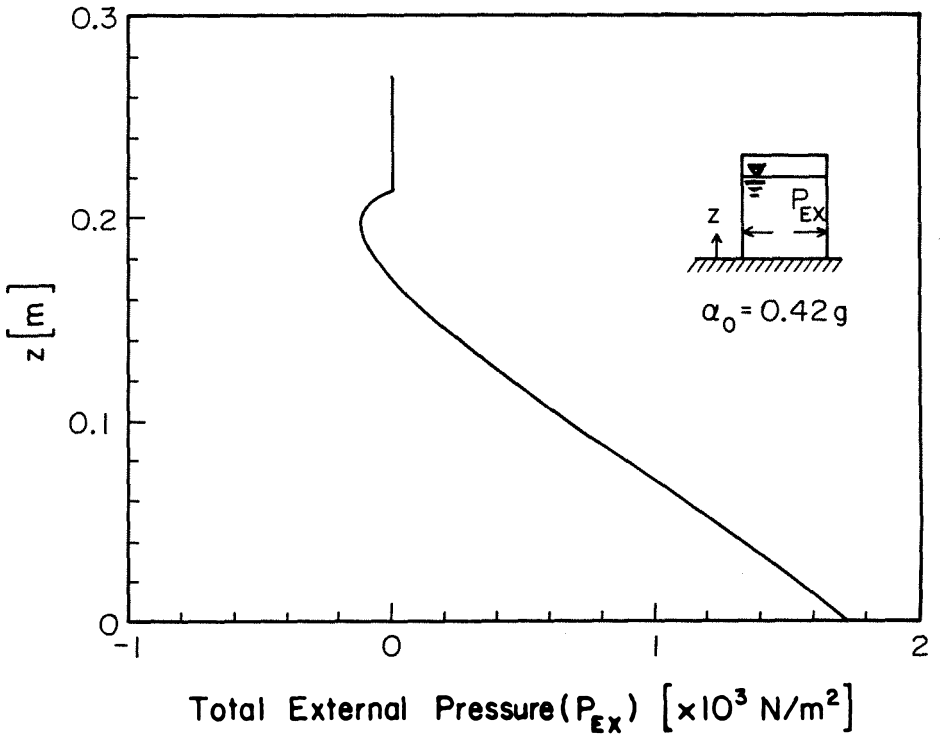

Figure 4.5.a External Pressure along the Shell Length

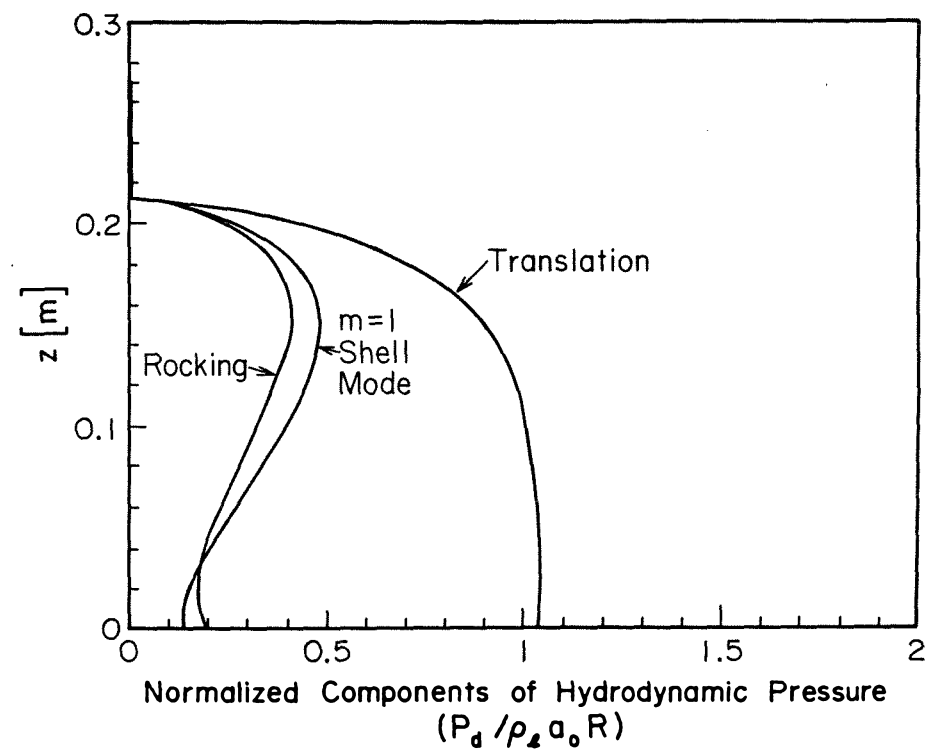

Figure 4.5.b Components of the External Pressure along the Shell Length

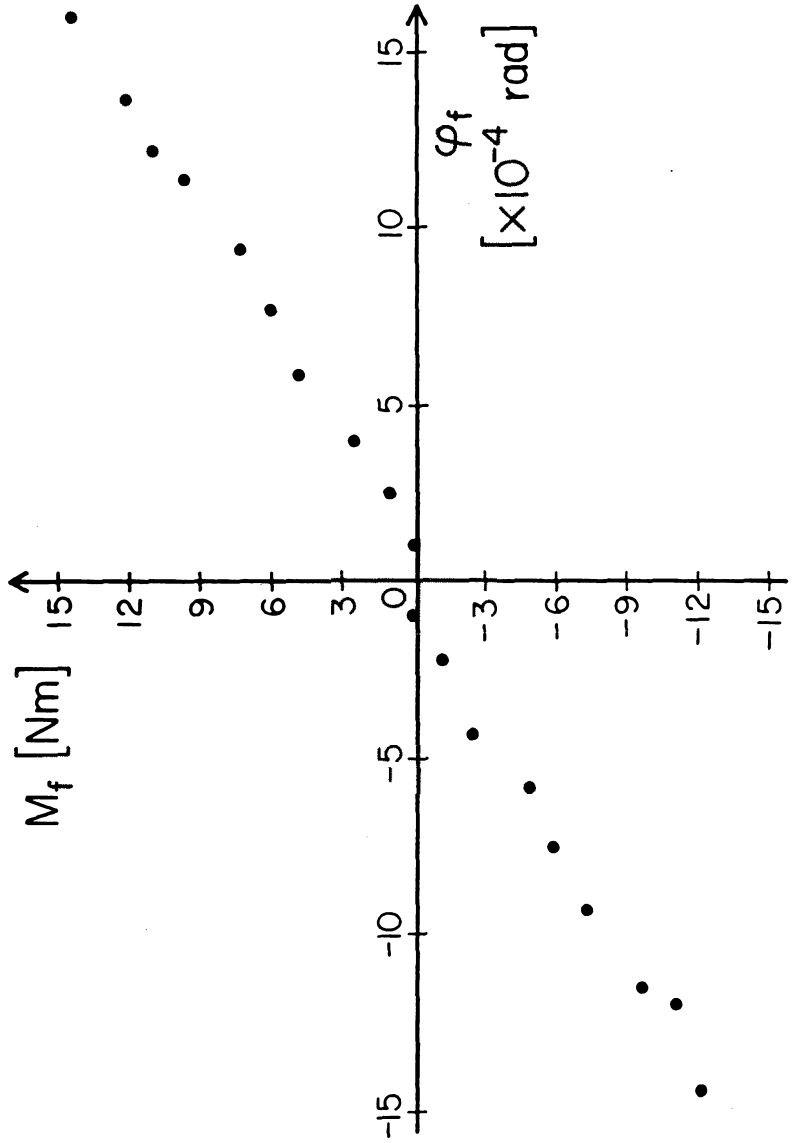

Figure 4.6 Moment vs Shaking Table Rotation

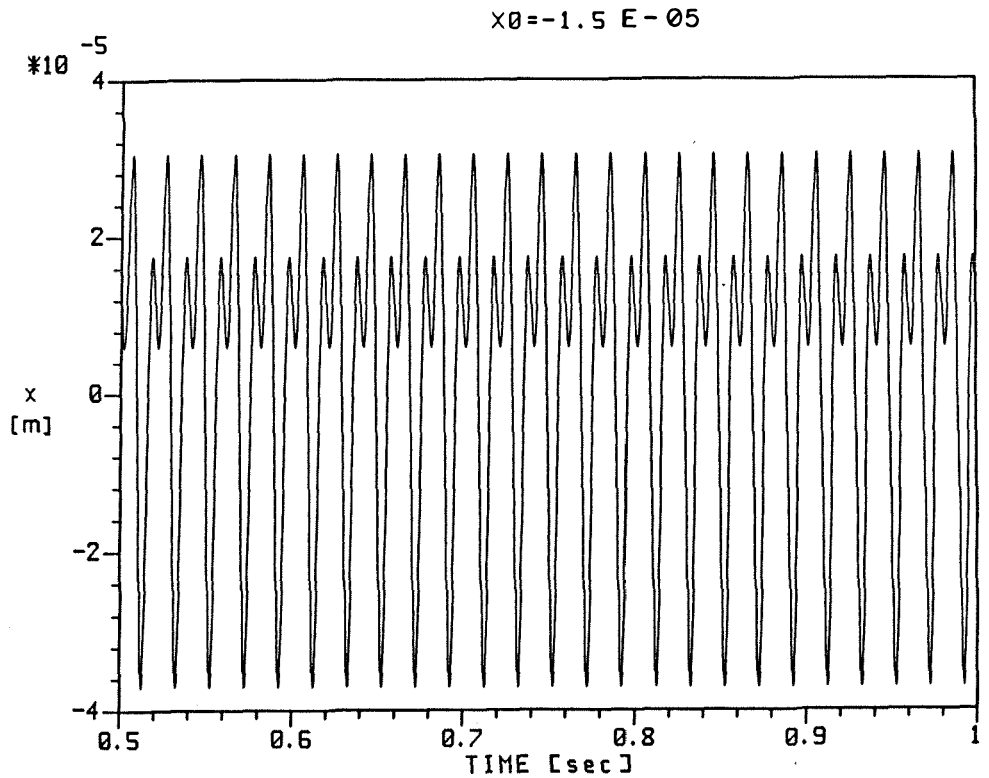

Figure 4.7.a Displacement History

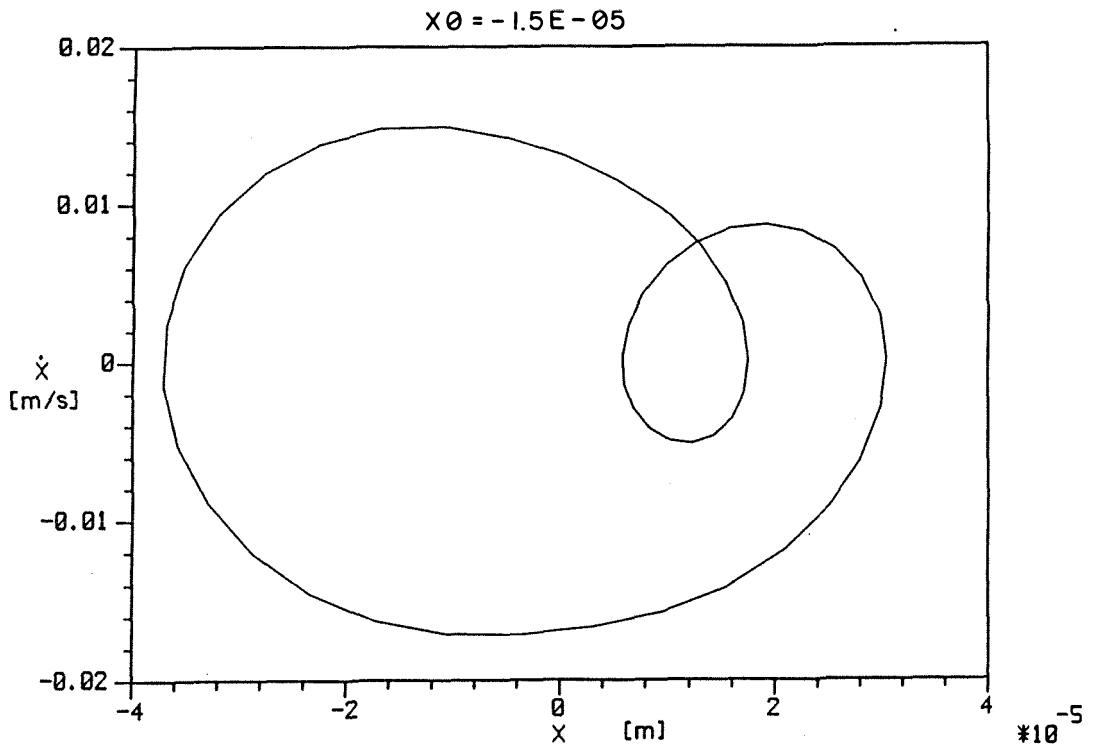

Figure 4.7.b Phase-Plane x-$\dot{x}$

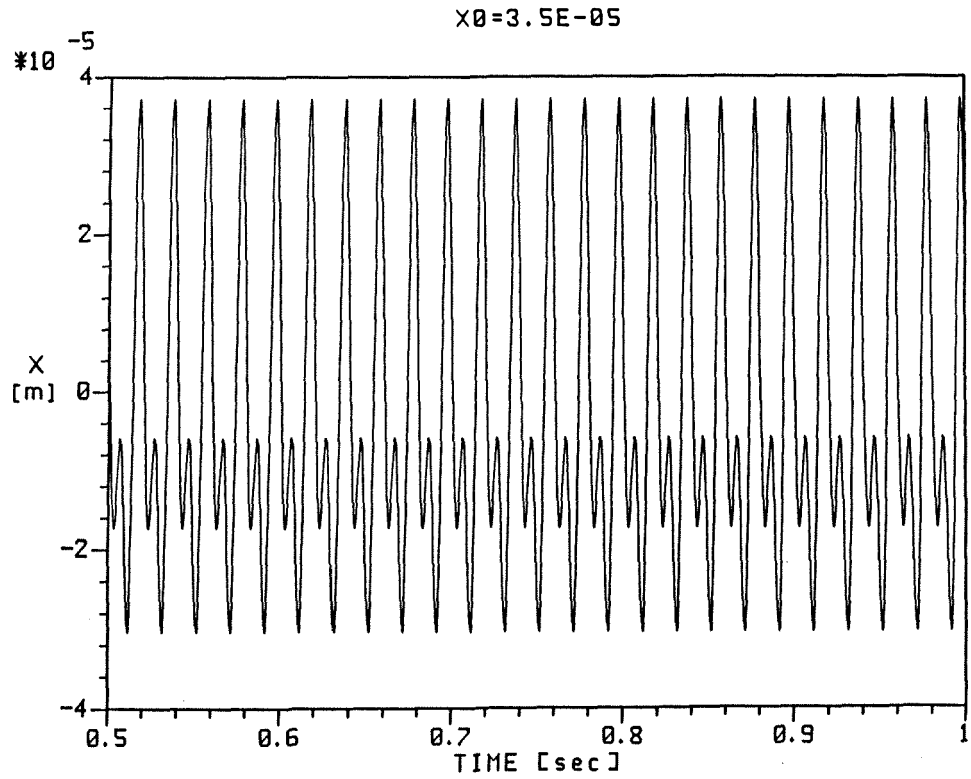

Figure 4.7.c Displacement History

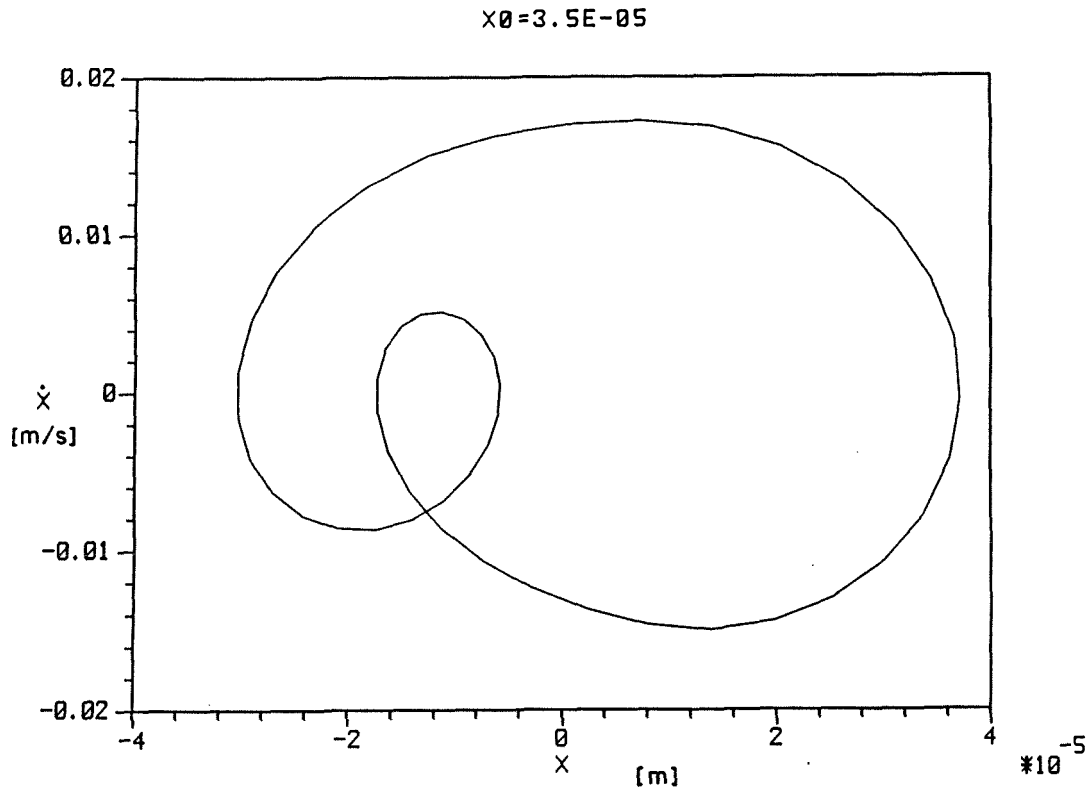

Figure 4.7.d Phase-Plane x-$\dot{x}$

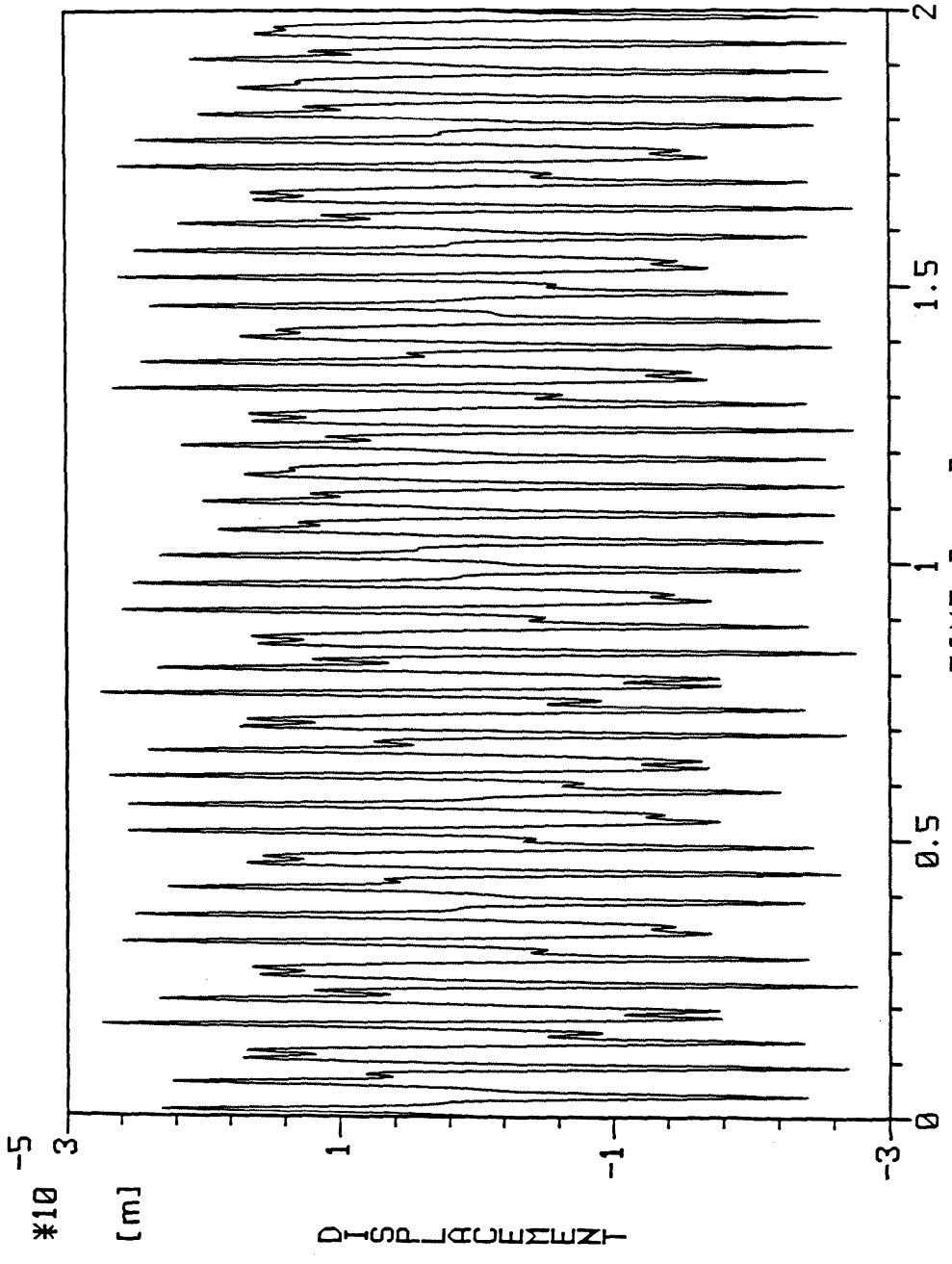

Figure 4.8.a Displacement History

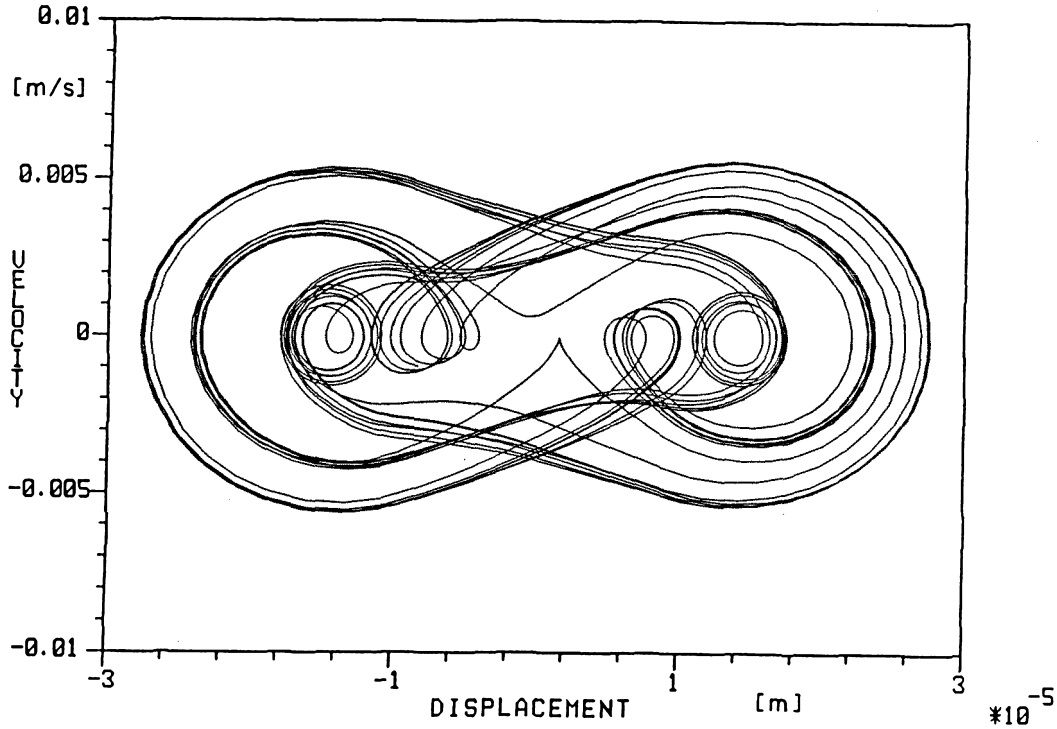

Figure 4.8.b Phase-Plane x-$\dot{x}$ (t= 3-4 sec)

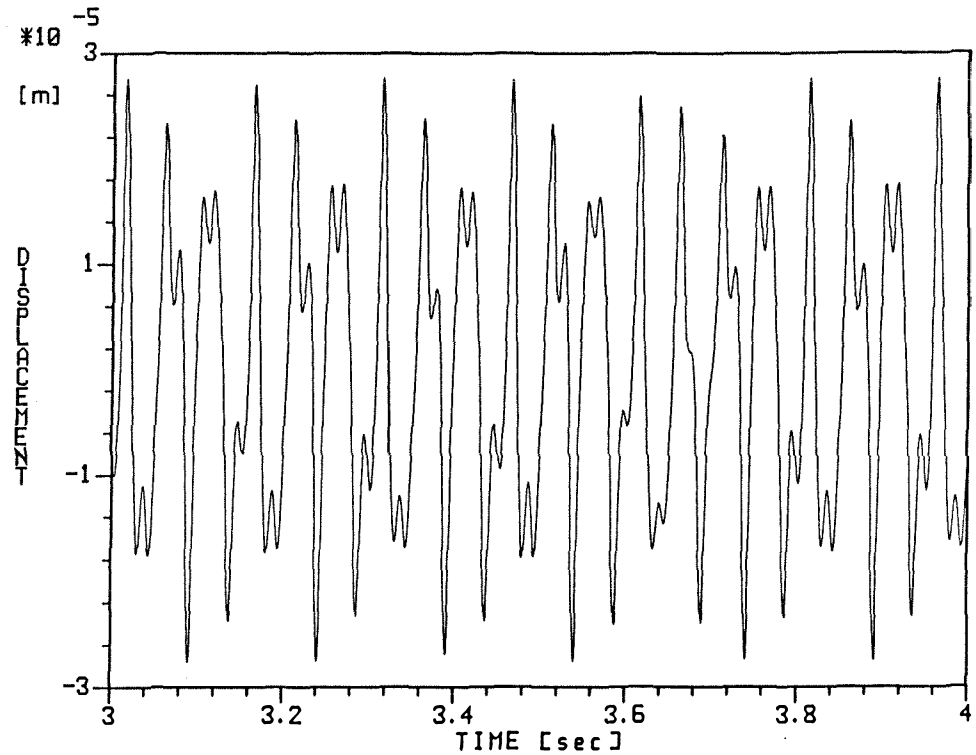

Figure 4.8.c Displacement History

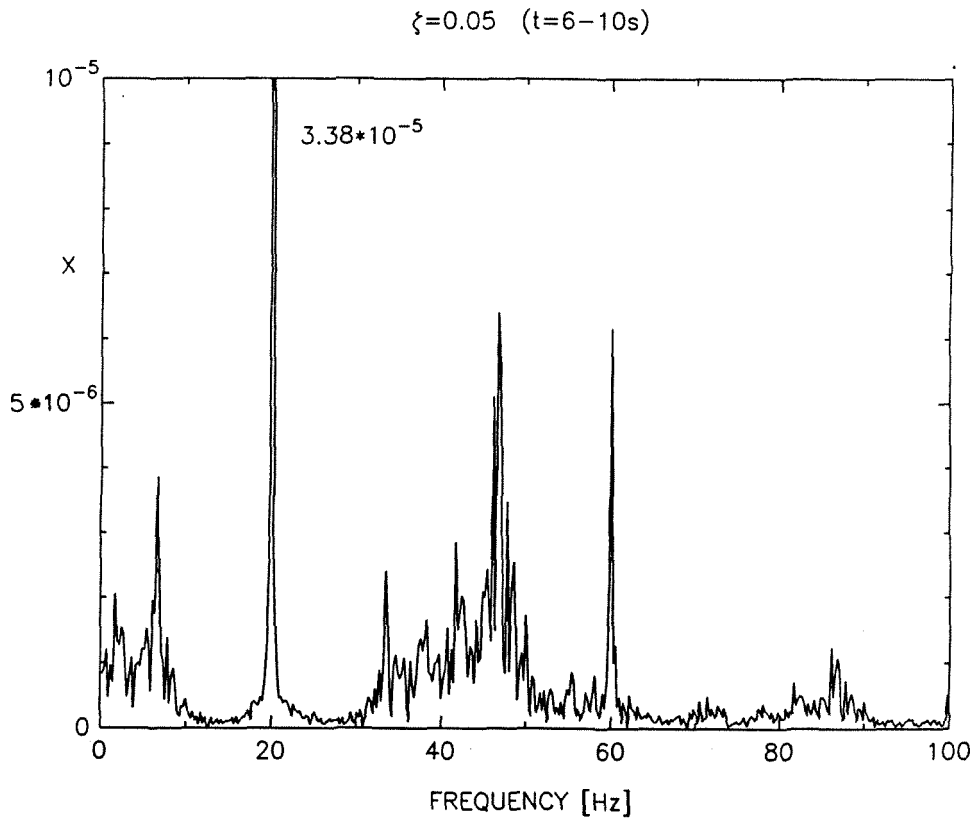

Figure 4.8.d Fourier Spectrum of the Displacement

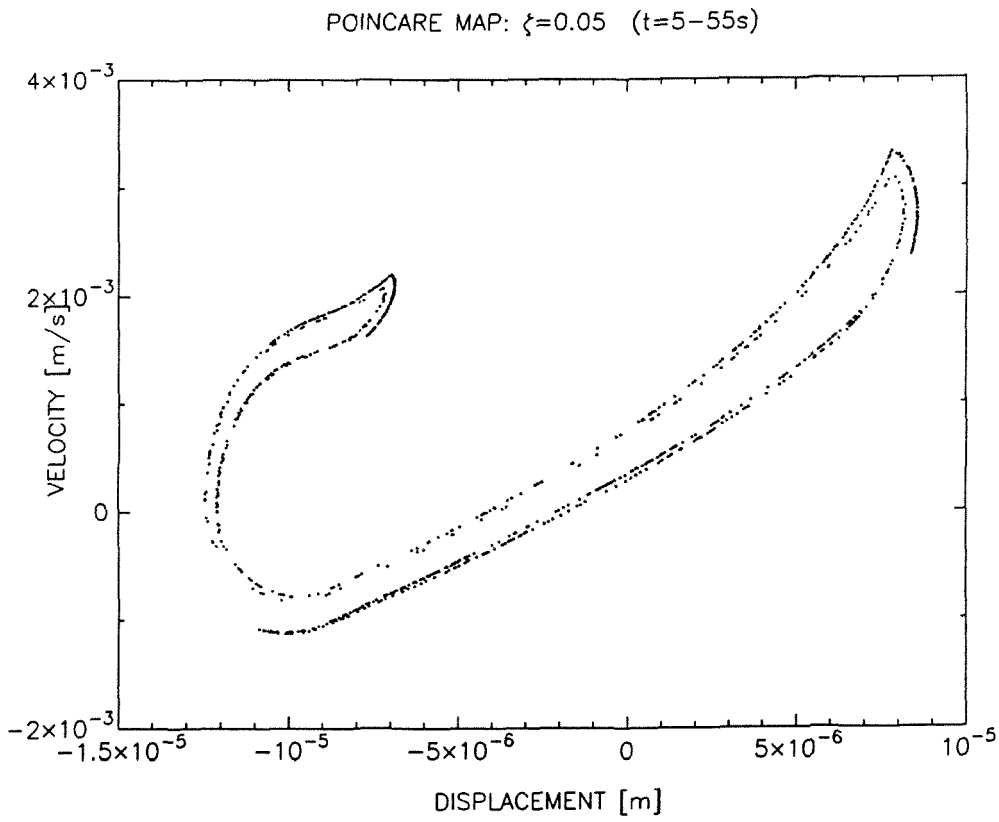

Figure 4.8.e Poincare Map

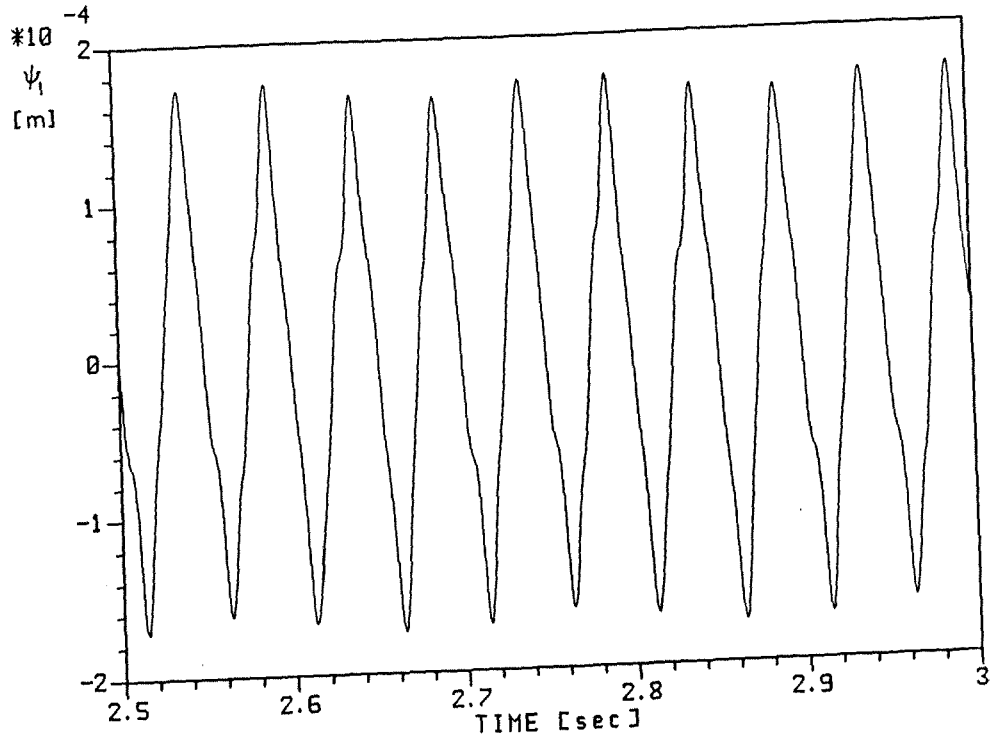

Figure 4.9.a History of ψ_1

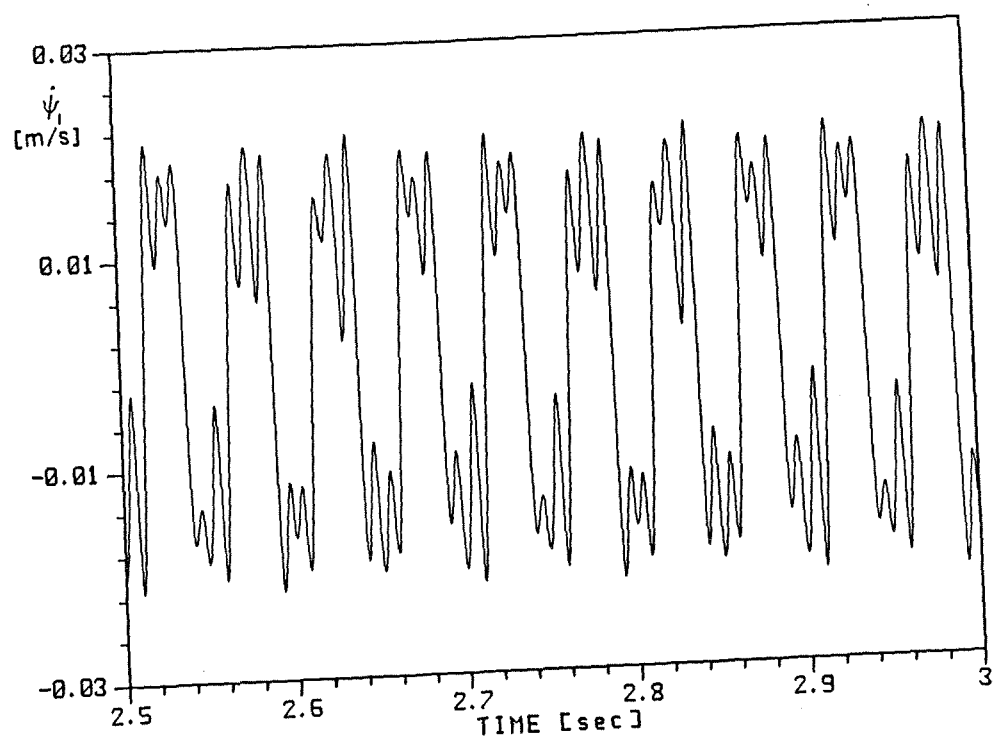

Figure 4.9.b History of $\dot{\psi}_1$

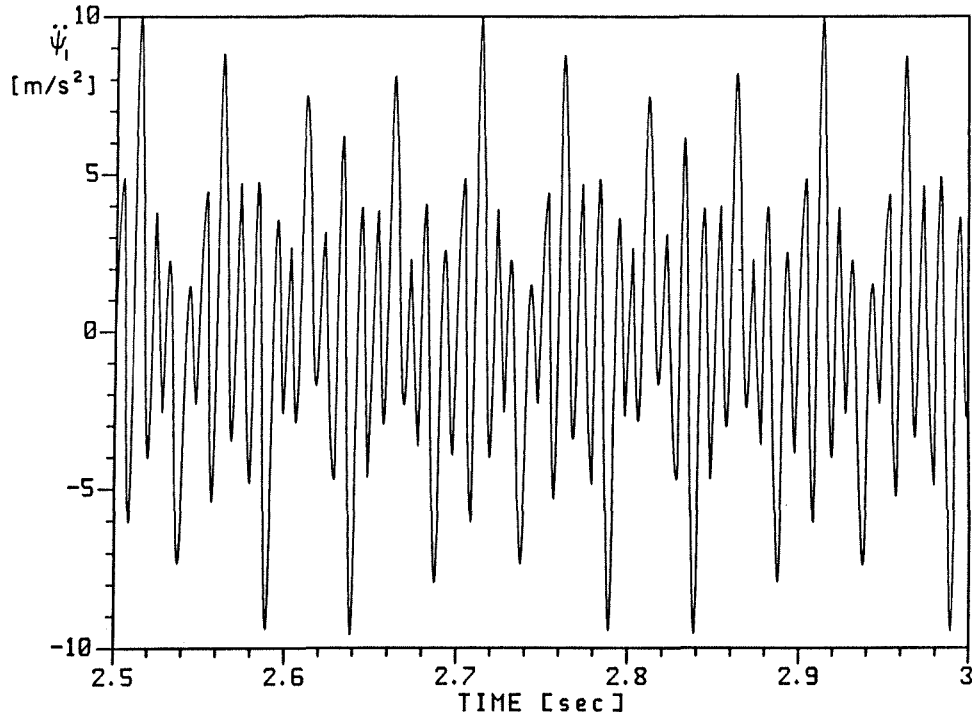

Figure 4.9.c History of $\ddot{\psi}_1$

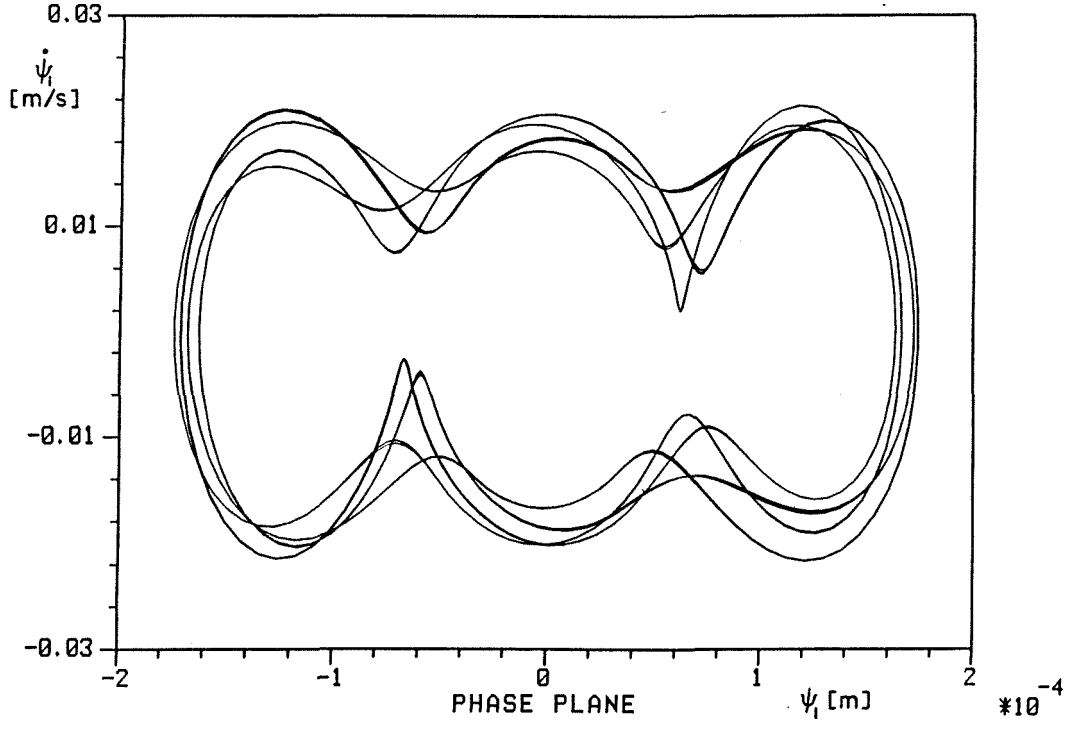

Figure 4.9.d Phase-Plane for the m=1 Shell Radial dof (t= 2.5-3 sec)

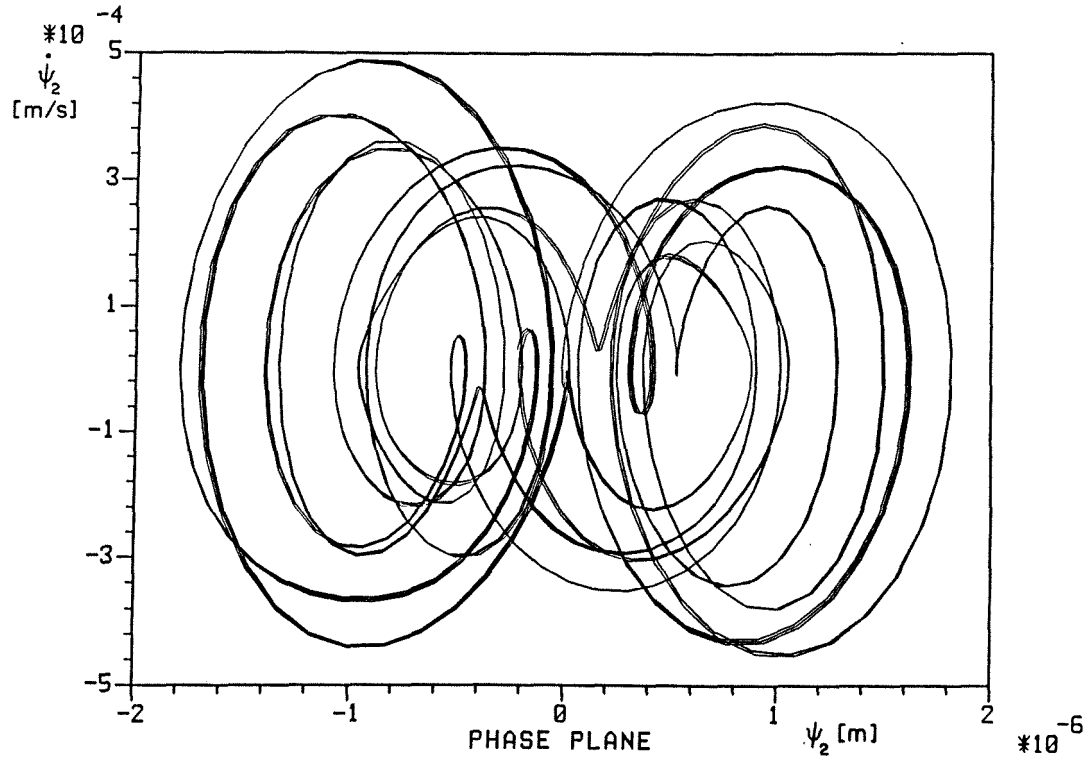

Figure 4.9.e Phase-Plane for the m=2 Shell Radial dof (t= 2.5-3 sec)

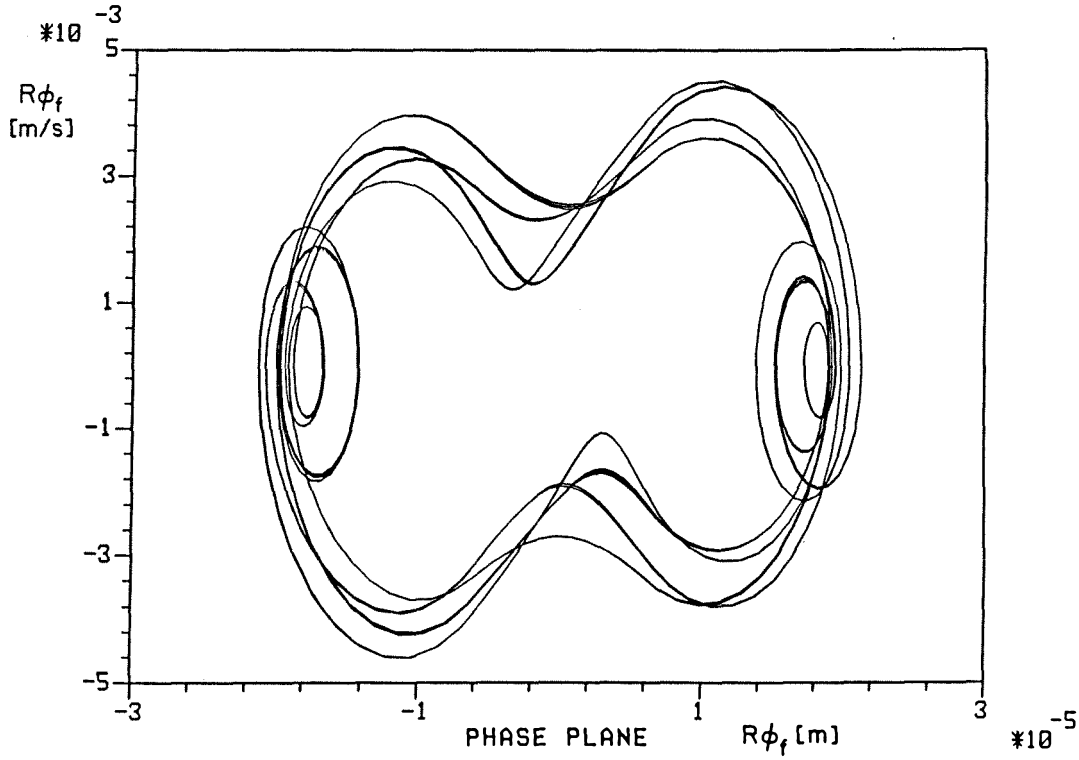

Figure 4.9.f Phase-Plane for the Foundation Rocking dof (t= 2.5-3 sec)

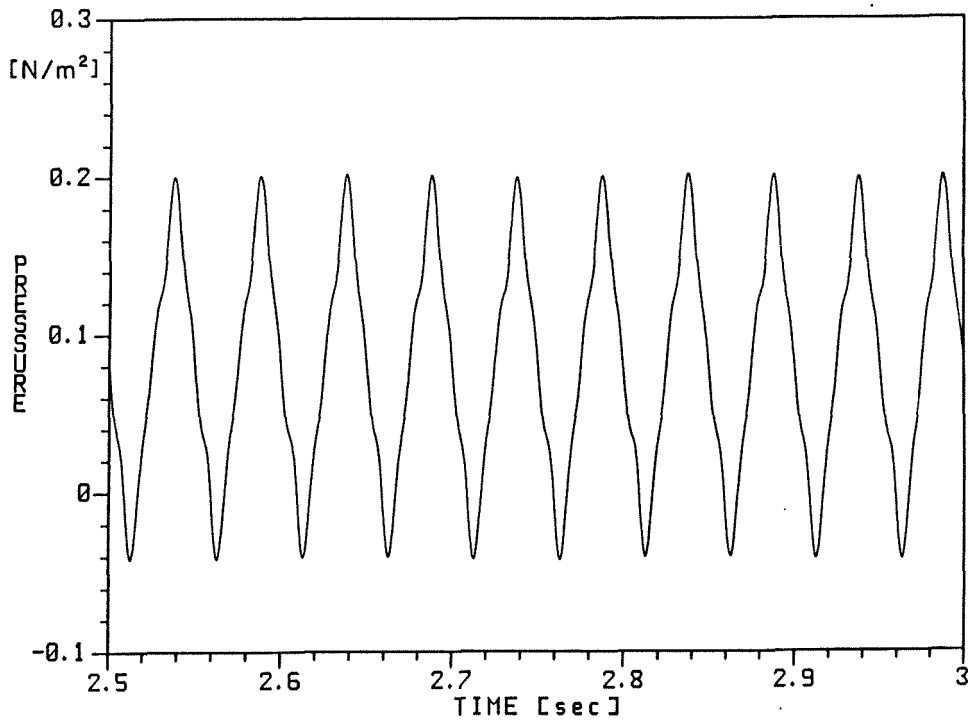

Figure 4.10.a External Pressure at r=R, z=0.92H and θ=0°

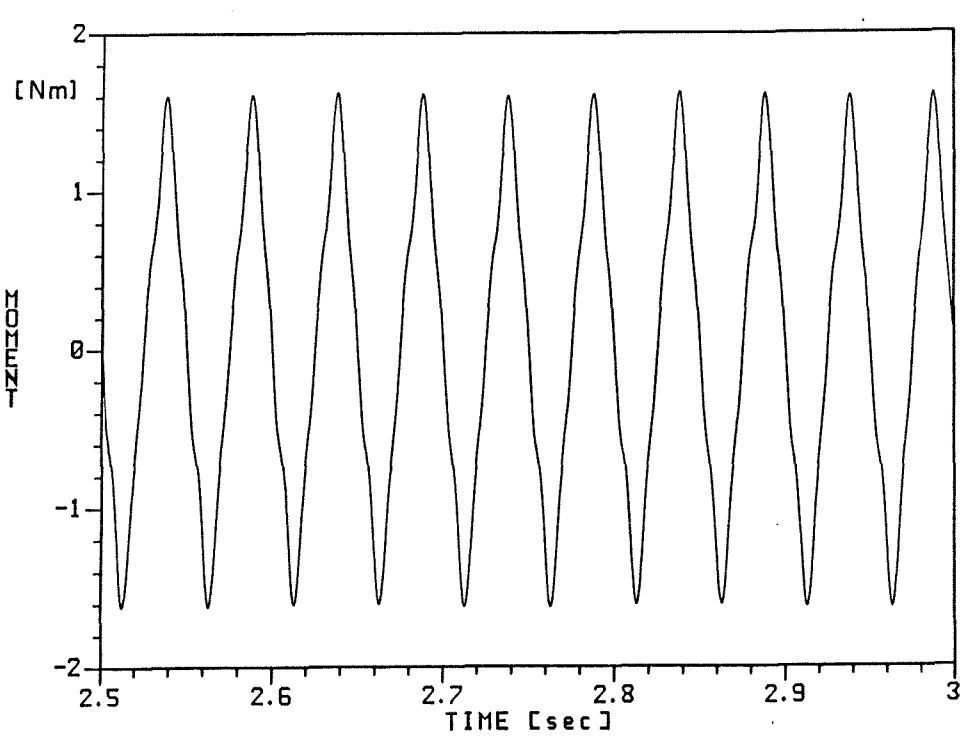

Figure 4.10.b Moment at the Tank Bottom

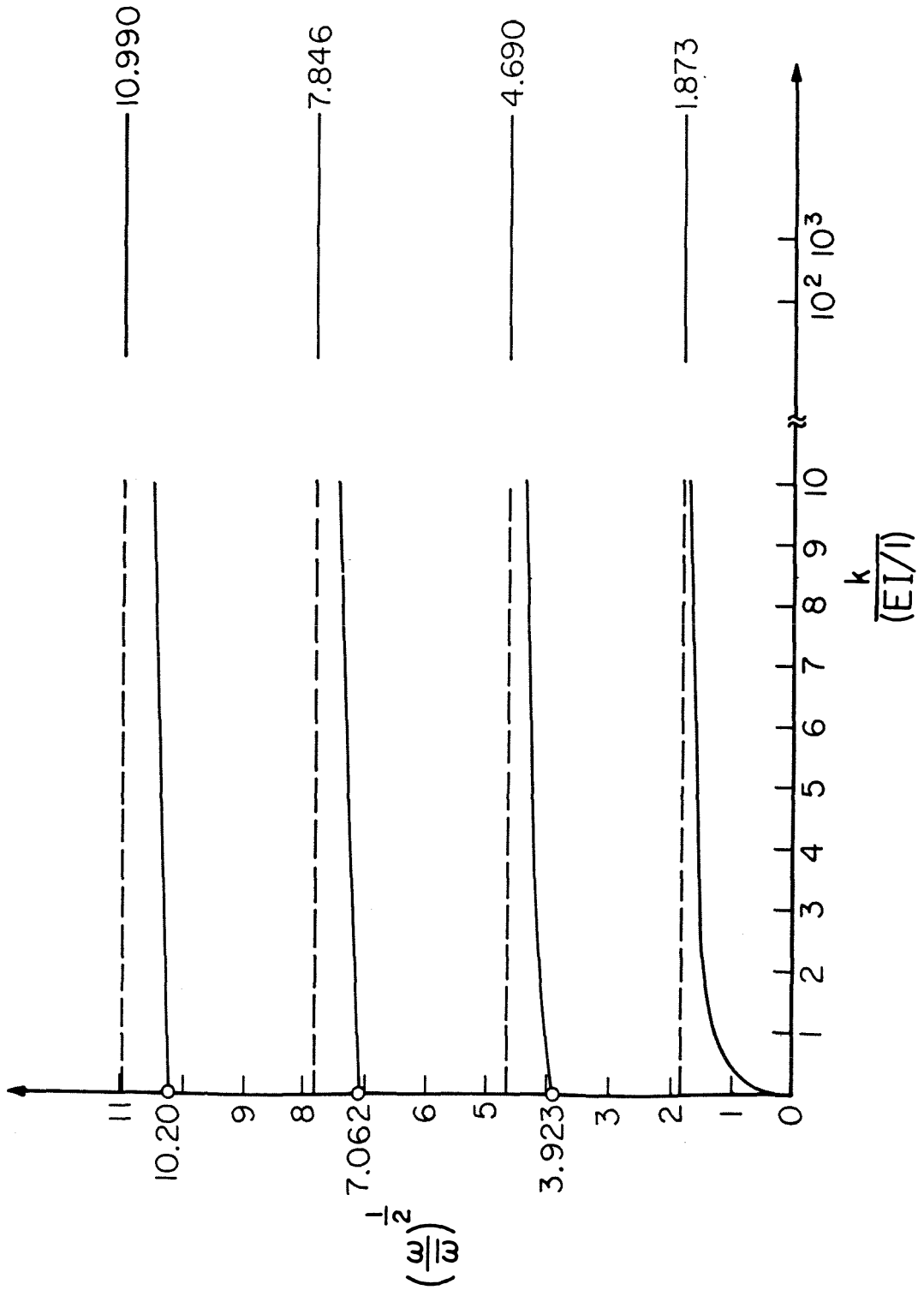

Figure 5.1 Beam Frequencies vs End Rotational Stiffness

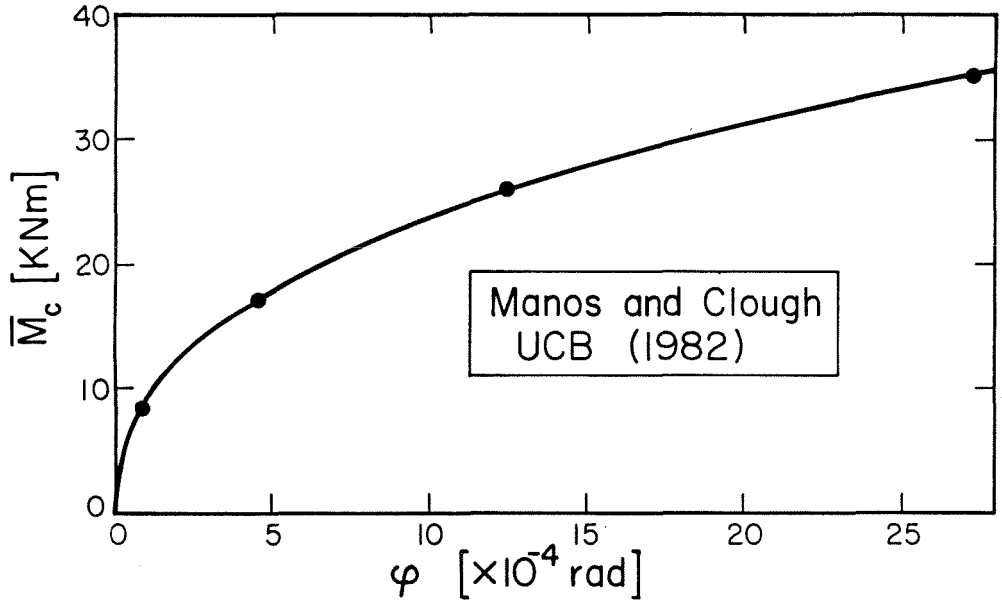

Figure 5.2 Moment vs Uplift Rotation for Tank of Reference [37]

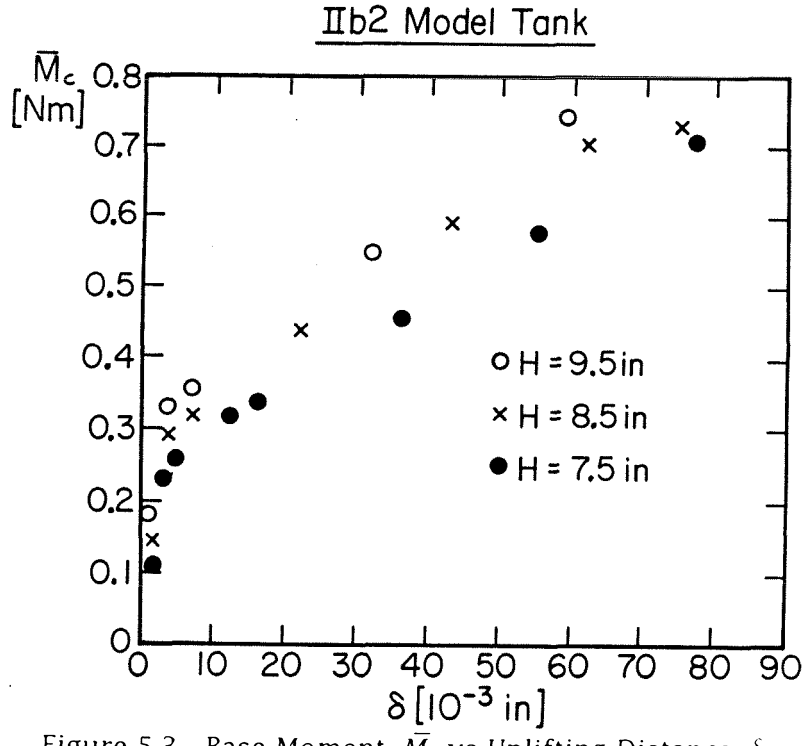

Figure 5.3 Base Moment, $\bar{M}_c$ vs Uplifting Distance, δ

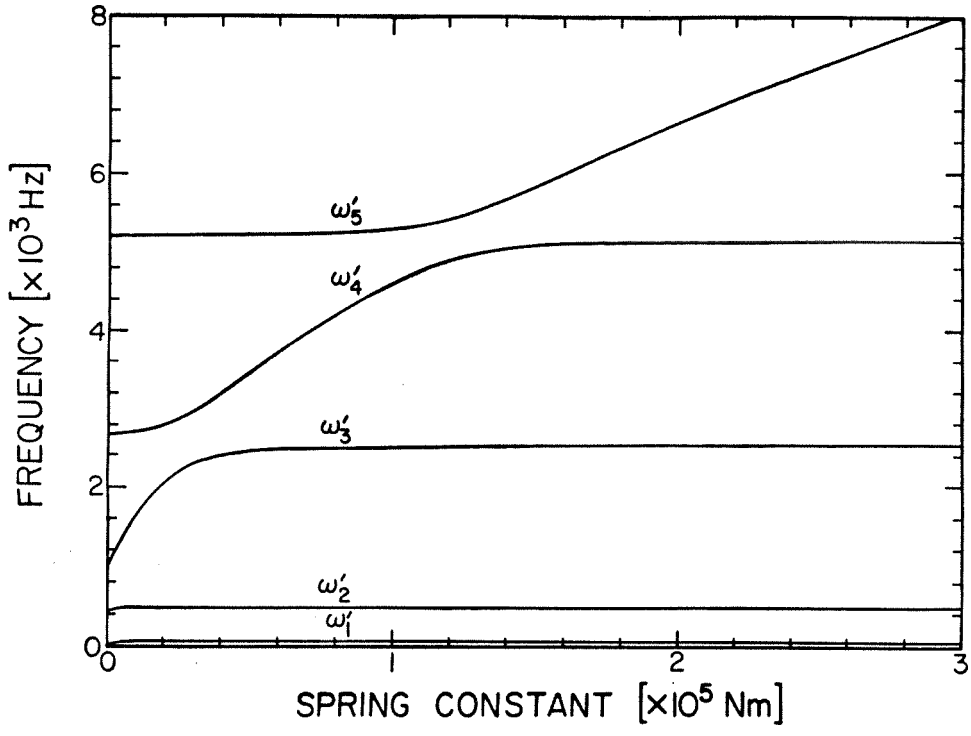

Figure 5.4.a Frequencies vs Uplift Spring Stiffness

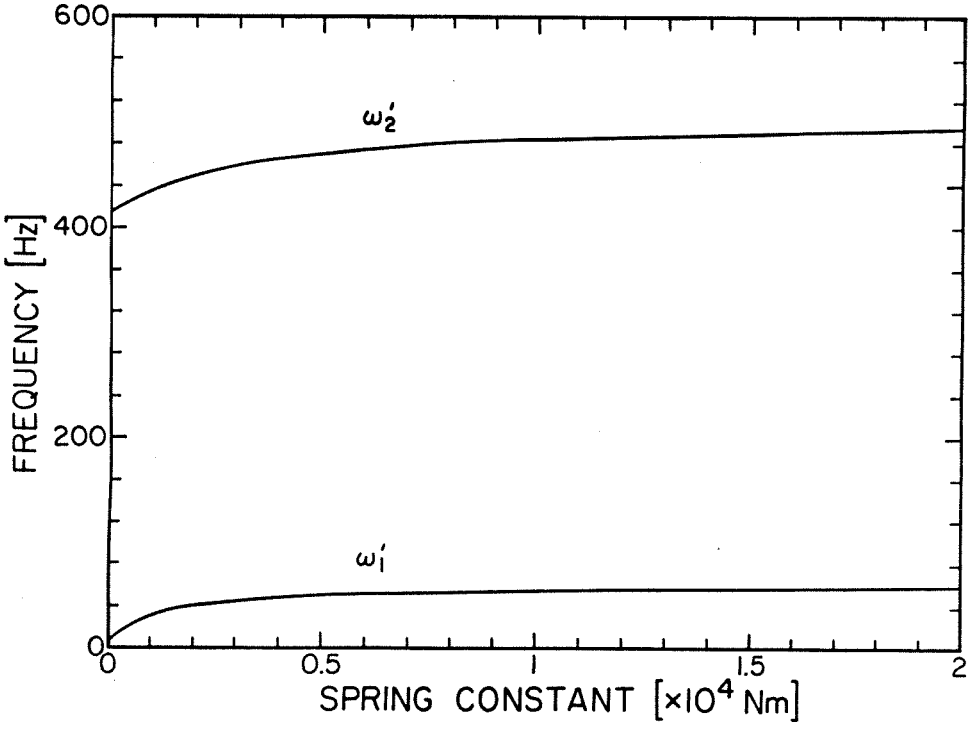

Figure 5.4.b Magnification of the Origin of Figure 5.4.a

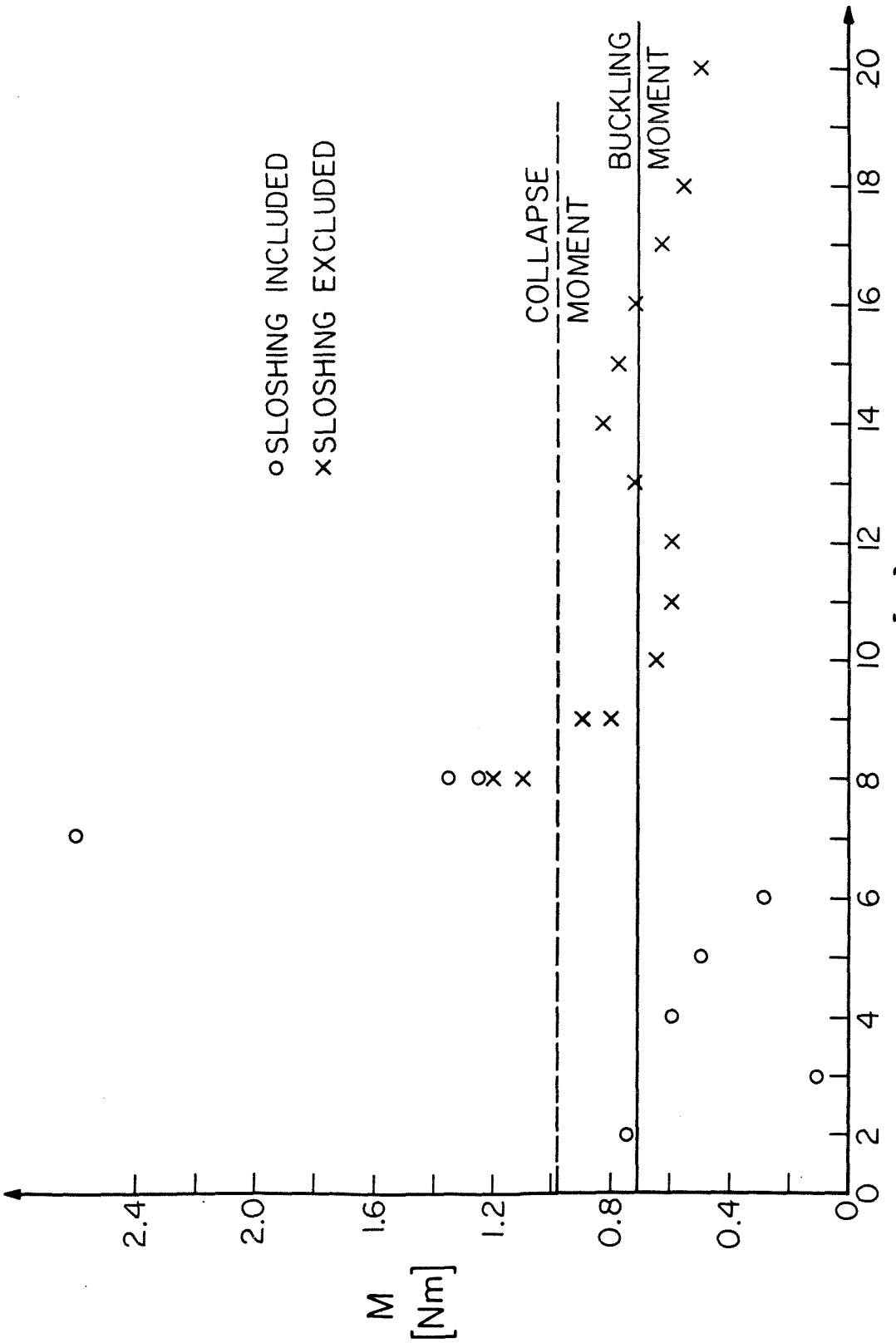

Figure 5.5 Computed Base Moment vs Excitation Frequency

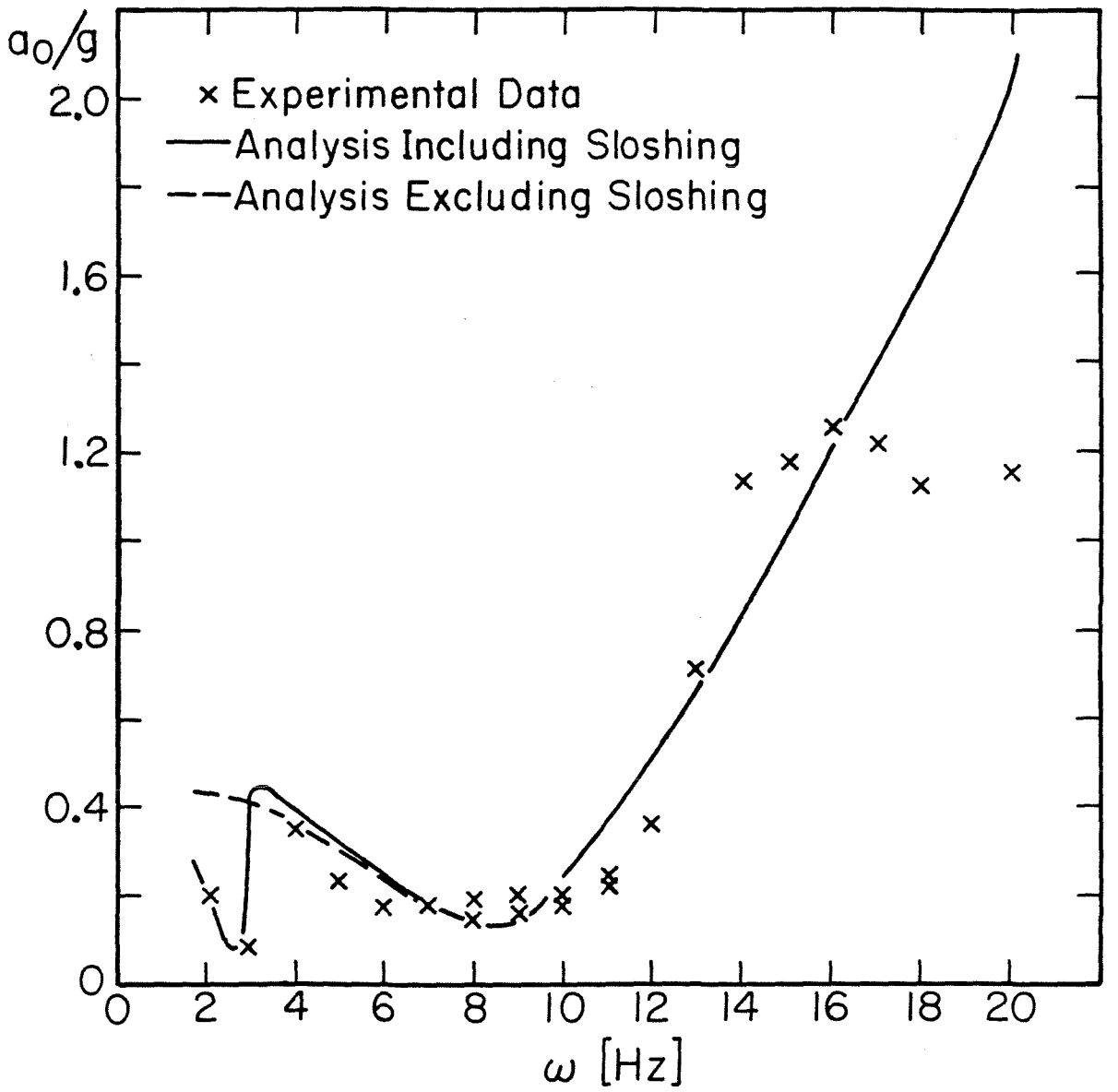

Figure 5.6 Critical Buckling Acceleration vs Excitation Frequency

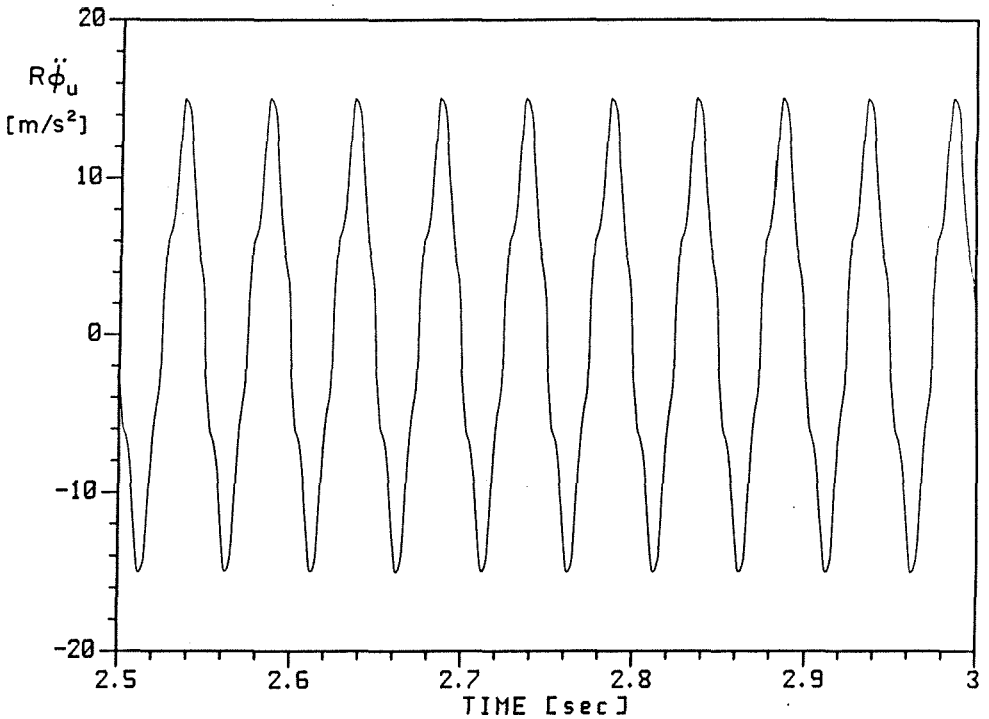

Figure 5.7.a History of Acceleration of Uplift dof

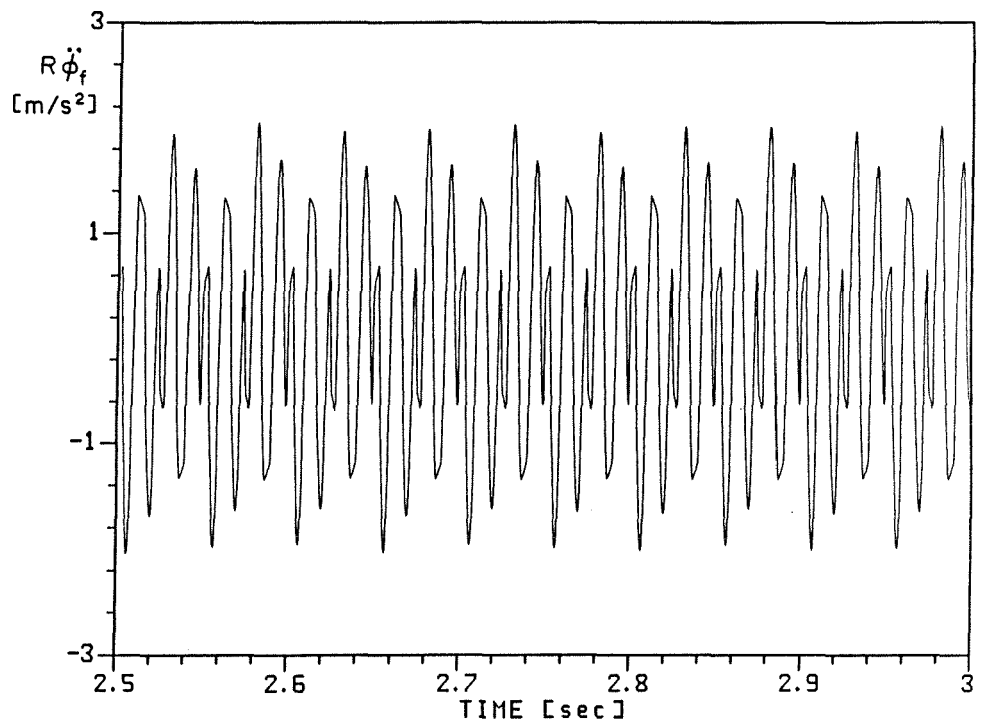

Figure 5.7.b History of Acceleration of Foundation Rocking dof

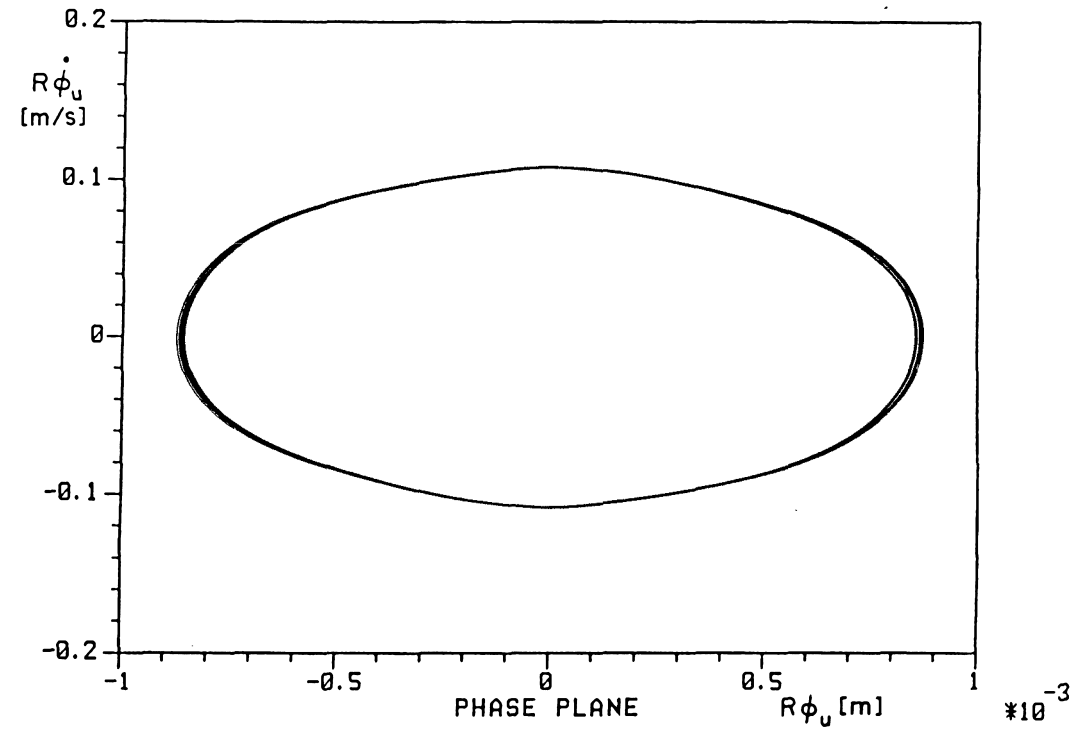

Figure 5.7.c Phase-Plane for the Uplift dof (t= 2.5-3 sec)

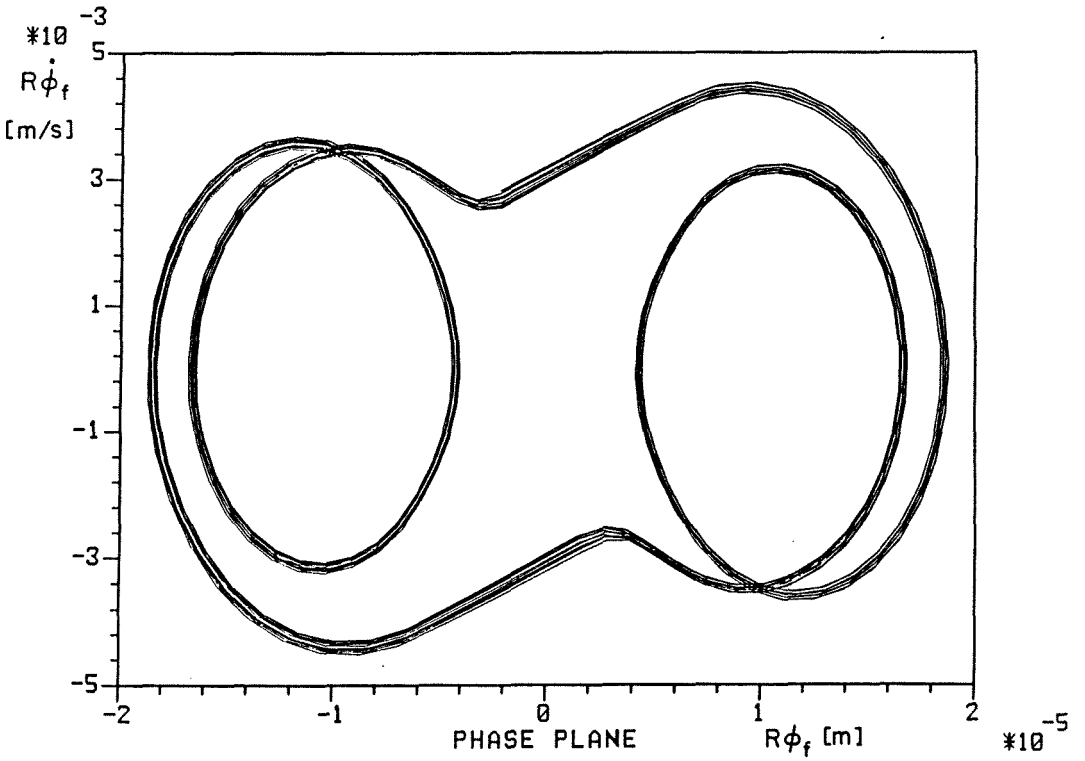

Figure 5.7.d Phase-Plane for the Foundation Rocking dof (t= 2.5-3 sec)

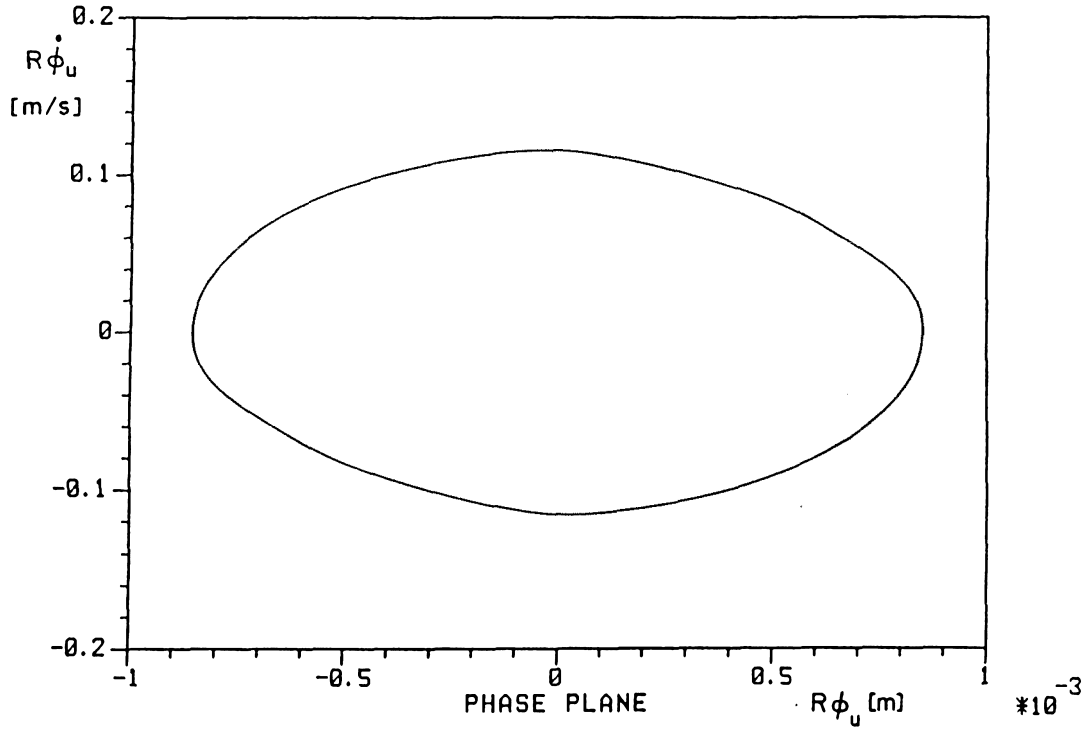

Figure 5.7.e Phase-Plane for the Uplift dof (t= 2.5-3 sec, $a_o(1-e^{-3t})$)

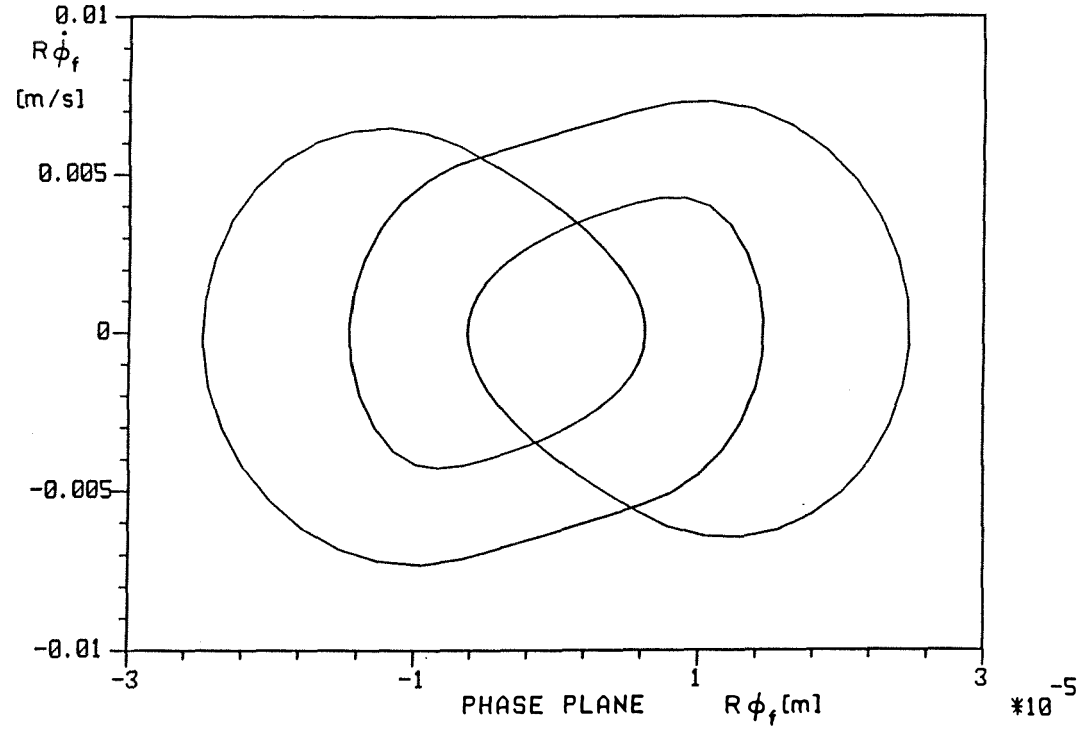

Figure 5.7.f Phase-Plane for the Foundation Rocking dof (t= 2.5-3 sec, $a_o(1-e^{-3t})$)

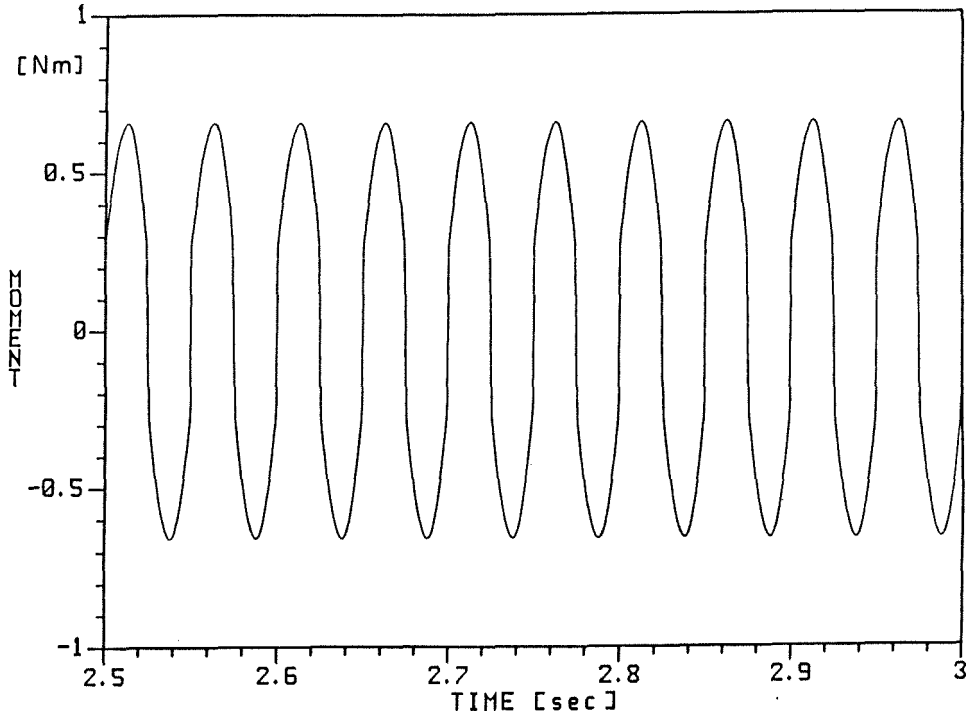

Figure 5.7.g History of Base Moment

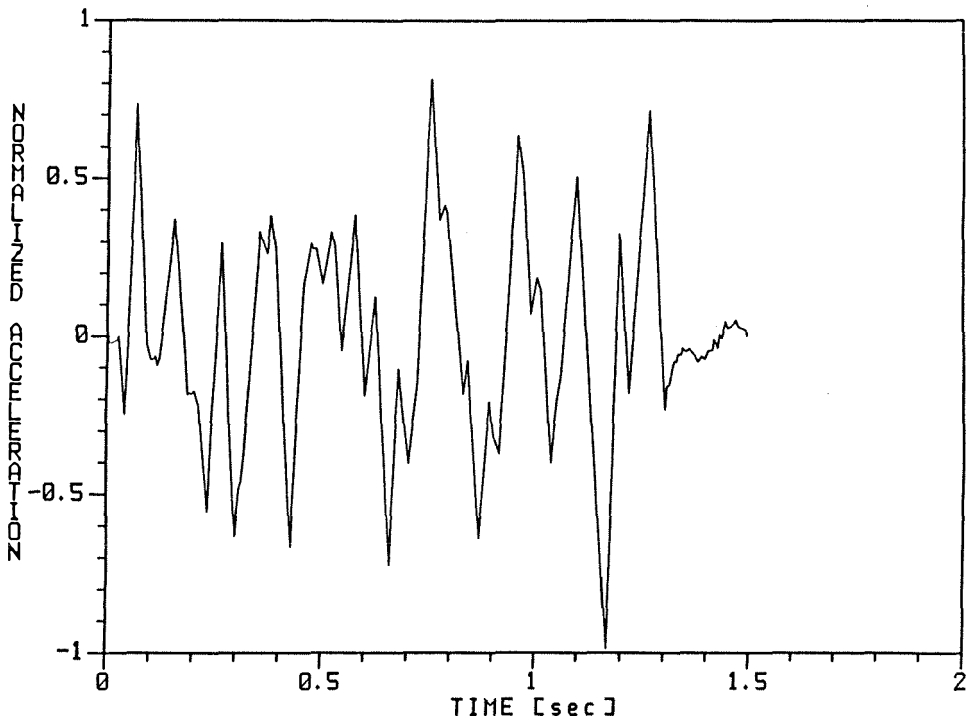

Figure 5.8 Normalized Base Acceleration History for the Transient Model Tests of Ref. [29], with Simulated Earthquake Excitation

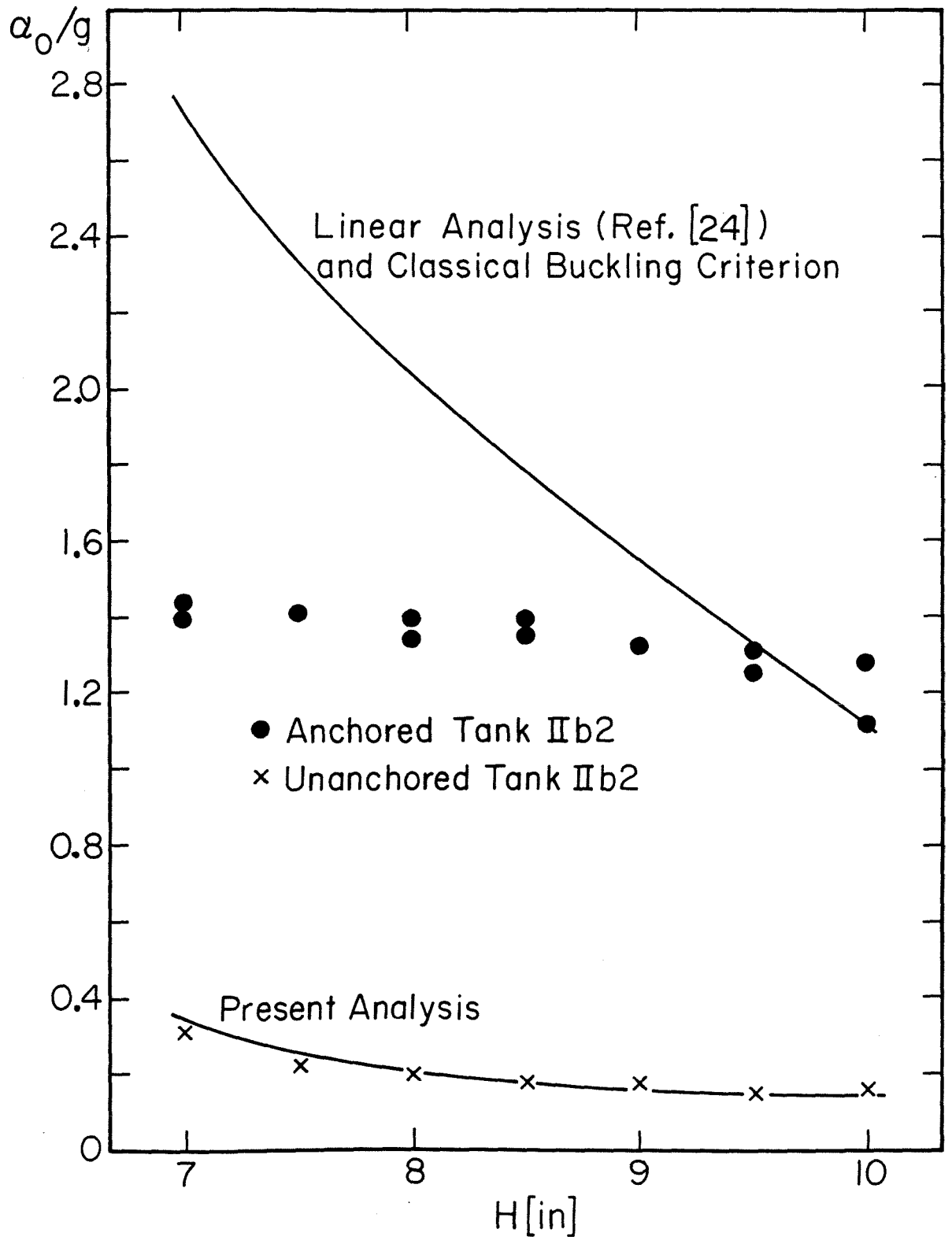

Figure 5.9 Critical Buckling Acceleration vs Water Depth (Transient Model Tests with Simulated Earthquake Excitation [29])

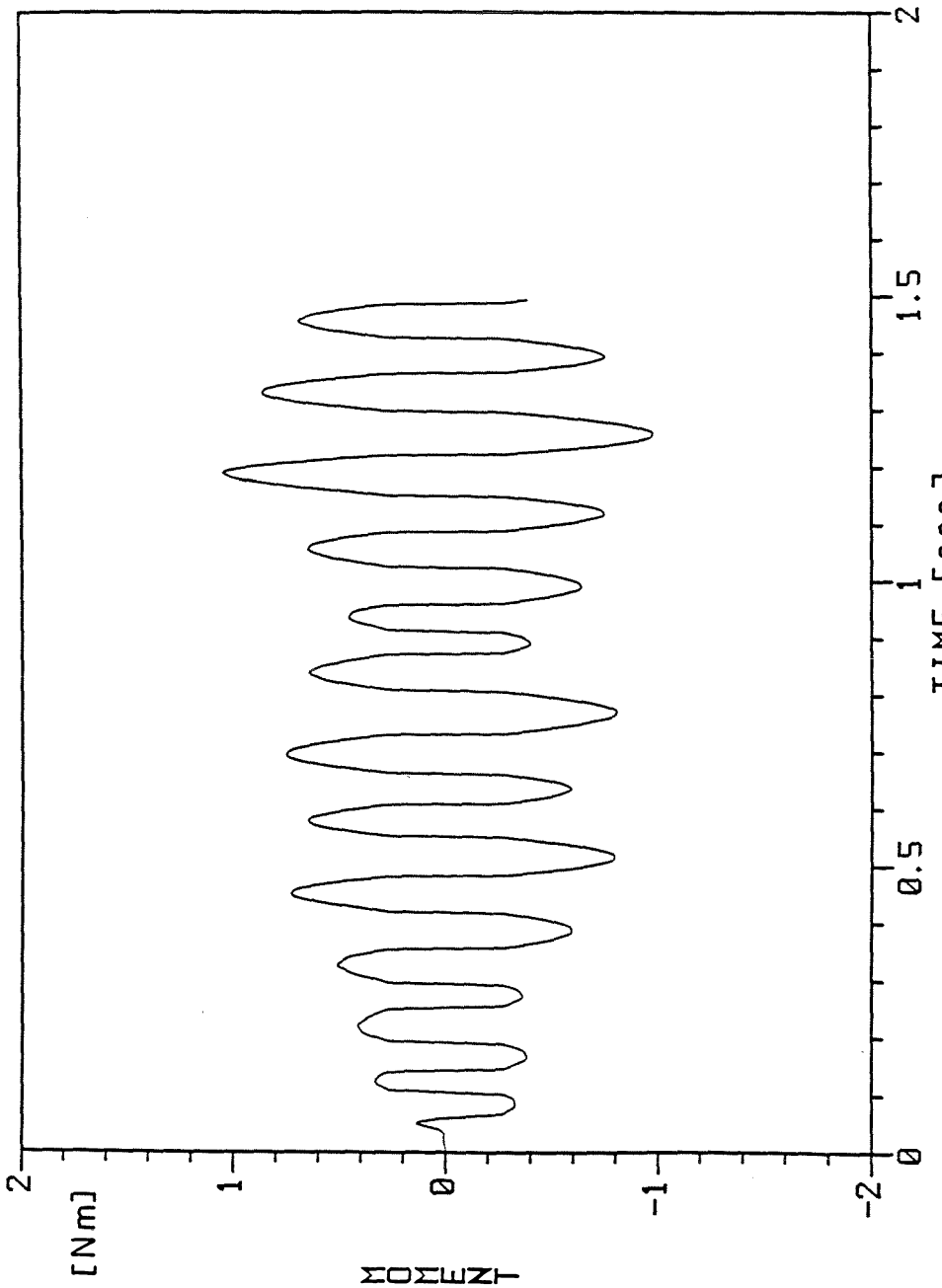

Figure 5.10 Base Moment History for Transient Tests (H= 7.5 in, a_o= 2.5 m/s^2)